NASA CONTRACTOR REPORT

NASA CR-379

FEASIBILITY OF STANDARD EVALUATION PROCEDURES FOR ABLATING MATERIALS

by Nevin K. Hiester and Carroll F. Clark

Prepared under Contract No. NASr-49(15) *by*
STANFORD RESEARCH INSTITUTE
Menlo Park, Calif.
for

NATIONAL AERONAUTICS AND SPACE ADMINISTRATION • WASHINGTON, D. C. • FEBRUARY 1966

NASA CR-379

FEASIBILITY OF STANDARD EVALUATION PROCEDURES FOR ABLATING MATERIALS

By Nevin K. Hiester and Carroll F. Clark

Prepared under Contract No. NASr-49(15) by
STANFORD RESEARCH INSTITUTE
Menlo Park, Calif.

for

NATIONAL AERONAUTICS AND SPACE ADMINISTRATION

For sale by the Clearinghouse for Federal Scientific and Technical Information
Springfield, Virginia 22151 – Price $5.00

ABSTRACT

Twelve plasma arc heater facilities participated in a round-robin study to determine the feasibility of a standardized ablation test procedure. Teflon and high-density phenolic-nylon models having the same shape and size were supplied by Stanford Research Institute, and were evaluated at various enthalpies and heating rates under supersonic conditions. Calorimeters and pressure probes were also supplied by SRI, and interpretation of the results indicated that the best description of the test environment was given by the stagnation point heating rate and pressure. The mass loss rates for both materials as obtained from all facilities could be correlated in terms of these two parameters with a standard deviation of approximately 11%.

CONTENTS

CONTENTS

ILLUSTRATIONS

TABLES

SYMBOLS

A^*	Nozzle throat area—ft^2
A	Area—ft^2
C_p	Specific heat—Btu lb^{-1} $°F^{-1}$
D_e	Nozzle exit diam.—inch
D_t	Nozzle throat diam.—inch
h_t	Total stream enthalpy—Btu lb^{-1}
h_{CW}	Cold wall enthalpy—Btu lb^{-1}
h_{HW}	Hot wall enthalpy—Btu lb^{-1}
$\Delta h_{\substack{calc \\ SRI \\ CW}}$	Enthalpy potential calculated from $\dot{q}_{\substack{SRI \\ CW}}$—Btu lb^{-1}
$\Delta h_{\substack{calc \\ FAC \\ CW}}$	Enthalpy potential calculated from $\dot{q}_{\substack{FAC \\ CW}}$—Btu lb^{-1}
$\Delta h_{\substack{calc \\ SRI \\ HW}}$	Enthalpy potential calculated from $\dot{q}_{\substack{SRI \\ HW}}$—Btu lb^{-1}
$\Delta h_{\substack{meas \\ CW}}$	Enthalpy potential from h_t measured by the facility—Btu lb^{-1}
$\Delta h_{\substack{sonic \\ CW}}$	Enthalpy potential h_t calculated by sonic flow method—Btu lb^{-1}
H_{eff}	Effective heat of ablation $\dfrac{\dot{q}_{HW}}{\dot{m}_t}$—Btu lb^{-1}
$\dot{m}_p$	Pyrolysis rate $\dot{m}_p = \dot{m}_V + \dot{m}_{CP}$—lb $sec^{-1} ft^{-2}$
$\dot{m}_t$	Total mass loss rate—lb $sec^{-1} ft^{-2}$
$(\dot{m}_t)_{PN}$	Total mass loss rate for phenolic-nylon—lb $sec^{-1} ft^{-2}$
$(\dot{m}_t)_{TFE}$	Total mass loss rate for Teflon—lb $sec^{-1} ft^{-2}$
$\dot{m}_V$	Vapor production rate $\dot{m}_V = \dot{m}_t - \dot{m}_{CR}$
$\dot{m}_{CP}$	Char production rate—lb $sec^{-1} ft^{-2}$
$\dot{m}_{CR}$	Char recession rate—lb $sec^{-1} ft^{-2}$
P_{t_1}	Arc chamber or plenum pressure—atm

P_{t_2}	Model stagnation pressure—atm
P_σ	Percent standard deviation
$\dot{q}_{CW}$	Heat transfer rate, cold wall—Btu $sec^{-1}ft^{-2}$
$\dot{q}_{HW}$	Heat transfer rate, hot wall—Btu $sec^{-1}ft^{-2}$
$\dot{q}_{FAC}$	Heat transfer rate, Facility calorimeter—Btu $sec^{-1}ft^{-2}$
$\dot{q}_{SRI}$	Heat transfer rate, SRI calorimeter—Btu $sec^{-1}ft^{-2}$
R	Model radius—ft
R_{eff}	Effective radius of curvature—ft
t	Run time—sec
T	Temperature—°F
T_{FS}	Model front surface temperature—°F
w	Weight—grams or pounds as indicated
W	Gas flow rate—lb sec^{-1}
Δy	Model core length measurements—inches
Δm	Model core mass charge—g
ρ	Density—lb ft^{-3}

I INTRODUCTION

Ablation - the use of a sacrificial material to protect underlying bodies during exposure to severe thermal environments, such as during atmospheric re-entry - is so complex and interrelated a process that it is almost impossible to separate the various steps out as individual contributions. As a result, and because of the urgent need for items of hardware, the empirical approach of screening a large number of materials in various simulation devices has received much attention. Unfortunately, the results have been difficult to cross-correlate, even those from ostensibly similar devices.

For this reason the National Aeronautics and Space Administration's Research Advisory Committee on Materials recommended the establishment of a national test program with the objective of providing, among other things, data as to the capability of various test devices to represent thermal flight environments, and standard test methods. Some question existed, however, as to the technical feasibility of producing standard test methods.

NASA gave The Stanford Research Institute a contract to conduct a round-robin test study to determine whether ablation results from different plasma arc heater facilities could be shown to be related. This work was to involve:

1. Definition of realistic environmental conditions.

2. Evaluation of extent to which these conditions are simulated by existing or projected test devices

3. Conduction of comparative ablation tests on standardized materials at selected organizations possessing suitable equipment, and provision of the specialized instrumentation and test models required

4. Correlation of test results with analyses to determine the feasibility of developing a standardized test.

II SUMMARY

Selection of test conditions, model dimensions, and materials for the round-robin ablation program was governed by possible Apollo reentry environments. Using the first two of these factors as criteria, the various supersonic arc-heated plasma jet facilities were reviewed analytically from published information, and their capabilities were determined by an inspection visit. Twelve were selected for participation in the study. Five were government organizations, namely:

A. Gas Dynamics Branch—Ames Research Center—NASA

B. Entry Structures Branch—Langley Research Center—NASA

C. Advanced Materials and Physics Division—Langley Research Center—NASA

D. Manned Spacecraft Center—NASA

E. Flight Mechanics Division—Wright-Patterson Air Force Base

The seven industrial organizations were:

A. AVCO Corporation

B. Boeing Company

C. General Dynamics

D. General Electric Space Technology Center

E. Giannini Scientific Corporation

F. Martin Company

G. North American Aviation, Incorporated

Test instruments and ablation models were supplied to each participant for use in the round-robin test program. The calorimeter and pressure probe were of the same size and configuration as the test models and the calorimeter had the same sensing area as the core of the model. The materials used in the models were:

1. Teflon, type TFE, white variety, density = 135 lb/cu ft

2. Phenolic-nylon (50—50%), density = 75 lb/cu ft

These represented low and high temperature ablators; the former is a subliming material, and the latter a charring type ablator.

Half of the facilities had provisions for two or less insertions during a test run. In these cases only one measurement of environment could be made in addition to exposure of the model. In the majority of cases this was determination of the heating rate by either the SRI or the facility calorimeter. As a result, a number of calibration runs were necessary so that more complete information, including stagnation pressure, could be estimated and reported for the model runs. Comparison of the stagnation pressure and heating rates as determined by various methods was therefore important.

The stagnation pressures determined with a facility probe, for those few facilities that did so, compared with the Institute probe with a standard deviation of 2.6%. It was therefore concluded that the use of either probe was satisfactory.

Comparison of the SRI calorimeter with those supplied by each facility was not as satisfactory. The standard deviation was 16%; in fact, the facility calorimeters tended to read a little higher than the SRI calorimeter. This in part can be explained by the smaller sensing areas of the facility calorimeters and the existence of plasma "coring" at a number of the facilities. It should be pointed out that these comparisons are based on the usual conversion procedure for calorimeter size and the use of a 0.55 ratio between flat-face and hemisphere readings. Some evidence was available from work done at FMD-Wright Patterson that, at high nozzle expansion ratios, departure from equilibrium can cause different readings in calorimeters depending upon the catalyticity of their surfaces.

The majority of the facilities used the energy balance technique for determining the total enthalpy of the plasma stream. This was not satisfactory in those cases where "coring" existed, such as at Boeing and General Electric. Comparison of these values with the enthalpy potentials calculated from the heating rates and stagnation pressure through the Fay-Riddell relation showed a standard deviation of 46%; this was reduced to 18% when the Boeing and General Electric data were eliminated.

Determination of the enthalpy by the sonic flow method was not an improvement over the energy balance value. Its standard deviation, when compared with the calculated enthalpies, was 29%.

The mass loss rate of Teflon was best correlated by the following relation:

$$(\dot{m}_t)_{TFE} = 0.0058(\dot{q}_{\substack{SRI \\ CW}})^{0.58}(P_{t_2})^{0.25}$$

with a standard deviation of 11%. Equally good correlations were obtained in terms of the stagnation pressure with the SRI calorimeter hot wall heating rate, and with the facility calorimeter cold wall heating rate. Correlation of the mass loss rate in terms of the measured enthalpy potential and stagnation pressure was much less satisfactory, having a standard deviation of 21%.

Minor adjustment of the exponents in a correlation similar to that shown above permits relation of the heat of ablation of Teflon to the calculated hot wall enthalpy potential as follows:

$$H_{eff} = \frac{\dot{q}_{\substack{SRI \\ HW}}}{(\dot{m}_t)_{TFE}} = 38.3\left(\Delta h_{\substack{calc \\ SRI \\ HW}}\right)^{0.49} .$$

This has a standard deviation of 21%. Comparison of this relation with linear forms proposed by others shows its validity for the wide range of experimental cooditions experienced in the round-robin test program.

Similar mass rate correlations are found for phenolic-nylon. For instance,

$$(\dot{m}_t)_{PN} = 0.0017(q_{\substack{SRI \\ CW}})^{0.56}(P_{t_2})^{0.13}$$

with a standard deviation of 11%. A somewhat similar correlation based on the facility calorimeter is equally good but a phenolic-nylon mass loss correlation in terms of the measured enthalpy potential has a standard deviation of 30%. A summary of these correlations for Teflon and phenolic-nylon is given in Table I.

Correlations of other char parameters with environmental conditions were not successful. The same was true for back surface temperature rise and front surface temperature. The latter difficulty was partially due to technique variations from facility to facility in measuring this value.

Table I

SUMMARY OF CORRELATIONS PREDICTING TOTAL MASS LOSS RATE, $\dot{m}_t$

TYPE OF CORRELATION	TEFLON	PHENOLIC-NYLON
SRI Calorimeter, cold wall heating rate (1)	$0.0058\left(\dot{q}_{\substack{SRI \\ CW}}\right)^{0.58}\left(P_{t_2}\right)^{0.25}$ ± 10%	$0.0017\left(\dot{q}_{\substack{SRI \\ CW}}\right)^{0.56}\left(P_{t_2}\right)^{0.13}$ ± 11%
SRI Calorimeter, cold wall heating rate (2)	$0.0060\left(\dot{q}_{\substack{SRI \\ CW}}\right)^{0.57}\left(P_{t_2}\right)^{0.25}$ ± 10%	$0.0018\left(\dot{q}_{\substack{SRI \\ CW}}\right)^{0.55}\left(P_{t_2}\right)^{0.13}$ ± 10%
SRI Calorimeter, cold wall heating rate (1,4)	$0.0065\left(\dot{q}_{\substack{SRI \\ CW}}\right)^{0.55}\left(P_{t_2}\right)^{0.23}$ ± 11%	$0.0013\left(\dot{q}_{\substack{SRI \\ CW}}\right)^{0.64}\left(P_{t_2}\right)^{0.18}$ ± 14%
Facility Calorimeter, cold wall heating rate	$0.011\left(\dot{q}_{\substack{FAC \\ CW}}\right)^{0.48}\left(P_{t_2}\right)^{0.29}$ ± 11%	$0.0034\left(\dot{q}_{\substack{FAC \\ CW}}\right)^{0.46}\left(P_{t_2}\right)^{0.18}$ ± 8%
Facility Calorimeter, cold wall heating rate (3)	$0.013\left(\dot{q}_{\substack{FAC \\ CW}}\right)^{0.44}\left(P_{t_2}\right)^{0.29}$ ± 18%	$0.0039\left(\dot{q}_{\substack{FAC \\ CW}}\right)^{0.44}\left(P_{t_2}\right)^{0.18}$ ± 9%
SRI Calorimeter, hot wall heating rate	$0.0076\left(\dot{q}_{\substack{SRI \\ HW}}\right)^{0.55}\left(P_{t_2}\right)^{0.27}$ ± 10%	
SRI Calorimeter, hot wall heating rate (4)	$0.0085\left(\dot{q}_{\substack{SRI \\ HW}}\right)^{0.51}\left(P_{t_2}\right)^{0.245}$ ± 11%	
Measured enthalpy potential	$0.0017\left(\Delta h_{\substack{meas \\ CW}}\right)^{0.59}\left(P_{t_2}\right)^{0.57}$ ± 21%	$0.0010\left(\Delta h_{\substack{meas \\ CW}}\right)^{0.49}\left(P_{t_2}\right)^{0.41}$ ± 30%

(1) Not including Giannini and Martin data

(2) Including Giannini and Martin data

(3) Includes all Martin replicate data

(4) Adjusted coefficients $a(\dot{q})^n(P_{t_2})^{(1-n)/2}$

III CONCLUSIONS

Based on the success in correlating the mass loss rate data, it is concluded that:

1. A procedure for comparing ablation results (on a given material) at each plasma arc heater facility is feasible through use of a standard mass-loss rate, heating rate, stagnation-pressure correlation

2. The applicability of the procedure outside the range of materials, model sizes, and arc heater operating conditions studied in this program is not known.

In addition to these conclusions other findings on the program are:

3. Stagnation pressure measurements as well as heating rates should be taken during each run

4. The calorimeter should be the same shape and size as the test sample, and the core on which measurements are taken should have the same diameter on both

5. A standard calorimeter (for example the SRI calorimeter used in this study) will provide consistent results from facility to facility

6. Determination of enthalpy by the energy balance method is not very satisfactory, especially if the plasma stream exhibits a severe heating rate gradient (that is, if there is a hot plasma core of about the same size as the test sample).

Another conclusion is:

7. A standard ablation test procedure should involve:

   a. Measurement of both heating rate and stagnation pressure in each run

   b. Use of a sample model and a standard calorimeter of the same shape and dimensions

   c. Use of a plasma column of at least 50% greater diameter than the test shroud, and with a low degree of enthalpy coring (as checked by pressure and heating rate traverses)

   d. Test durations equivalent to heating loads of at least 1,000 Btu/sq.ft. for Teflon and 6,000 Btu/sq.ft. for phenolic-nylon samples

A final conclusion was:

8. Additional work is necessary to determine the generality of the test correlation, extend the range of conditions studied, and explain the significance of the form of the correlation.

IV SCOPE

Early in the program, representatives of the Ames Research Center, Langley Research Center, Manned Spacecraft Center, and Stanford Research Institute met to determine the test conditions, model dimensions, and materials to be evaluated. Initially it was proposed that the enthalpy and heating fate conditions be selected in terms of possible Apollo environments. However, such values were difficult to attain in plasma arc devices and as a result, an enthalpy of 5,000 Btu lb^{-1} and heating rate of 150 Btu sec^{-1} ft^{-2} were chosen as a common point for all facilities. The other test conditions were to be selected, insofar as possible, to provide a series of points running generally along a constant stagnation pressure line for the Teflon models, as well as a series of points at a constant value of enthalpy for the phenolic-nylon models, plus several cross-comparison points.

The heating rates, of course, are those for the model geometry chosen. The flat-faced, shroud design, indicated in Fig. 1, was selected because of its ease of construction and on the basis that it represents a design adopted by many testing organizations.

Two materials were selected for the study, namely:

1. Teflon, type TFE, white variety, density = 135 lb/ft^3
2. Phenolic-nylon (50-50%), density = 75 lb/ft^3.

These were chosen as representative types of low and high temperature ablators. Teflon is also an important material for this program because it offers an independent means of determining the enthalpy and, as a subliming material, serves as a control specimen for the test series. Phenolic-nylon is, of course, a charring ablator.

The round robin would then consist of the exposure of these models under the conditions indicated at various arc-heated plasma jet facilities. The participants would supply information about test conditions and the Institute would measure the physical and chemical changes in the models.

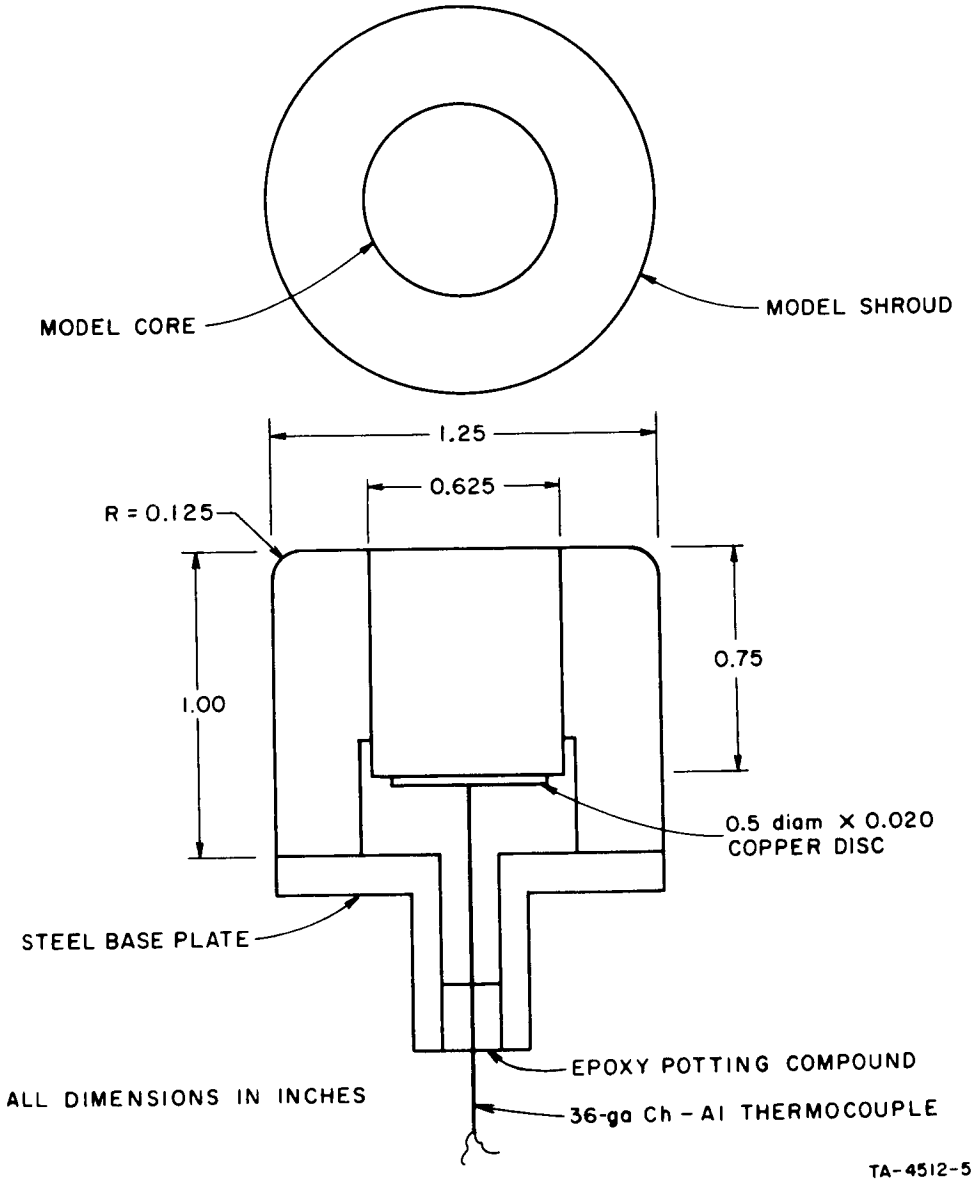

FIG. 1 DIMENSIONS OF TEFLON AND PHENOLIC-NYLON MODELS

V SELECTION OF PARTICIPATING ORGANIZATIONS

The choice of testing facilities to be contacted was governed by two primary factors: first, that the test device could accommodate the model size of 1¼ inches diameter within the plasma stream; and second, that it would operate in the range of test conditions desired.

Based on Vought Astronautic's Report No. 00.49 of 18 April 1962 (*A Survey of Plasma Arc Heaters*), twenty organizations were chosen for initial contact. Subsequent discussions with interested parties led to inclusion of an additional twelve. Each of these was notified of the details of the round-robin ablation program, and asked to indicate its interest in participating and to advise as to the operating capabilities of its arc-heated plasma jet facility.

Expressions of interest were received from twenty of the thirty-two organizations; one—the Itek Division of Vidya Corporation—withdrew because of lack of a supersonic facility at that time. This was in excess of the number of participants planned for inclusion, so arrangements were made to visit and assess as many of these as possible. To assist in this, an evaluation form was completed during the visit to each facility, at which time the program was discussed in detail. In addition to obtaining factual information about the plasma arc heater, the Stanford Research Institute representative made a subjective rating of the quality of the equipment, the degree of sophistication of the instrumentation of the facility, and the experience of the test personnel.

The results of this assessment are shown in Table II, which covers the interested commercial organizations. Three were not visited—Douglas Aircraft, Johns Hopkins University, and Republic Aircraft. In these cases the tabulated information was determined from correspondence.

The evaluation form called for information on actual electric arc heater performance plus operating limits on enthalpy, arc chamber pressure, and power input. These data were used to estimate the operating envelopes for each of these supersonic facilities. The results of these calculations, which were performed in accordance with the method of

Table II

SUMMARY OF COMMERCIAL FACILITIES

ORGANIZATION	PLASMA HEAD	P_{t_1} (ATM)		$\dot{q}$ max 1.25 in. FF h = 5,000	T_{fs}	INSERTIONS	SUBJECTIVE RATING (1)	MOTION PICTURES
		min	max					
Giannini Scientific Corporation	Giannini	0.02	0.36	165	Yes	3	E	Yes
AVCO Corporation	AVCO	0.013	0.13	55	Yes	4	E	Yes
General Dynamics	Vidya Rotating Arc	0.5	35	170	No	4	M	--
Goodyear	Vidya Rotating Arc	0.1	1.0	170	No	8-13	M	Yes
Martin Company	Modified Giannini	0.005	0.2	85	Yes	3	M	Yes
Boeing Company	Boeing Rotating Arc	0.1	0.5	95	No	1	M	Yes
North American Aviation	Modified Thermal-Dynamics	0.3	5.5	300	No	2	M	Yes
General Electric Space Technology Center	Tandem-Gerdien	1.0	1.6	130	Yes	1	M	No
Douglas	Radial Arc Jet	0.2	14	200 (2)	Yes	1	S	Yes
University of Chicago	Air Stabilized Arc	0.1	1.0	subsonic	Yes	1	S	Yes
Space Dynamics	Space Dynamics	0.01	100	?	No	1	S	Yes
Johns Hopkins University	JH Rotating Arc	1.5	2.6	130	No	1	S	No
McDonnell	McDonnell Vortex Stabilized	0.3	2.0	240	No	1	S	No
Republic Aircraft	Thermal-Dynamics	1	5.0	subsonic	Yes	6	S	Yes

(1) Facility capability considering equipment, instrumentation, and personnel: E if extensive; M if moderate; S if some.

(2) h = 4,000 max.

Winovich,[1] are contained in Technical Report No. I[2] on this contract. The values headed $\dot{q}^{max}_{h=5,000}$ in Table II were taken from these envelopes as the maximum heating rate (in Btu $ft^{-2}sec^{-1}$) shown by the envelope for an enthalpy of 5,000 Btu/lb.

The five interested government organizations were not summarized in Table II because they would be participating in any case. They were:

a. Gas Dynamics Branch—Ames Research Center—NASA

b. Entry Structures Branch—Langley Research Center—NASA

c. Advanced Materials and Physics Division—Langley Research Center—NASA

d. Flight Mechanics Division—Wright-Patterson Air Force Base

e. Manned Spacecraft Center—NASA.

The last of these has a subsonic facility which was included to provide a comparison between the two test regimes.

The limitation on participants was due to a ceiling on funds for subcontracting the round-robin tests. It was therefore necessary to rate the commercial organizations to permit selection of those to be funded. The important factors considered in weighing these facilities were:

1. Heating rate capabilities of the test facility, and number of insertions possible per run

2. Apparent quality of the facility's equipment, instrumentation, and personnel, as subjectively rated during the visit discussed previously

3. Ability to measure front surface temperature

4. Unit cost and total cost for performing the program.

A summary evaluation based on these factors is contained in Table III.

Two of the organizations proposed participation at no cost so that they could gain additional experience and know-how from the study and its results. This permitted inclusion of more organizations within the funds available. The ultimate decision was to include the first eight companies listed in Table III (down through General Electric), plus the five government organizations already mentioned. Subsequent to awarding of the contracts, Goodyear withdrew, because of an accident to its facility. This then provided twelve participants in the final program.

Table III

RATING OF COMMERCIAL FACILITIES*

ORGANIZATION	$\dot{q}_{max}$ / $h = 5,000$	T_{fs}	INSERTIONS	SUBJECTIVE RATING	COST/MODEL	BID COST	TOTAL RATING
Giannini Scientific Corporation	1	½	2	4	1	1	9½
AVCO Corporation	½	½	2	4	1	1	9
General Dynamics	½	0	2	3	2	1½	9
Goodyear	1	0	2	3	1½	1	8½
Martin Company	½	½	2	3	1½	1	8½
Boeing Company	½	0	0	3	2	1½	7
North American Aviation	1	0	1	3	1	1	7
General Electric Space Technology Center	½	½	0	3	½	½	6
Douglas	½	½	0	2	1½	1	5½
University of Chicago	½	½	0	2	1	1	5
Space Dynamics	½	0	0	2	½	½	3½
Johns Hopkins University	½	0	1	2	0	0	3½
McDonnell	1	0	0	2	0	0	3
Republic Aircraft	½	½	0	2	0	0	3

*Weighting based on following criteria applied to information given in Table I

$\dot{q}_{max\ (1.25\ in.\ FF)}$ $_{h=5,000}$: 1 if > 150 Btu $sec^{-1} ft^{-2}$; otherwise ½

T_{fs}: ½ if yes; otherwise 0

Insertions: 2 if ≥ 3; 1 if 2; otherwise 0

Subjective Capability Rating: 4 if extensive; 3 if moderate; 2 if some

Cost/Model: 2 if \$0; 1½ if < \$500; 1 if < \$1,000; ½ if < \$1,500; otherwise 0

Bid Cost: 1½ if \$0; 1 if < \$10,000; ½ if < \$15,000; otherwise 0.

VI ABLATION MODELS AND SRI INSTRUMENTATION

Ablation models and test instruments as shown in Figs. 2 and 3 were sent to each of the selected participants. A more detailed description of these are in the following sections.

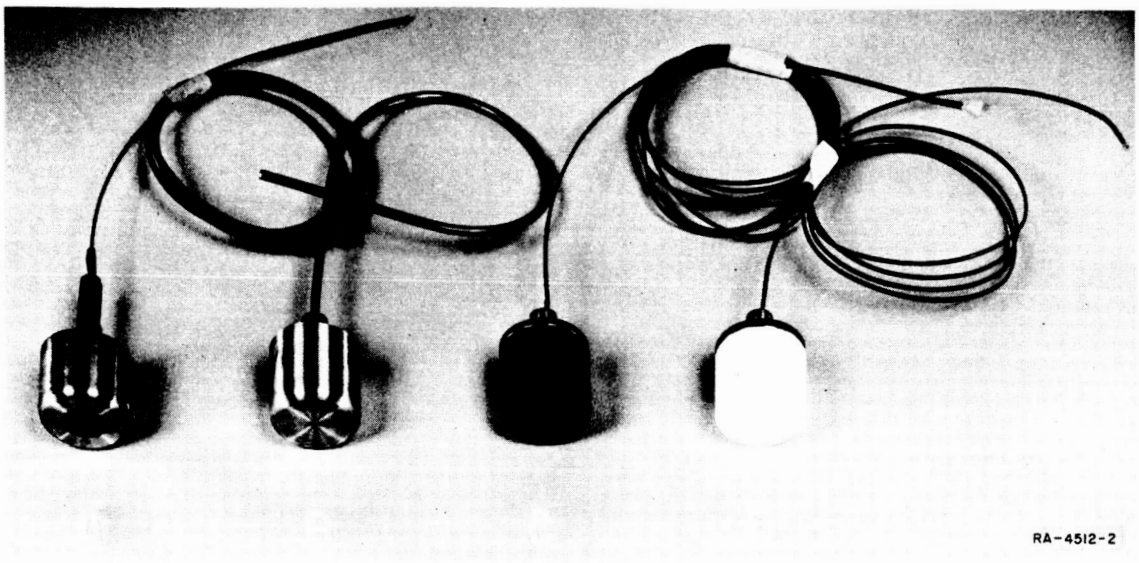

FIG. 2 ASSEMBLED INSTRUMENTS AND TEST SPECIMENS
A. Transient Calorimeter
B. Pitot Probe
C. Phenolic-Nylon Model
D. Teflon Model

A. DESCRIPTION OF MODELS

The Teflon models used in the round-robin ablation program were machined from forty cylinders, 1.5 inches in diameter by 6 inches long, furnished to Stanford Research Institute by the Ames Research Center. The cylinders were molded by the R. S. Hughes Company of Los Angeles of virgin DuPont TFE 7 white Teflon molding powder. The average specific gravity of the cylinders was 2.177 (135.6 lb/cu ft). Ames Research Center made X-ray photographs of the cylinders at 120° planes and found no inclusions or voids.

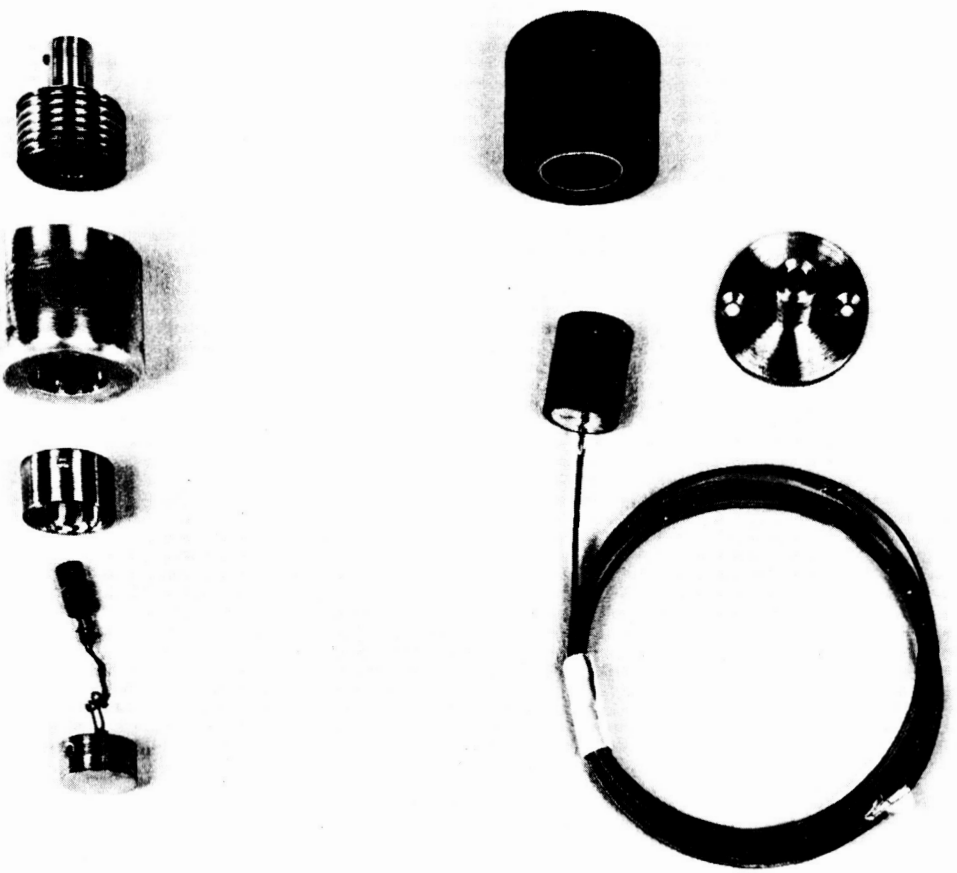

RA-4512-3

FIG. 3 EXPLODED VIEW OF CALORIMETER AND MODEL
A. Transient Calorimeter
B. Phenolic-Nylon Test Specimen

The phenolic-nylon models were machined from 12 cylindrical slabs 8 inches in diameter by 1¾ inch thick. These slabs were molded at the Ames Research Center with proportions of 50 percent phenolic and 50 percent nylon, using techniques developed at Langley Research Center. The phenolic and nylon molding powders were first screened to a -30 mesh and mixed together for 4 hours in a ball mill. The molding powders were then placed in a special mold and held for 10 minutes under 30 inches Hg vacuum. The temperature of the mold was increased gradually to 200°F and held for

4 hours. Pressure was then placed on the mold (700 psi) and the temperature was raised to 300° and held for 45 minutes. The slabs were removed from the mold, cut in half, and inspected for uniformity. Each slab was numbered and each half lettered A or B. The material was then post-cured for 4 hours at 200°F, followed by 16 hours at 300°F. The average specific gravity of all slabs was 1.191 (74.3 lb/cu ft) and the lot-to-lot variation in density was less than 0.5 percent. From 6 to 7 models were machined from each half slab and each model was labeled, designating its origin. For example, Model No. P2B2 was machined from phenolic slab No. 2, B half, Model No. 2.

The shape and dimensions of all of the Teflon and phenolic-nylon models were identical and were as shown in Fig. 1. The model shrouds and cores were weighed (with an analytical balance) before assembly to the nearest 0.001 g and the length and diameter of the cores were measured to the closest 0.001 inch with a micrometer.

The model back surface thermocouples were constructed by resistance-welding 36-gage chromel-alumel wire, and silver-soldering the thermocouple to a 0.5-inch diameter by a 0.020-inch-thick copper disc. The copper discs were then cemented to the back of the core and the core pressed into the shroud. The 36-gage wire gave some breakage problem in transit and should be increased in diameter to 30 gage in future studies.

The model back support plate was constructed of mild steel, and initial test results indicated that the metal back plate was possibly affecting the back surface temperatures. The facilities were therefore requested to provide low thermal conducting model holders that would protect the metal support plate from the jet stream. Future models should use a machinable low thermal conductivity material to support the model.

B. DESCRIPTION OF SRI CALORIMETER AND PITOT PROBE

In addition to the Teflon and phenolic-nylon models, each participating facility was furnished with a standard calorimeter and pitot probe.

The SRI calorimeter was a transient slug type based on a design used at Ames Research Center. The dimensions of this calorimeter were chosen so that in configuration and size it would be similar to the model. The slug diameter was 0.625 inch, which was equal to the core diameter of all samples and the slug was constructed of oxygen-free copper plated with

one-half-mil-thick nickel plate. As shown in Fig. 4, the slug was supported and positioned in the calorimeter shroud with three 0.097-inch-diameter sapphire bearings resting on knife edges. The slug was thereby electrically and thermally insulated from the surrounding copper shroud. The temperature of the slug was sensed by a 36-gage chromel-alumel thermocouple peened into a hole in the base of the slug. Studies at Ames Research

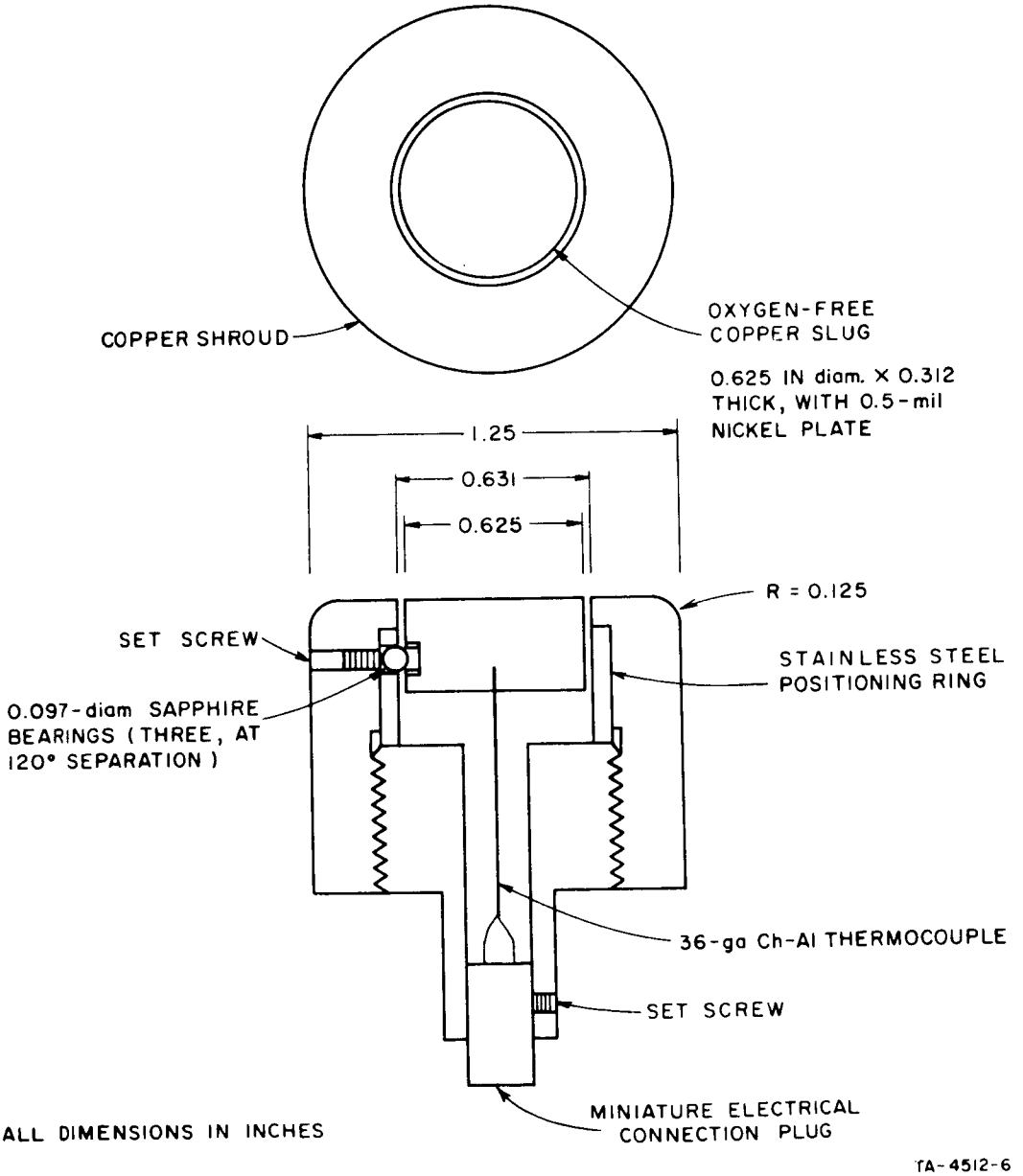

FIG. 4 DESIGN AND DIMENSIONS OF SRI CALORIMETER

Center during this program indicated that these calorimeters had less than one percent heat loss per secood when exposed to the jet stream for the normal 2 to 3 seconds.

The weight of each calorimeter slug was determined to the nearest 0.001 gram and this was stamped on the base of the calorimeter. Each facility was provided with a plot of the specific heat of the copper slug versus temperature. The heat flux was calculated by the facility, with the following relationship.

$$\dot{q}_{\substack{SRI \\ CW}}(\text{in Btu sec}^{-1}\text{ft}^{-2}) = 1.036 \times \text{slug weight (in grams)} \times (C_p)_{Av.T} \times \frac{\Delta T(\text{in } ^\circ F)}{\Delta t(\text{in sec})} \quad (1)$$

Some facilities used a fixed average heat content for the copper slug rather than using the actual average slug temperature. This technique is acceptable if a uniform procedure of a fixed initial temperature and exposure time is followed.

The SRI pitot probe is shown in Fig. 5; it was uncooled copper with a 0.0625 inch pressure tap located in the center of the face. Again the dimensions and configuration were identical to those of the models.

C. QUALITY CONTROL TESTS ON PHENOLIC-NYLON MATERIAL

As reported previously, the twelve lots of phenolic-nylon material were molded at Ames Research Center under carefully standardized procedures and exhibited a very low variation in density. However, to insure further that each lot would exhibit a similar response to a given thermal environment, a series of quality control ablation tests were made at the Ames Research Center, using one model from each of eleven lots of the phenolic-nylon material. The data for these runs are given in Appendix B, Table B-13. The mean values of tunnel conditions and the ablation results for the quality control runs are listed in Table IV, with the percent standard deviation that was experienced for each variable.

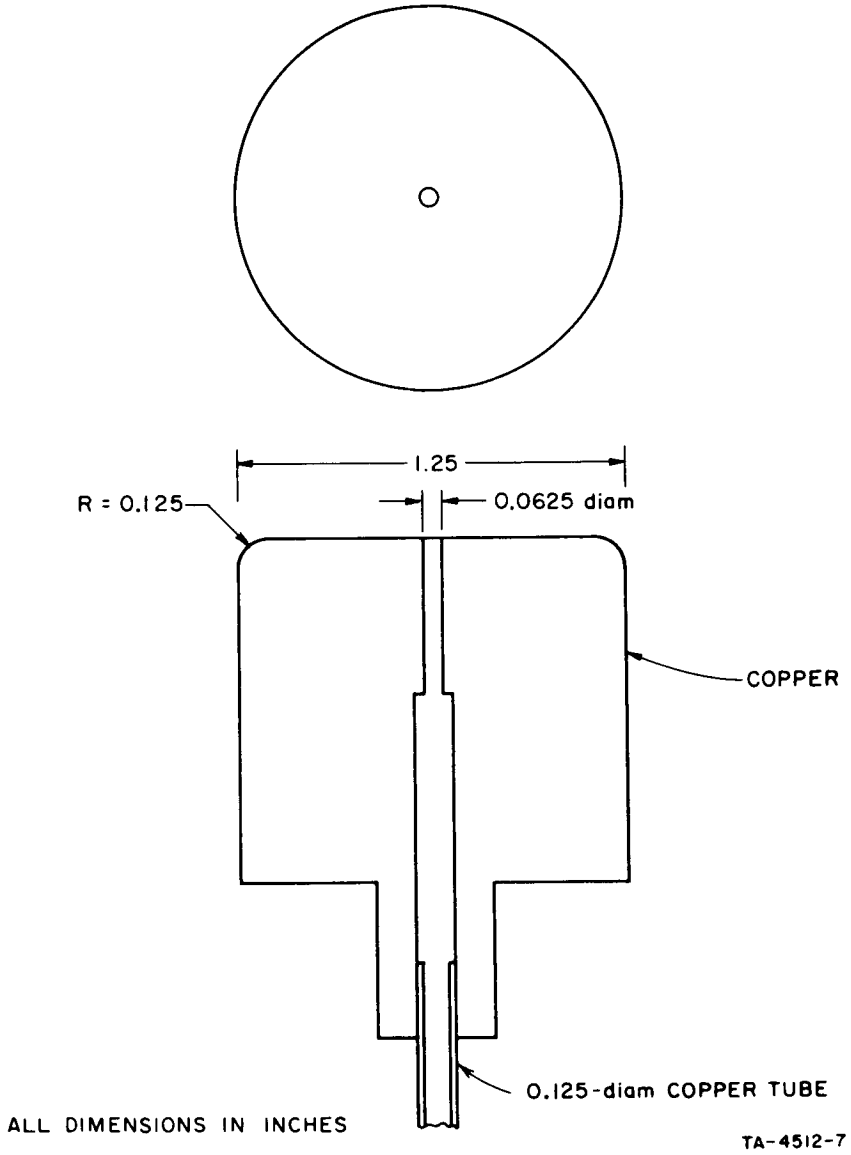

FIG. 5 DESIGN OF SRI PITOT PROBE

Table IV

RESULTS OF PHENOLIC-NYLON QUALITY CONTROL TESTS

VARIABLE	MEAN VALUE	STANDARD DEVIATION
Total Enthalpy h_t (Btu lb^{-1})	5,150	5 %
Heating Rate $\dot{q}_{CW}$ SRI (Btu $sec^{-1} ft^{-2}$)	265	10 %
Model Stagnation Press. P_{t_2} (atm)	0.187	2 %
Plenum Press. P_{t_1} (atm)	0.925	2 %
Run Time t (sec)	40	2 %
Core Weight Loss (lb)	0.00242	2.1%
Core Char Weight (lb)	0.0066	2.6%
Recession (ft)	0.0074	6.6%
Char Thickness (ft)	0.00979	2.5%
Pyrolysis Zone (ft)	0.0141	3.6%

Statistical analysis of the results indicated that the observed deviations could have been caused by the perturbations in heating rate that occurred from run to run. It was therefore concluded that the material response of all eleven lots of phenolic-nylon to a thermal environment was virtually constant.

D. MEASUREMENTS OF THE TESTED MODELS

In order to reduce the variations that might result from the participating facilities each using different measurement techniques, all models were returned to the Institute after completion of the tests for weighing and measuring. The model base plate was removed first and the recession or change in length of the model core determined by averaging several micrometer readings. The model core was then pressed out of the shroud and the copper thermocouple disc removed, including any remaining cement. The weight losses of the shroud and core were determined with an analytical balance.

The char cap was removed from the phenolic-nylon core and the substrate scraped back to the start of the pyrolysis zone. The cores were reweighed and measured to give information leading to the char thickness, weight, and density. The phenolic-nylon cores were then sectioned and the pyrolysis zone determined with a measuring microscope. The pyrolysis

zone was defined as the distance from the scraped char base back to where there was no discernible color change in the virgin plastic. This area was a sharply defined yellow band.

VII EXPERIMENTAL PROCEDURES

At the time that the ablation models and instruments were furnished to each facility, suggestions were made as to the operating conditions for each run.* These suggestions were based on the predicted operating envelopes derived from the data supplied by each participant. This information was gained by correspondence and subsequent visits to each organization. At the same time, descriptive information about the facilities, their measurement techniques, and their operational procedures was obtained. The following sections provide this information.

A. DESCRIPTION OF FACILITY EQUIPMENT AND INSTRUMENTATION

The equipment and instruments that were used by each facility for the round-robin ablation tests are summarized in Appendix A at the end of this report. This information was based partly on the "Facility Evaluation" form completed for each facility at the start of the program and also on data collected at the time the model tests were witnessed. A detailed description of each facility is beyond the scope of this report, and the information contained in Appendix A is intended only to provide a brief summary of pertinent information on equipment and instruments used at each facility during these tests.

B. DESCRIPTION OF MEASUREMENT TECHNIQUES

The data on the ablation models, with their corresponding tunnel conditions, for all participating facilities are presented in Appendix B. Part of the "as received" information from each facility was corrected to provide a uniform set of units, and the data were also rearranged into a standard presentation form. Generally, however, the tables contain all of the data received from each facility, in its original form. That is, if the calibration runs were originally reported separately by the facility, they are also reported separately in Appendix B.

---

* Exposure times for the models were designated as 30 seconds for Teflon and a heat load (heating rate times test duration) of 6,000 Btu ft^{-2} for phenolic-nylon.

A few facilities reported the gross and net power to the arc heater and the resulting efficiencies. These data were omitted because some facilities considered them proprietary and also because they were not particularly pertinent to this study. Although the basic test conditions were set by Stanford Research Institute, an effort was also made not to influence the measurement techniques and methods used by each facility.

The measurements made at SRI on all ablation models tested during the round robin are presented in the last five columns of each table in Appendix B. The weights listed in these tables are for the 0.625-inch-diameter cores with an equivalent area of 0.00213 sq ft. The various mass loss rates for all models were calculated and are presented in Appendix C, along with other calculated values derived from the primary information contained in Appendix B.

Following is a brief description of the various techniques that were used to measure the variables reported in Appendix B.

1. Enthalpy Measurement

In most cases, the participating facilities measured enthalpy with techniques that gave the mean or average enthalpy of the entire jet stream. A few organizations had enthalpy probes, but said they had experienced problems in their use and reported no data. As a result, no comment can be made on the enthalpy profile or "core" flow of the various plasma jet streams during this study.

Eight of the twelve facilities measured the mean total enthalpy by a single technique; two facilities used two methods, one used three, and one used four. The energy or heat balance method was used by ten of the twelve participating facilities to measure average enthalpy; the sonic flow method was used by three, and the pressure rise method, which is also based on sonic flow, was used by two. Three calculated a localized enthalpy from heat transfer data, and one measured average enthalpy with a total calorimetry technique.

All of the above techniques for measuring enthalpy are simple in concept, but can give difficulties in application. The difficulties arise from insufficient precision in measurement or an inability to make an accurate measurement.

a. HEAT BALANCE ENTHALPY

The heat balance method for determining enthalpy was generally considered the most reliable by the participating facilities because of its simplicity in concept. The calculation is made by subtracting the heat losses in the arc generator and nozzle as indicated by the cooling water, from the gross power input and dividing the resulting net power by the mass gas flow. This calculation, however, may require making from five to ten separate readings, each with its attendant error, and the accumulated errors can be considerable. Accurate measurement of the slight temperature rise in the cooling water is probably the greatest source of error. The accuracy of this method is usually best at high power and high gas flow rates, where the measurement errors are at a minimum.

b. SONIC FLOW ENTHALPY

The sonic flow method of measuring enthalpy can give satisfactory results provided that the plenum pressure can be accurately measured. The sonic enthalpy is a power function of the mass gas flow, reservoir pressure, and nozzle throat area that can be approximated by the following relation:[1]

$$h_t = \left(\frac{280 P_{t_1} A^*}{W}\right)^{2.5} \qquad (2)$$

It is usually possible to determine the throat area and mass gas flow to a good degree of accuracy; however, measuring a true static chamber pressure is more difficult. Most arc heaters are vortex or magnetically stabilized and this can result in a dynamic pressure component. In addition, the methods used for secondary gas injection and the location of the pressure taps can result in errors. All errors are further amplified when raised to the necessary power shown in Equation (2). A correction for frozen flow, that increases with increasing enthalpy, must be added to the calculated sonic enthalpy. The method is generally more accurate at lower enthalpies and is not applied to enthalpies in excess of 10,000 Btu/lb.

c. PRESSURE RISE METHOD

The pressure rise method[1] is a special application of the sonic flow method. Briefly, the enthalpy is determined by setting the ratio of the starting pressure (cold gas flow) to the running pressure (hot gas flow). For the condition of constant mass flow through the arc heater, the pressure rise ratio (P_{t_1} cold/P_{t_1} hot) uniquely determines the enthalpy. Constant flow is achieved by metering the gas flow from a high pressure source. The method is subject to some of the measurement problems outlined under the sonic flow method, but is also an excellent method for rapidly calibrating tunnel conditions.

d. COLD WALL HEAT FLUX ENTHALPY METHOD

The enthalpy can also be calculated from the cold wall heat flux, using the relations of Fay-Riddell[3] or Lees.[4] This method has the advantage of measuring the enthalpy in a location similar to that of the exposed model. The method, however, is subject to variations in heat flux resulting from geometry and surface chemistry effects that will be detailed in a later section.

e. TOTAL CALORIMETRY METHOD

The average enthalpy of the stream was measured at General Electric by directing the entire jet from the nozzle through a heat exchanger that removed part of the energy. The heat removed by the exchanger, plus the exiting gas temperature and mass flow rate, was then used to determine the original enthalpy of the gas stream. The enthalpy during the model runs was calculated by General Electric from the pretest calibration runs with the semi-empirical relation:

$$\frac{h}{h_r} = \frac{PE^{0.5} W_r^{0.5}}{P_r E_r^{0.5} W^{0.5}} \qquad (3)$$

where

h = enthalpy

P = plenum pressure

E = input power

W = air mass flow rate

Subscript r refers to pretest calibration runs.

The total calorimetry method is effectively a macroscopic enthalpy probe and can give problems similar to those experienced in determining the nozzle and arc heater losses when using the energy balance method.

2. HEAT FLUX MEASUREMENTS

Two facilities measured the cold wall heat flux primarily with only the SRI calorimeter, whereas the remaining ten facilities measured heat flux with both the SRI calorimeter and a facility calorimeter. The facility calorimeters are described in the instrumentation section of Appendix A, Tables A-1 to A-12, and are summarized in Table V. With two exceptions, these calorimeters were "in-house" designs, with four being transient types and six steady-state types. Six of the facility calorimeters had hemispherical shapes and four were flat-faced. A wide range of shroud diameters and sensing areas was present in the facility calorimeters and six different metals were used for the surface of the sensing area. It should be emphasized that while the heat transfer data in Appendix B have been adjusted as indicated for shroud shape and diameter, no adjustment has been made for different sensing areas and surface materials, and therefore the reported heat fluxes are the integrated averages of the respective sensing areas. No heat flux traverses were made during this study and as a result no comment can be made on the uniformity of the jet streams.

Table V

FACILITY CALORIMETER DESCRIPTION

FACILITY	CALORIMETER DESCRIPTION				
	Calorimeter Type	Shape	Surface Material	Shroud Diam. (in.)	Sensing Diam. (in.)
SRI	Transient	Flat Face	Nickel plate on copper	1.25	0.625
Ames Research Center—NASA	Used SRI Calorimeter Only				
Entry Structures Branch—Langley Research Center—NASA	Transient	Hemisphere	Stainless Steel	1.50	1.50
Applied Materials and Physics Division—Langley Research Center—NASA	Transient	Hemisphere	Stainless Steel	2.00	2.00
Manned Spacecraft Center—NASA	Hy-Cal	Flat Face	Constantan	1.25	0.15
Flight Mechanics Division—Wright-Patterson Air Force Base	Steady State	Hemisphere	Silver	1.00	1.00
AVCO Corporation	Transient	Flat Face	Copper	1.25	0.375
Boeing Company	Steady State	Hemisphere	Platinum plate on copper	2.00	0.74
General Dynamics	Transient	Flat Face	Copper	1.25 1.00 0.75	0.625 0.50 0.375
General Electric Space Technology Center	Used SRI Calorimeter Primarily				
Giannini Scientific Corporation	Steady State	Hemisphere	Copper	0.625	0.625
Martin Company	Steady State	Flat Face	Copper	1.00	0.375
North American Aviation, Incorporated	Steady State	Hemisphere	Copper	0.50	0.50

a. TRANSIENT CALORIMETERS

The transient calorimeters used in this study were generally of the slug type. This type of calorimeter consists of a metal slug of known mass, heat capacity, and area, usually set in an insulating shroud. The calorimeter is exposed to the jet stream for a few seconds and its temperature rise rate is measured. The heat transfer rate is then calculated with the relation:

$$\dot{q}_{cw} = \frac{wC_p\Delta T}{A\Delta t} \qquad (4)$$

where

w = mass of calorimeter slug
C_p = specific heat of slug
A = sensing surface area
$\frac{\Delta T}{\Delta t}$ = slug temperature rise rate

The SRI calorimeter described previously was a slug-type design and this design was also utilized in the General Dynamics and General Electric calorimeters. The Martin calorimeter that was used to calibrate their steady state calorimeter, was a slug-type design.

The two Langley facilities used a thin-walled shell version of the slug calorimeter. The metal hemispherical shell was instrumented with a number of thermocouples to give an indication of the heat flux distribution over the hemisphere. The AVCO calorimeter is a special version of the slug calorimeter where the sensing thermocouple is placed 0.020 inches from the sensing surface of a relatively long slug (1.5 inches) and the temperature-time history is evaluated with a computer program to yield the cold wall heat flux.

b. STEADY STATE CALORIMETERS

The steady-state facility calorimeters used in this study were primarily of the water-cooled, temperature-rise type. The heat flux to a known surface area is extracted with a known water flow and the temperature rise of the water measured. The heat flux is calculated with the relation:

$$\dot{q}_{cw} = \frac{\dot{w} C_p \Delta T}{A} \qquad (5)$$

where

$\dot{w}$ = cooling water flow rate
C_p = specific heat of water
ΔT = temperature rise of the cooling water
A = sensing surface area.

The water-cooled, temperature-rise-design calorimeter was used by Giannini, North American, Boeing, and FMD-WPAFB. When the calorimeter sensing area covered the entire hemisphere, the $\dot{q}_{cw}$ had to be corrected

to give the heat transfer rate $\dot{q}_{CW}$ at the stagnation point. This was usually done by the facility, using the relation $\dot{q}_{CW} = 2.1\ \dot{q}_{AV_{CW}}$.

The Martin steady state calorimeter measured the temperature difference between two axially located thermocouples mounted in a cooled block. This type of calorimeter is sometimes referred to as a heat meter type, heat flux being determined from the temperature difference and the thermal conductivity of the block. Martin calibrated this calorimeter with a transient slug type.

The principle described above is also used in the commercial calorimeter used by Manned Spacecraft Center. This calorimeter was made by Hy-Cal Engineering and is usually referred to as a foil or asymptotic calorimeter. The temperature difference is measured between the center and the cooled periphery of a thin metal disc. The heat flux is determined from the temperature difference and the thermal properties of the thin disc.

3. Pressure Measurements

The uncooled, SRI pitot probe described previously was used by six facilities to measure the model stagnation pressure. Five facilities used in "in-house"-design, water-cooled pitot probes with diameters ranging from 0.5 inches to 1.25 inches. Four facilities had cross checks between the SRI probe and the facility probe. The pressure was measured by a wide variety of methods described under the instrumentation section of Appendix A. In two cases, a manometer was used for the pressure measurement; however, in most cases an electrical pressure transducer with some form of electrical readout was used. In all cases, the model stagnation pressure was measured only on the center line of the stream, and, as a result no comment can be made on the pressure profile of the various jets.

The expansion of the jet in the nozzle was monitored and controlled at most organizations by matching the test chamber pressure to the nozzle exit pressure. This was done to ensure balanced and repeatable flow conditions in the area of the model. The control was usually accomplished by bleeding air into the test chamber or by throttling the vacuum line. At some facilities, the expansion of the jet was controlled by visual observation of the stream.

The pressure measuring instruments were calibrated by the facilities, utilizing various methods depending on their pressure range. Dead weight testers were usually used for high pressures; manometers for moderate pressures; and McLeod gages for low pressures.

4. Front Surface Temperature

The front surface temperature of the ablating models was measured by seven of the participating facilities. In all but one case, the instruments used were monochromatic optical pyrometers that measured the brightness temperature of the model. One facility, General Electric, used a two-color pyrometer. The pyrometers were calibrated by the facilities, using techniques such as viewing a standard light source, or viewing a black body source and comparing the results with those from a standard pyrometer. Allowances were also made in the calibration for optical absorption by intervening viewing ports in the test chamber. Part of the "as-received" data had been corrected to an assumed emissivity and the remainder of data assumed an emissivity of unity. The front surface temperature data in Appendix C all has been corrected to an assumed emissivity of 0.85 for comparison.

5. Gas Flow Rate

Ten of the twelve organizations measured the gas flow rate with some flow-restrictive device such as an orifice plate. Four of these facilities specified that they were using the orifice with critical or choked flow conditions. Five other facilities used standard orifice plates and in one additional case a Venturi section, but did not specify whether they were operating in the sonic region. One group used a variable area or rotometer type of instrument to measure gas flow and one used a turbine meter.

The inlet gas temperature was usually monitored but only in one case was the inlet gas controlled to a fixed temperature.

The flow meters were calibrated by the facilities by such techniques as weighing the gas bottles or by measuring the pressure rise rate in a tank of known volume.

C. METHOD OF OPERATION

The facilities determined the values of the operating variables for the run conditions requested by Stanford Research Institute by making a series of calibration runs, using trial and error methods. As a result, facilities with more experience could usually reach the desired conditions more rapidly than a group with limited experience. The facilities were requested to put primary importance on achieving the desired enthalpy and heating rate and place secondary importance on the model stagnation pressure.

The sequence that was followed by the facility to make the requested measurements of tunnel variables, during both the calibration and model runs, were largely dictated by the facility insertion capability. Facilities that had a four-insertion capability could make all of the requested measurements during a single run and did not require separate calibration runs; tunnels with a single insertion had, of course, to make separate runs for each measurement. Table VI indicates the insertion capability of each group and the groupings of each measurement within single runs.

As is shown in Table VI, several facilities also reported estimated data for the model runs, based on information gained from calibration runs. These data were treated in correlating the results as if they had been determined directly.

Various methods were used to reproduce tunnel conditions from run to run. Most facilities set the gas flow rate, measured the net power, and calculated a run enthalpy. Some groups set the gas flow rate and arc current or total arc power and assumed constant efficiency. A few facilities set the gas flow rate, and adjusted power to give a set plenum pressure; this technique is effectively using the sonic flow method for enthalpy.

Table VI

SEQUENTIAL ORDER OF TEST MEASUREMENT

COMPANY	FACILITY DESCRIPTION TABLE NUMBER	NUMBER OF INSERTIONS	DATA DETERMINED DURING SAME RUN								
			Model $\dot{q}_{SRI}$ $\dot{q}_{FAC}$ P_{t_2}	Model $\dot{q}_{SRI}$ P_{t_2}	Model $\dot{q}_{FAC}$ P_{t_2}	$\dot{q}_{SRI}$ $\dot{q}_{FAC}$ P_{t_2}	Model $\dot{q}_{SRI}$	Model $\dot{q}_{FAC}$	$\dot{q}_{SRI}$ $\dot{q}_{FAC}$	$\dot{q}_{SRI}$ P_{t_2}	$\dot{q}_{FAC}$ P_{t_2}
AVCO Corporation	B-6	4	J								
Boeing Company	B-7	4	J								
General Dynamics	B-8	4	J								
Flight Mechanics Division—Wright-Patterson Air Force Base	B-5	3		M		C					
Giannini Scientific Corporation	B-10	3			M	C					
Martin Company	B-11	3			M	C					
Ames Research Center—NASA	B-1	2		I			M			N	
Applied Materials and Physics Division—Langley Research Center—NASA	B-3	2		I			M		C	C	
Manned Spacecraft Center—NASA	B-4	2						M	C		
North American Aviation, Incorporated	B-12	2	II				M			C	C
Entry Structures Branch—Langley Research Center—NASA	B-2	1	III								
General Electric Space Technology Center	B-9	1		IV							

J Separate calibration runs not required

M Model runs

C Calibration runs

N Calibration run data not reported to SRI

I P_{t_2} estimated and reported for model runs from calibration runs

II P_{t_2} and $\dot{q}_{FAC}$ estimated and reported for model runs from calibration runs

III P_{t_2}, $\dot{q}_{FAC}$ and $\dot{q}_{SRI}$ estimated and reported for model runs from calibration runs

IV P_{t_2} and $\dot{q}_{SRI}$ estimated and reported for model runs from calibration runs

VIII EVALUATION OF TEST CONDITIONS

As was pointed out earlier, the initial intent of the round-robin was to have at least one common operating point, *i.e.*, a heating rate of 150 Btu $ft^{-2}sec^{-1}$ at an enthalpy of 5,000 Btu lb^{-1} for each facility. When it became obvious that this was no longer possible, as was shown by the individual facility envelopes contained in Technical Report No. I, each participant was asked to study a range of the conditions achievable with respect to both enthalpy and arc chamber pressure. The actual test values used are given in Tables B-1 to B-12, which contain the experimental results reported by each participant. These operating conditions have been plotted on the predicted facility envelopes from Technical Report No. I and are shown in Figs. 6 to 15. Where information is available these data

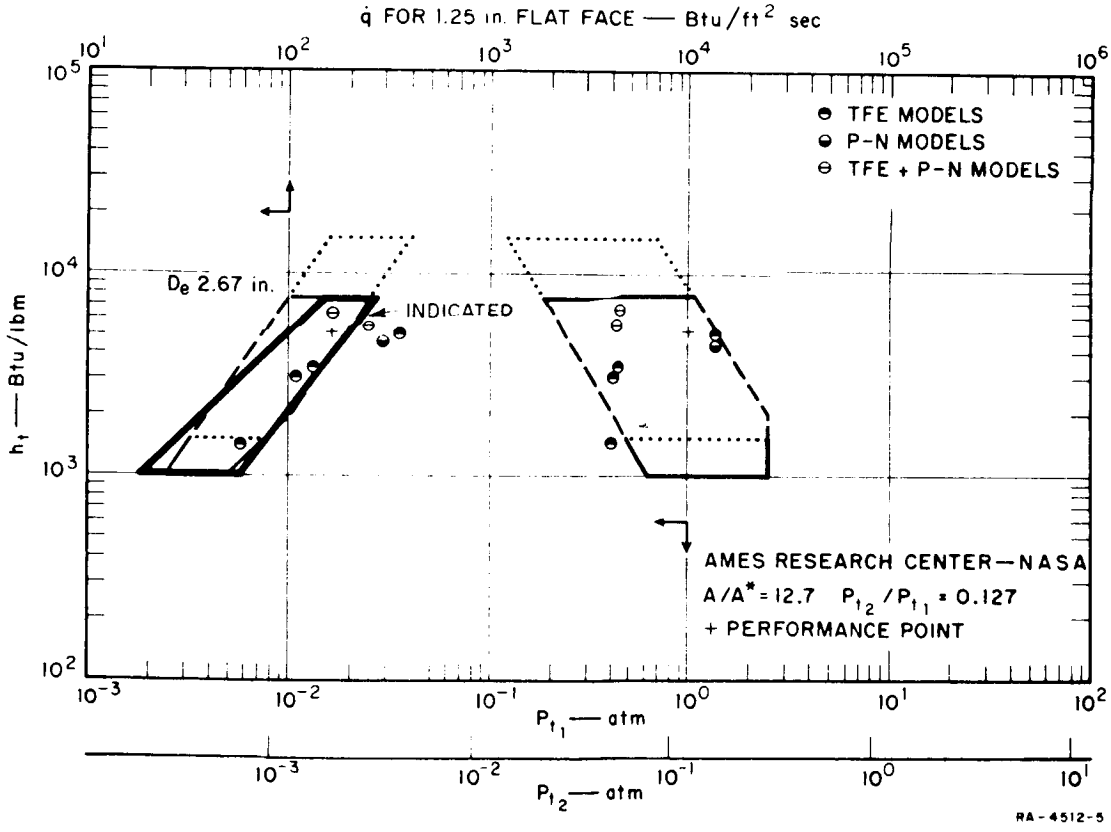

FIG. 6 ESTIMATED AND INDICATED ENVELOPES FOR AMES RESEARCH CENTER, NASA

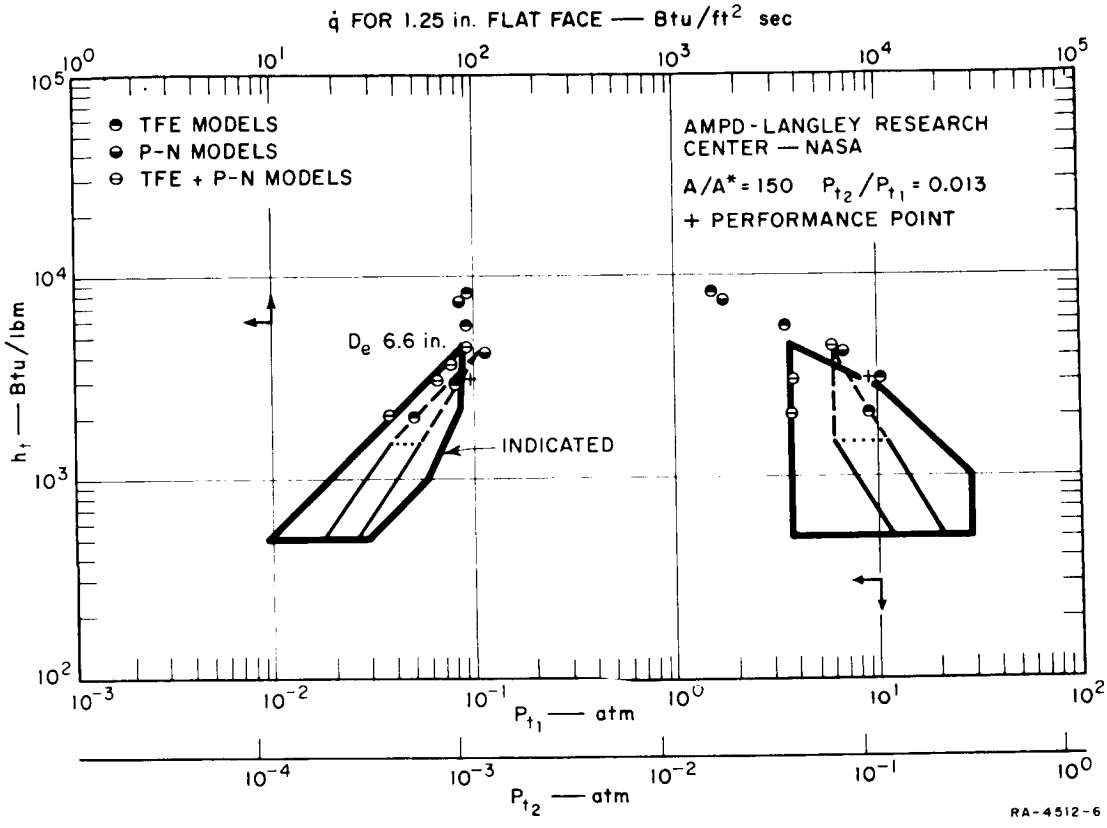

FIG. 7 ESTIMATED AND INDICATED ENVELOPES FOR APPLIED MATERIALS AND PHYSICS DIVISION — LANGLEY RESEARCH CENTER, NASA

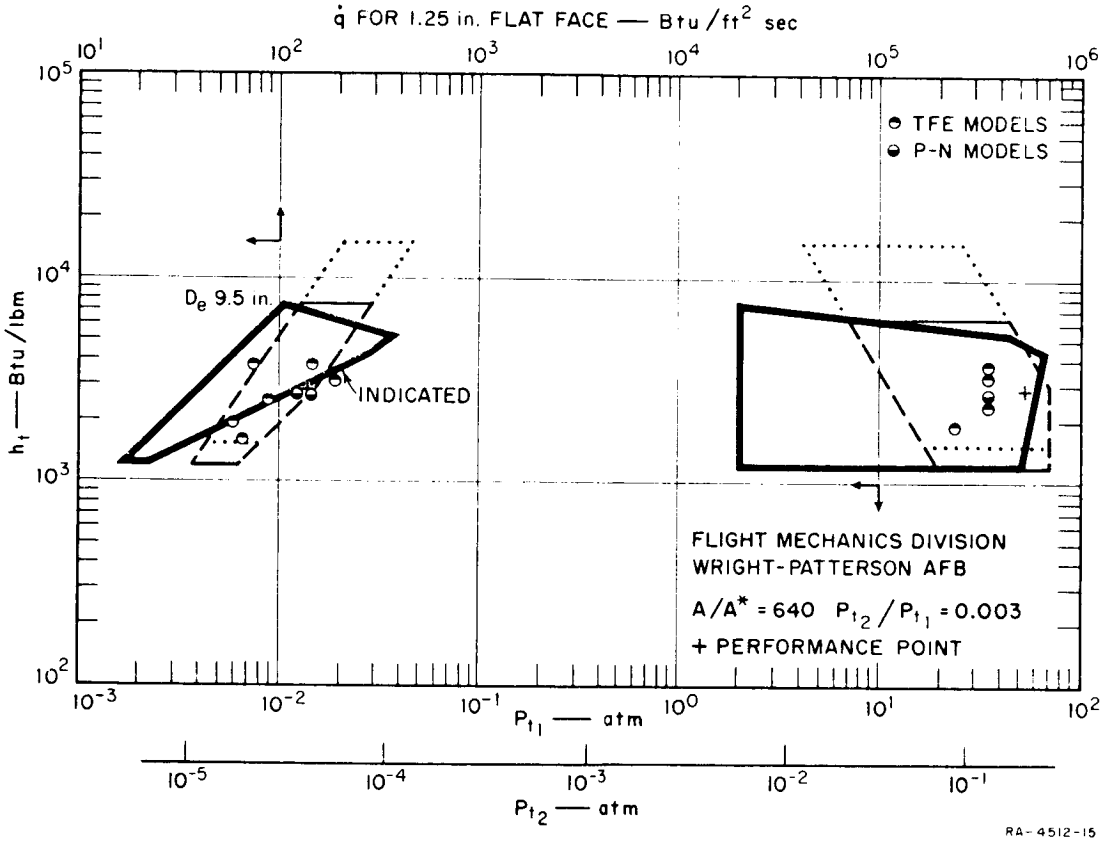

FIG. 8 ESTIMATED AND INDICATED ENVELOPES FOR FLIGHT MECHANICS DIVISION, WRIGHT-PATTERSON AIR FORCE BASE

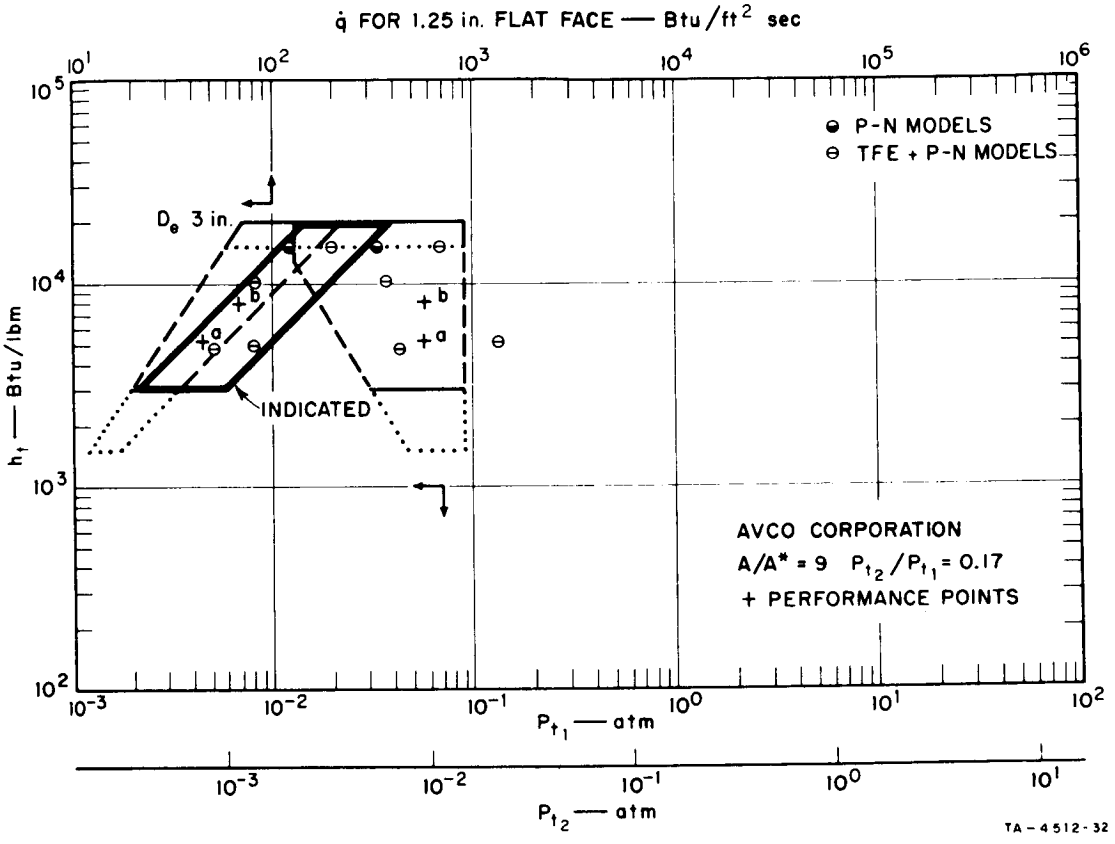

FIG. 9 ESTIMATED AND INDICATED ENVELOPES FOR AVCO CORPORATION

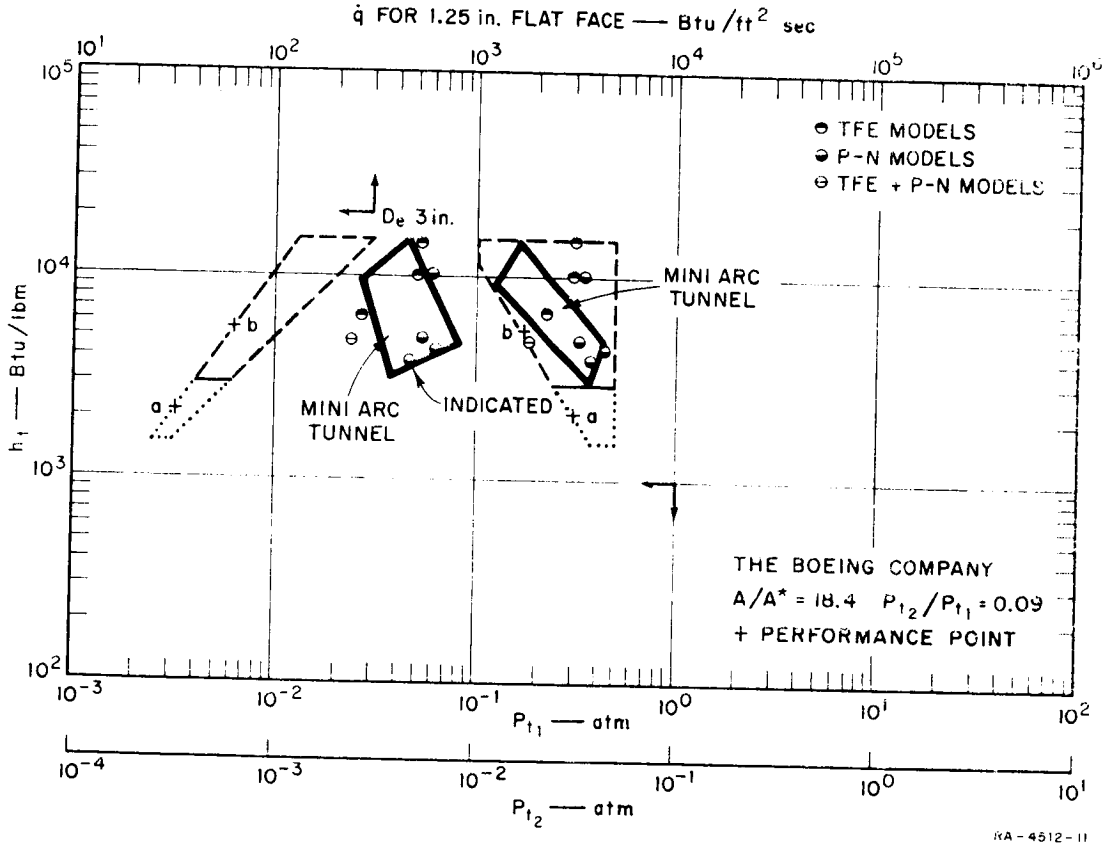

FIG. 10 ESTIMATED AND INDICATED ENVELOPES FOR THE BOEING COMPANY

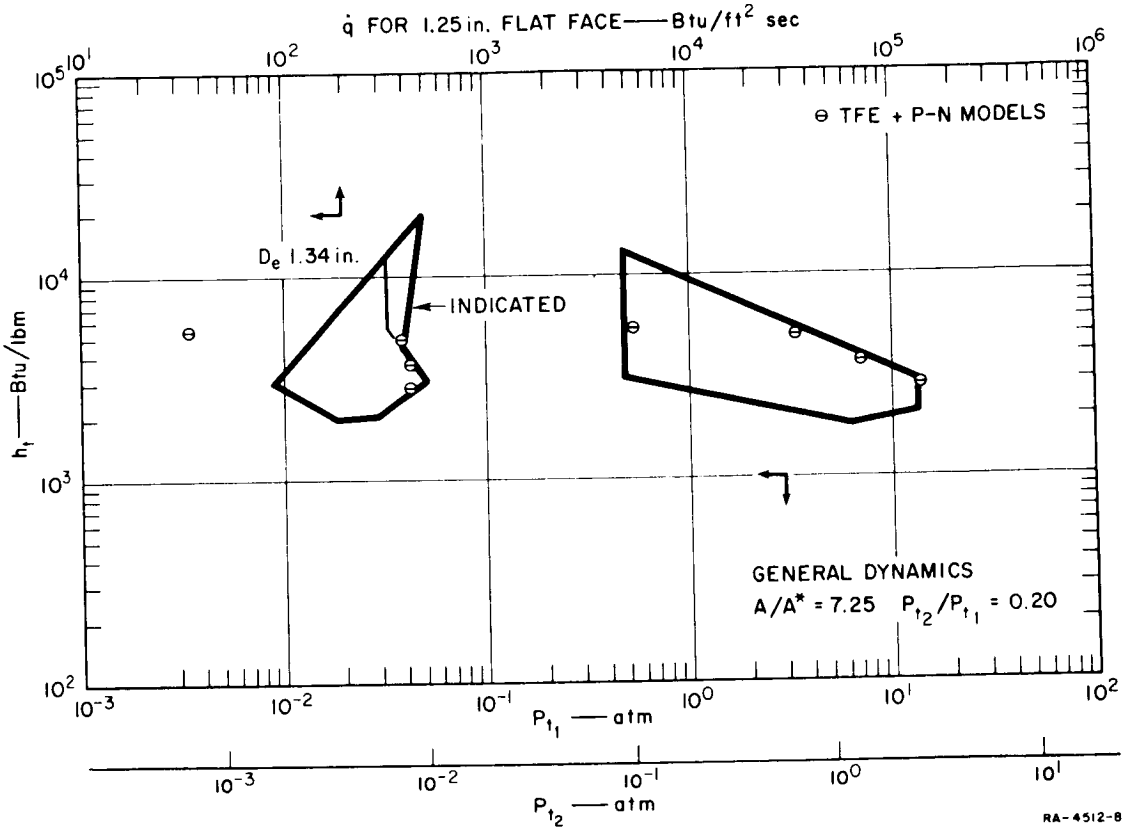

FIG. 11 ESTIMATED AND INDICATED ENVELOPES FOR GENERAL DYNAMICS

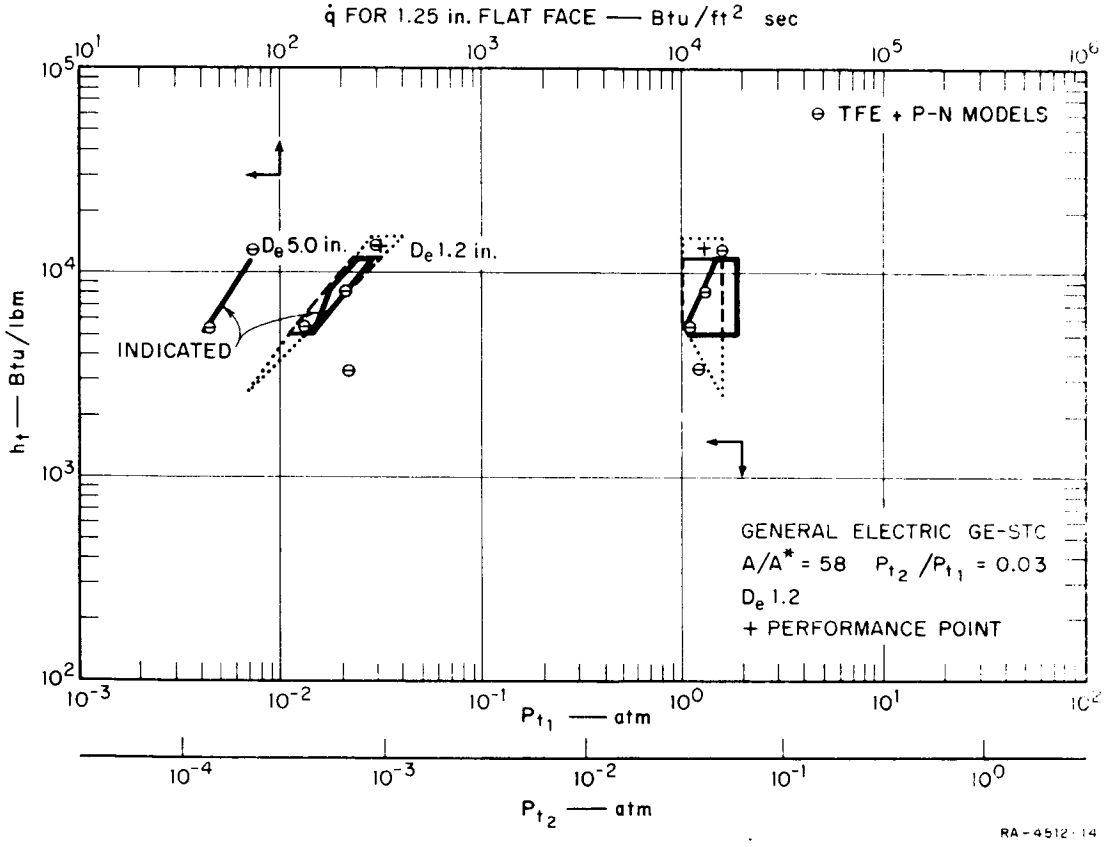

FIG. 12 ESTIMATED AND INDICATED ENVELOPES FOR GENERAL ELECTRIC SPACE TECHNOLOGY CENTER

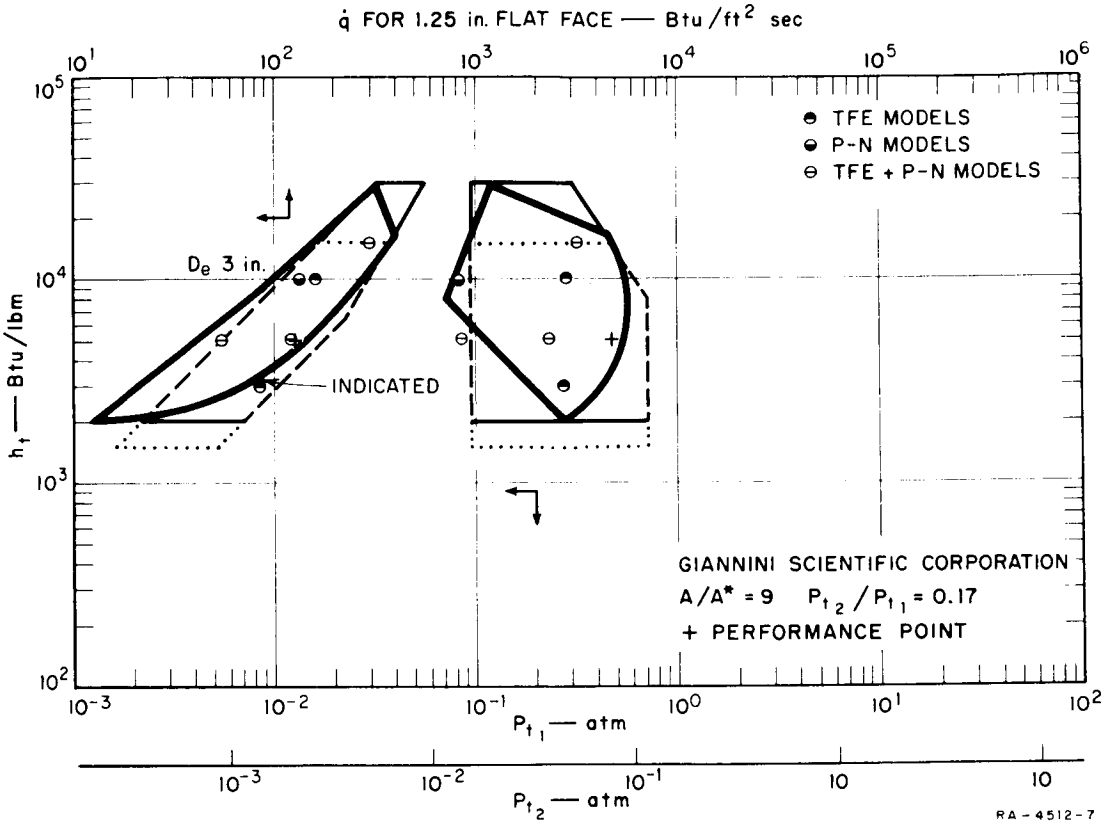

FIG. 13 ESTIMATED AND INDICATED ENVELOPES FOR GIANNINI SCIENTIFIC CORPORATION

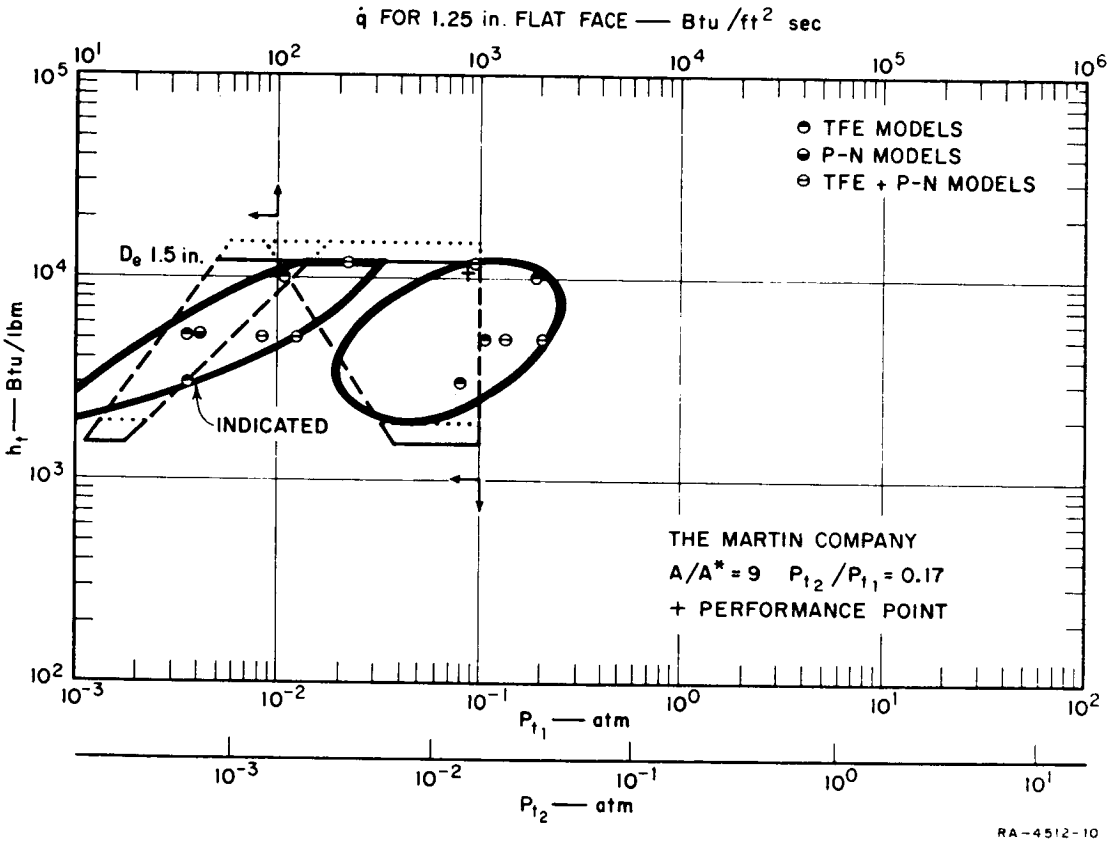

FIG. 14 ESTIMATED AND INDICATED ENVELOPES FOR MARTIN COMPANY

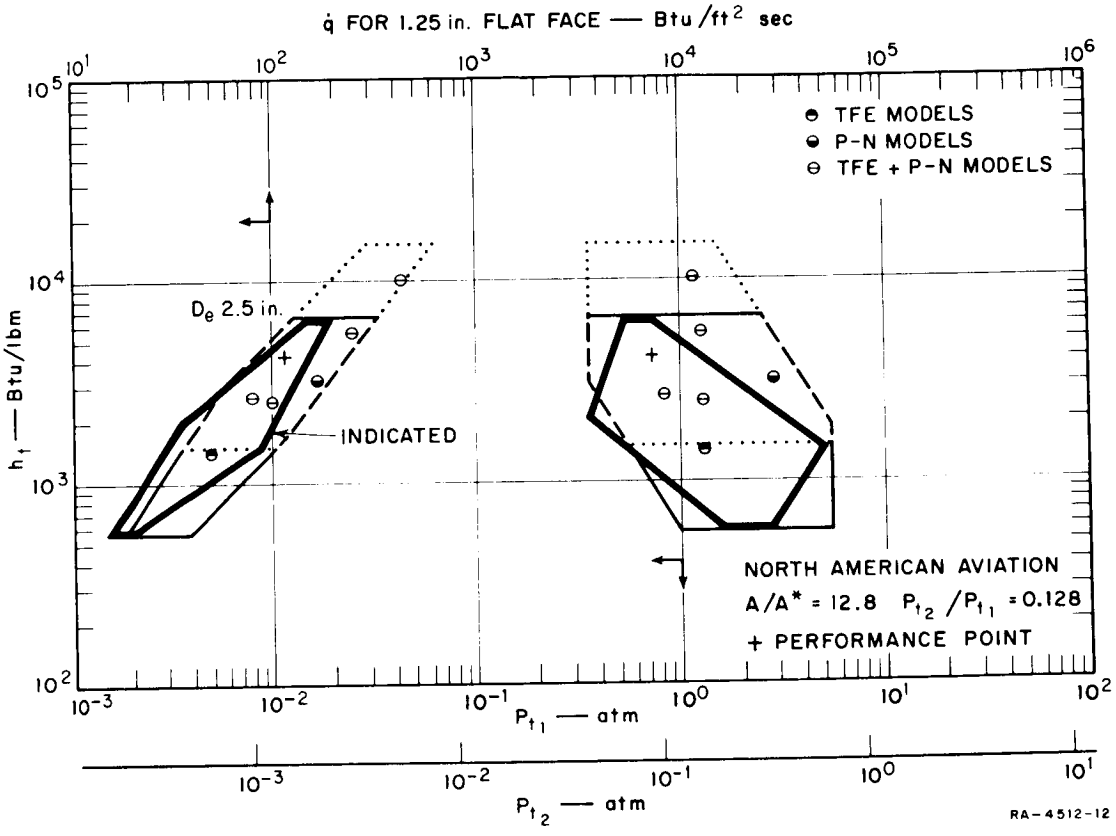

FIG. 15 ESTIMATED AND INDICATED ENVELOPES FOR NORTH AMERICAN AVIATION, INCORPORATED

are plotted on both the heating rate-stagnation pressure and enthalpy-arc chamber pressure envelopes. In the case of General Dynamics, the predicted envelope has been changed from that shown in Technical Report No. I as a result of later arc heater modifications.

The lack of common operating points made it necessary to determine how consistent the experimental results were, both internally at a given facility and externally between facilities. Demonstration of this consistency would then permit cross-correlation of the ablation data reported by each participant. This section describes the comparison of operating data.

A. STAGNATION PRESSURE

Several of the facilities inserted their own pressure probes during the same runs for which the SRI pressure probe was used. In all cases, as shown by Fig. 16, the results compared very closely. The plot is made on a logarithmic scale so that the percentage variation is more readily apparent. The percent standard deviation of the points from the correlation line is calculated as shown in the next paragraph.

For a correlation

$$Y = X \quad ; \tag{6}$$

being evaluated, the square of the residuals, on a logarithmic basis, is

$$(\text{Residual})^2 = (\log Y - \log X)^2 \quad . \tag{7}$$

This will be the same, whether measured parallel to the Y or the X axis. The residual representing the standard deviation will then be

$$\sigma = \pm \log \left(\frac{Y}{X}\right)_{\sigma} = \left[\frac{1}{N-1} \sum_{i=1}^{N} \log^2 \left(\frac{Y_i}{X_i}\right)\right]^{1/2} \quad . \tag{8}$$

Geometrically, this deviation is at a 45° angle to the correlation, since it is parallel to the Y or X axis. The deviation, σ_N, normal to the correlation is therefore

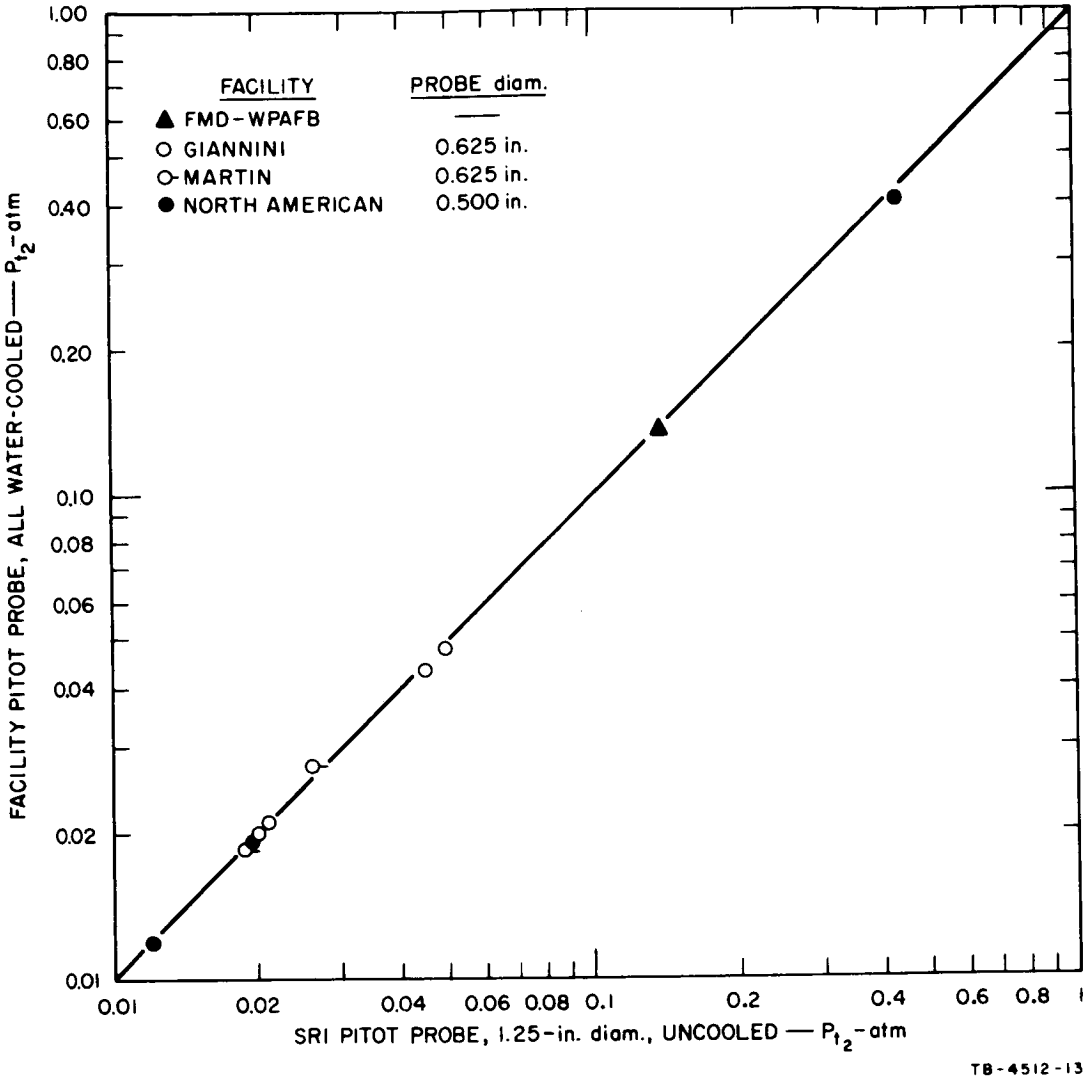

FIG. 16 MODEL STAGNATION PRESSURE MEASURED WITH FACILITY AND SRI PITOT PROBES

$$\sigma_N = \frac{\sigma}{\sqrt{2}} = \pm \log \left[\left(\frac{Y}{X} \right)_{\sigma}^{1/\sqrt{2}} \right] . \qquad (9)$$

Its antilog will be a ratio greater than one, and the reciprocal of this ratio. These ratios can be expressed in the percentage form, with the range shown, as follows:

$$P_\sigma = +100\left[\left(\frac{Y}{X}\right)_\sigma^{1/\sqrt{2}} - 1\right] \quad \text{and} \quad -100\left[1 - \left(\frac{X}{Y}\right)_\sigma^{1/\sqrt{2}}\right] . \qquad (10)$$

The larger of these will be the positive form, although the two will approach each other as the ratio approaches one. The term P_σ will be referred to hereafter as the percent standard deviation.

For the present case, the percent standard deviation between the two stagnation pressure measurements is

$$P_\sigma = +2.6\% \quad \text{and} \quad -2.5\% .$$

From this, it was decided that the type and diameter of the probe, within the limits of those used, was not critical, and that the stagnation pressure measurements could be considered as accurate and comparable.

Certain aspects of the stagnation pressures reported should be realized, however. In the case of five facilities no actual measurements were made during the runs. The values reported for Ames Research Center and AMPD—Langley Research Center were estimated by determining the P_{t_2}/P_{t_1} ratio during calibration runs and then multiplying it by the arc chamber pressure, P_{t_1}, measured during model runs. North American measured stagnation pressures during pre- and post-test calibrations at each operating point and then averaged these values for the comparable model run. General Electric and ESB—Langley Research Center reported values of stagnation pressure measured during a separate run at the same operating condition as the model run. All of these procedures were generally used because of a deficiency of insertion supports.

B. SHOCK PRESSURE RECOVERY RATIO

The flow of air through an arc heater and a nozzle must obey the first law of thermodynamics. When this flow is hypersonic, there generally will be some dissociation and ionization of the air, and the species involved may not reach thermal equilibrium. For a given nozzle, the dissociation, as well as the enthalpy of the air and the arc chamber pressure, affects the shock pressure recovery ratio at the model. Fortunately, this ratio, P_{t_2}/P_{t_1}, is insensitive to these factors compared with the effect of the area ratio of the nozzle. For instance, for a range of enthalpies from 2,000 to 8,000 Btu lb^{-1} and a range of arc chamber

pressure from 10 to 10,000 atmospheres, the shock pressure recovery ratio varies with area ratio as follows:[5,6]

A/A*	3.5	35	350	3,500
P_{t_2}/P_{t_1}	0.40-0.50	0.045-0.055	0.0050-0.0055	0.00055-0.00060
Mach No.	2.5	4.0	5.5	8.2

The P_{t_2}/P_{t_1} ratio tends to spread somewhat as the arc chamber pressure decreases. As a matter of interest, the mach number for each of the area ratios is also given above for $h_t = 5,000$ and $P_{t_1} = 7$.

A comparison of the actual value of P_{t_2}/P_{t_1} with the predicted value can thus be used to determine either whether the arc chamber pressure has been correctly measured or whether the plasma stream is expanding properly through the nozzle. This comparison is made in Appendix C, where it can be seen that most of the facilities have ratios reasonably close to the values expected.

Ames Research Center had slightly high values, but the stagnation pressure was not actually measured during the runs. The low values at General Dynamics were not of concern, since the use of nitrogen in the plasma arc precluded their inclusion in the correlations involving these pressures. Somewhat high values were reported at General Electric and FMD--Wright-Patterson; these were associated with very high nozzle expansion ratios. Some of the Martin pressure ratios were high by as much as a factor of three. This was not unexpected, since Martin representatives made particular references during the runs to recurring difficulties in measuring arc chamber pressures.

C. STAGNATION POINT HEATING RATE

As was pointed out earlier, the heating rate data were measured with the SRI colorimeter and a variety of facility calorimeters. The effect of the instrument design must be considered before comparing the results.

1. Effect of Calorimeter Design

The main aspects in which the various calorimeters differed were: shape, diameter, size of sensing area, and surface material of the sensing area. The effects of each of these are discussed in the following sections.

a. SHAPE AND DIAMETER

For a given set of tunnel conditions, the shape and diameter of a calorimeter determine the velocity gradients over the surface, and thereby the heat transfer to the surface. It is generally accepted that under supersonic conditions the heat flux to different-sized calorimeters with the same shape will vary inversely with the square root of the calorimeter radius or diameter. Thus, the heat flux will decrease with increasing calorimeter size according to the following relation.

$$\frac{\dot{q}_1}{\dot{q}_2} = \left(\frac{R_2}{R_1}\right)^{0.5} = \left(\frac{D_2}{D_1}\right)^{0.5} \tag{11}$$

The above relation was used to correct any facility flat-faced calorimeter data when there was a difference in diameter compared with the SRI calorimeter.

The participating facilities were in general but not exact agreement on how calorimeter shape affects the heat transfer measurement. The theoretical relations describing heat transfer are usually based on heat flux to a hemispherical shape. Heat transfer to other shapes is thus expressed as some factor times the heat flux to an equal-diameter hemispherical shape. An informal survey made of some of the participating facilities indicated that they used the following factor for shape correction from hemisphere to flat-face: five facilities used 0.55; one each used 0.50, 0.56, 0.63, and 0.67.

The heat flux data from the five facilities that used hemispherical calorimeters and that had equivalent data for the SRI flat-faced calorimeter were analyzed and found to follow the relation:

$$\dot{q}_{\text{Flat face}} = 0.54 q_{\text{Hemisphere}} \tag{12}$$

This was based on the average of 30 data sets.

Since this factor agreed well with the results reported in Ref. (7), it was decided to adjust all facility hemispherical calorimeter data where necessary to a flat-face value with the 0.55 factor. The use of this factor is the equivalent of saying that the radii will follow the relation:

$$R_{Effective} = R_{Hemisphere} = 3.3R_{Flat\ face} \quad (13)$$

b. SENSING AREA

All arc jets have some degree of nonuniformity or enthalpy profile across the jet. This is largely the result of heat losses to the walls of the arc heater and nozzle, and it causes a condition sometimes referred to as "peaking" or "coring." Models or calorimeters placed on the center line of a cored stream will indicate a higher heat flux resulting from a higher gas enthalpy than is indicated by the average jet enthalpy. The SRI calorimeter was designed with a slug diameter equal to the model core diameter so that the two surface areas would be sensing the same integrated heat flux.

If coring is present, a calorimeter with a large sensing area will usually indicate a lower heat flux than a calorimeter with a small sensing area. This type of phenomenon occurred during the round-robin testing at General Electric. This facility initially experienced considerable trouble with a loose connection in the SRI calorimeter. After this was repaired, it was found that the 0.25-in.-diameter General Electric slug calorimeter indicated a heat flux 1.35 times greater than the heat flux indicated by the 0.625-in.-diameter SRI calorimeter. A heat flux traverse of the stream was made by moving the location of the slug and varying its diameter. The results of this study are shown in Fig. 17. The coring problem in this case was probably aggravated by the model diameter's being nearly equal to the nozzle exit diameter, causing stream blockage.

A similar pattern was present in the Boeing jet, as can be seen in Fig. 18. This plot was furnished by the facility and was based on a previous study. This facility has since improved its apparatus and has achieved a much flatter profile.

Since no heat flux , stagnation pressure, or enthalpy profiles were developed during this study for other facilities, no comment can be made on the uniformity of their jets.

A problem was encountered at AVCO, in that the SRI calorimeter gave a very noisy signal. The problem was never completely solved, and could account in part for the AVCO calorimeter's reading from 20% lower to 60% higher than the SRI calorimeter. The low values were for SRI

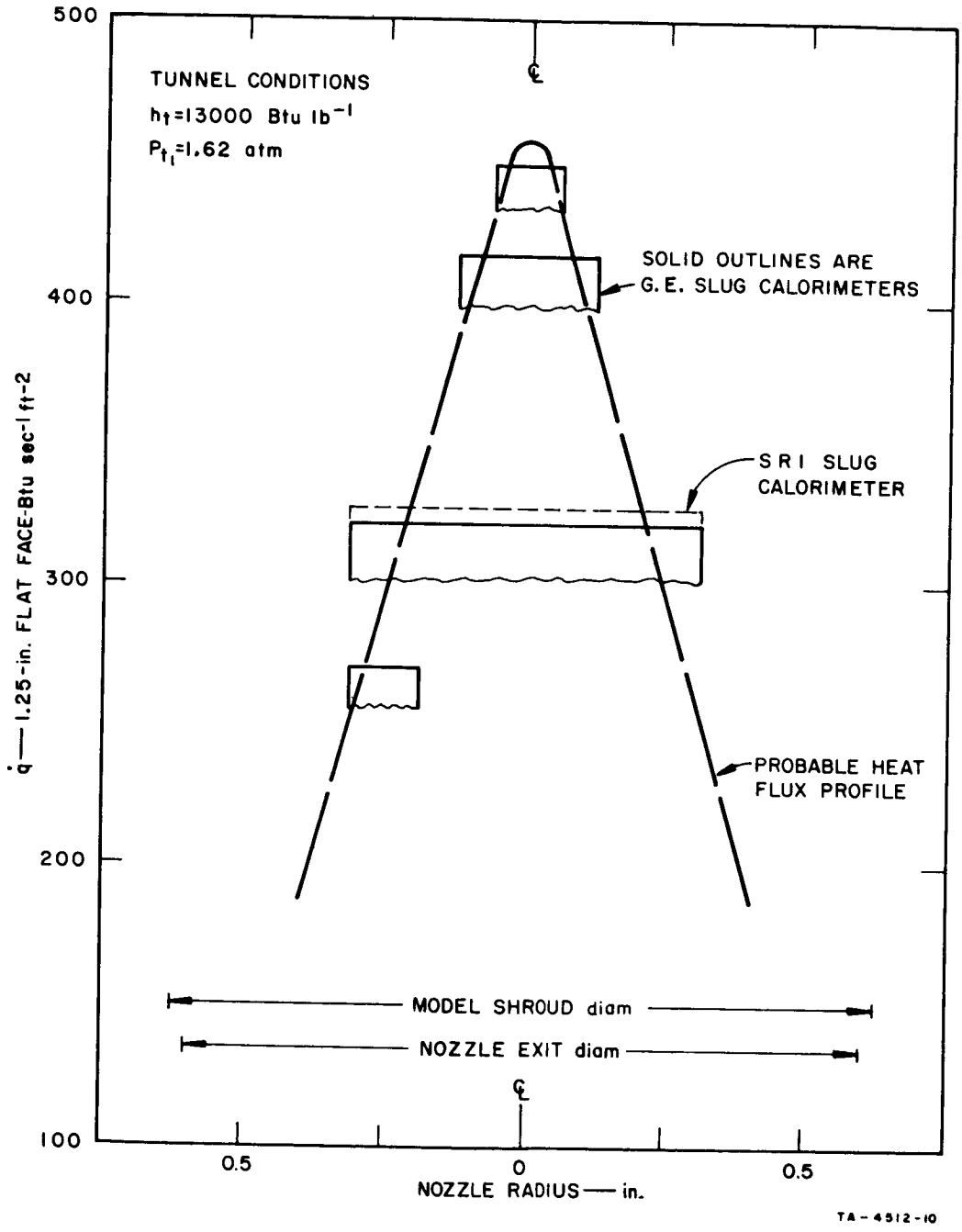

FIG. 17 GENERAL ELECTRIC HEATING RATE PROFILE

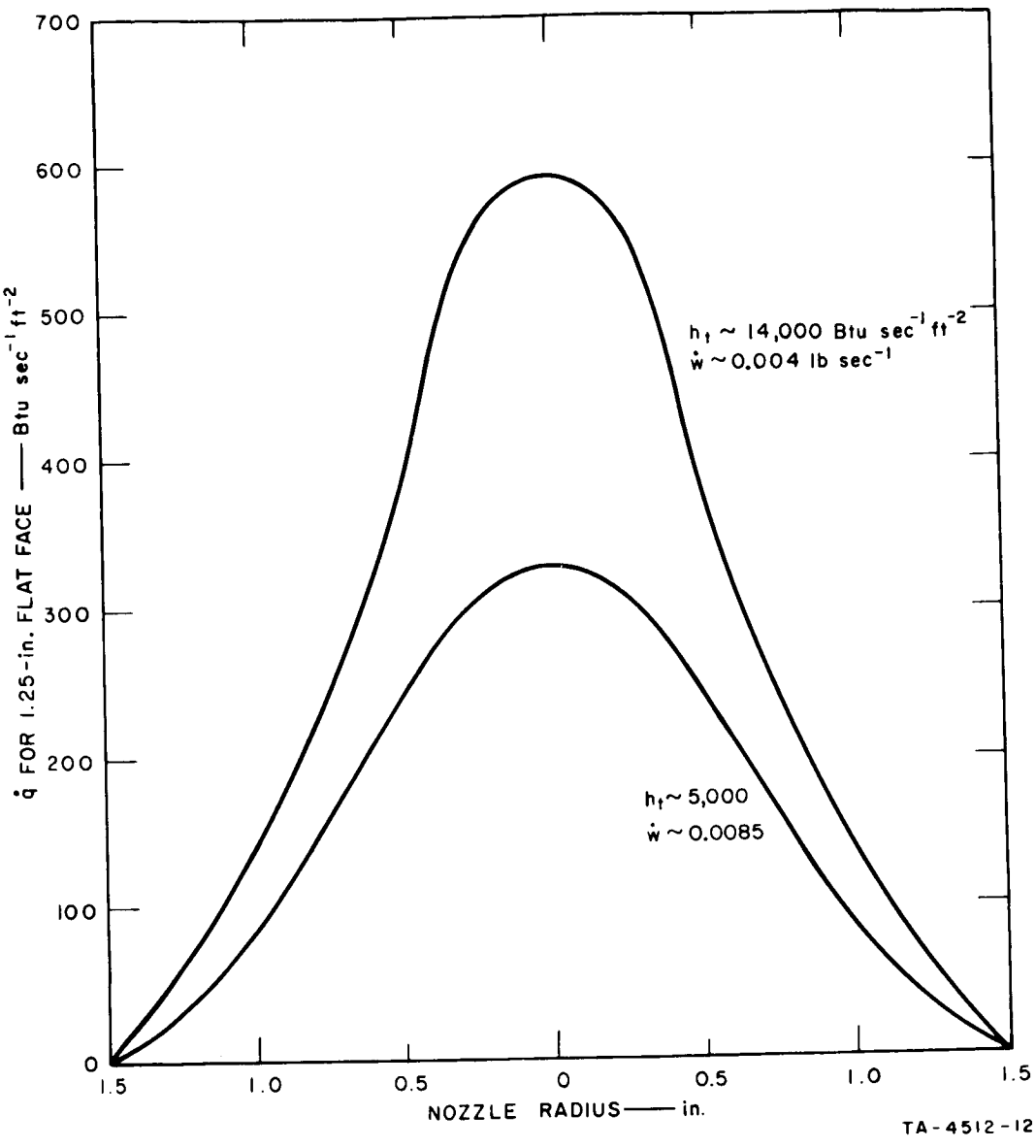

FIG. 18 THE BOEING COMPANY HEATING RATE PROFILE

calorimeter readings of 50 Btu $ft^{-2}sec^{-1}$; above 70, the AVCO calorimeter read from 20-50% high, increasing to 40-60% high at SRI calorimeter readings of 200 Btu $ft^{-2}sec^{-1}$. There were, however, differences in the two calorimeters such as sensing area, surface material and basic design that might account for the discrepancies in measured heat flux.

c. SURFACE MATERIAL

The plasma arc generator has been the most versatile test device developed for simulating free flight conditions. Such flight variables as enthalpy and impact pressure can be closely reproduced in an arc generator tunnel. The primary difference between arc tunnel testing and free flight conditions is the result of possible nonequilibrium conditions in the arc jet.

In free flight, the air preceding the vehicle shock wave is initially at rest and is thought to be in equilibrium up to about sixty miles altitude. The gases behind the shock wave are also thought to be in equilibrium, except possibly in the re-expansion area around the vehicle. By contrast, in plasma tunnel testing, the gas preceding the model shock wave has been heated to a very high temperature, and when expanded through a supersonic nozzle with a large expansion ratio, it probably is is not in equulibrium.

Recombination of the disassociated gas molecules behind the model shock wave may be promoted by the catalytic activity of the surface and will release energy to the surface.[8] Although the mechanism of recombination is not fully understood, it is known to be a function of such variables as: the atomic concentration in the boundary layer; the temperature of the gas and surface; and the catalytic activity of the surface material.

FMD—Wright-Patterson conducted a study to determine the effects of calorimeter surface material on the heat transfer measurement. The nickel plate was removed from the slug surface of three SRI calorimeters and replaced with silver, copper, and silicon monoxide surfaces. The calorimeters were chemically cleaned before each exposure. The data from this study are included in Table B-5, Appendix B, and are presented in Fig. 19.

If the heat transfer results in Table B-5 are arranged by material and the arbitrary value of 1.0 is allotted to the nickel, the silver surface would indicate a heat flux value 1.21 times higher, the copper 1.03, and the silicon monoxide 0.74. These results agree quite well with the catalytic activities indicated in Ref. 8.

The effect of surface materials on the measured heat transfer has been investigated further by FMD—Wright-Patterson in studies not

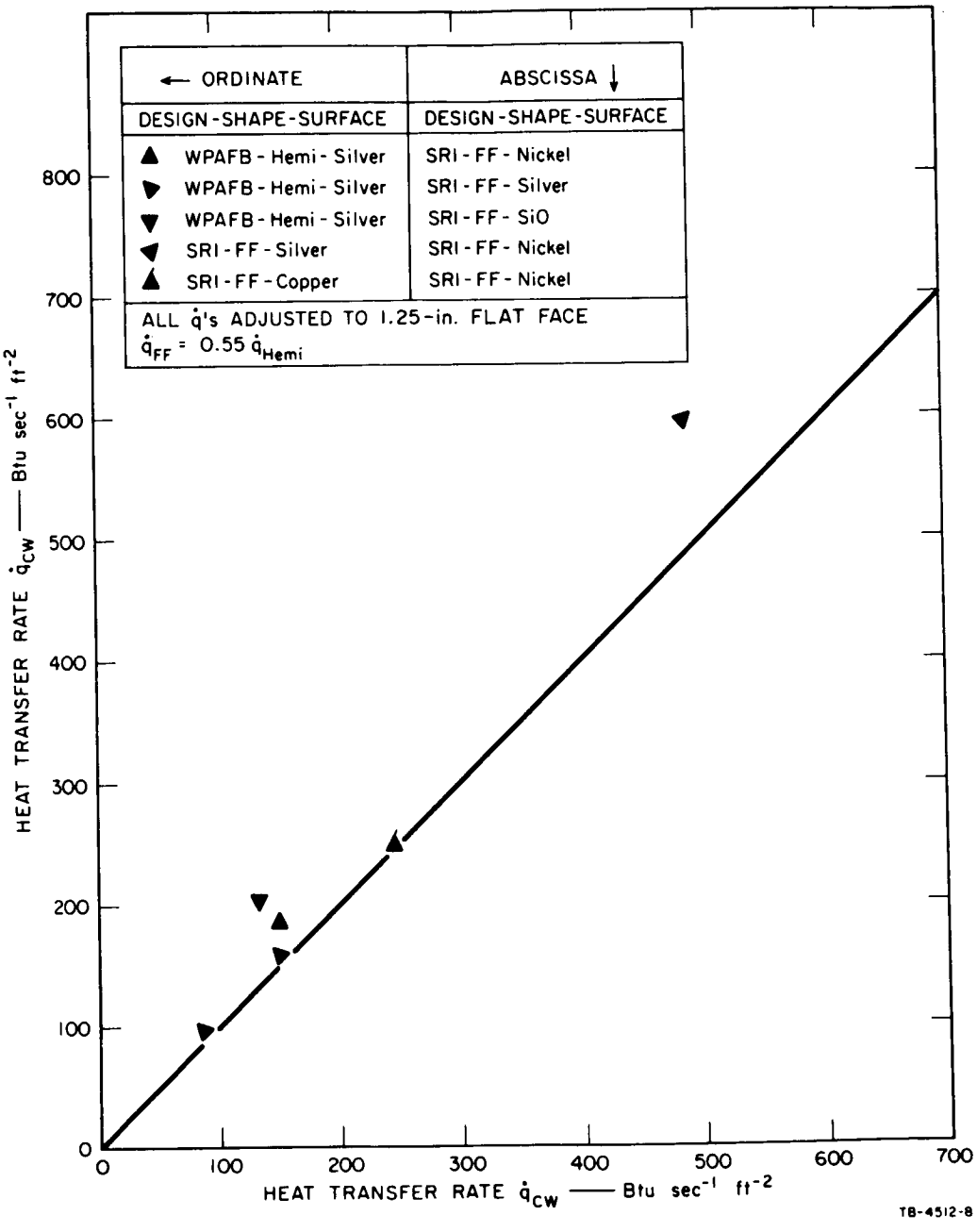

FIG. 19 EFFECT OF CALORIMETER SURFACE MATERIAL ON THE HEAT TRANSFER MEASUREMENT

included in this report. The study conducted during the round-robin program was not extensive, but did substantiate the previous studies; *i.e.*, for this facility and for the indicated operating conditions, the measured heat flux was dependent on the calorimeter surface material. For the current program, however, comparison of results using calorimeters with copper or nickel containing surfaces should not affect the results appreciably.

2. Comparison of Results

As was pointed out earlier, a variety of calorimeters was used by the various facilities for determining stagnation point heating rate. The effect of shape and shroud diameter were discussed above, and methods for correcting these rates to a common basis were given. Using these relations, the facility heating rates reported in Appendix B have been adjusted to a 1.25-in., flat-face calorimeter and are tabulated in Appendix C.

A plot of the adjusted facility values against the SRI calorimeter values, which are already based on a 1.25-in., flat-face calorimeter, are shown in Fig. 20. For the case at hand, the correlation being tested is

$$\dot{q}_{FAC}^{ADJ} = \dot{q}_{SRI} \quad , \tag{14}$$

so, in accordance with Eq. (6),

$$Y = \dot{q}_{FAC}^{ADJ} \tag{15}$$

$$X = \dot{q}_{SRI} \quad . \tag{16}$$

Then, in Fig. 20, which represents both model and calibration runs, the value of the percent standard deviation, P_σ, for this correlation is +16 and −14 percent.

Two facilities, Ames and General Electric, are not represented on the plot, since no facility calorimeter was compared with the SRI-furnished instrument during the experiments. Also, as is shown in Table VI, comparisons for two of the facilities (North American and ESB—Langley) depended on data not obtained during the same run. If these last two are left out of the correlation, the percent standard deviation becomes 18 percent.

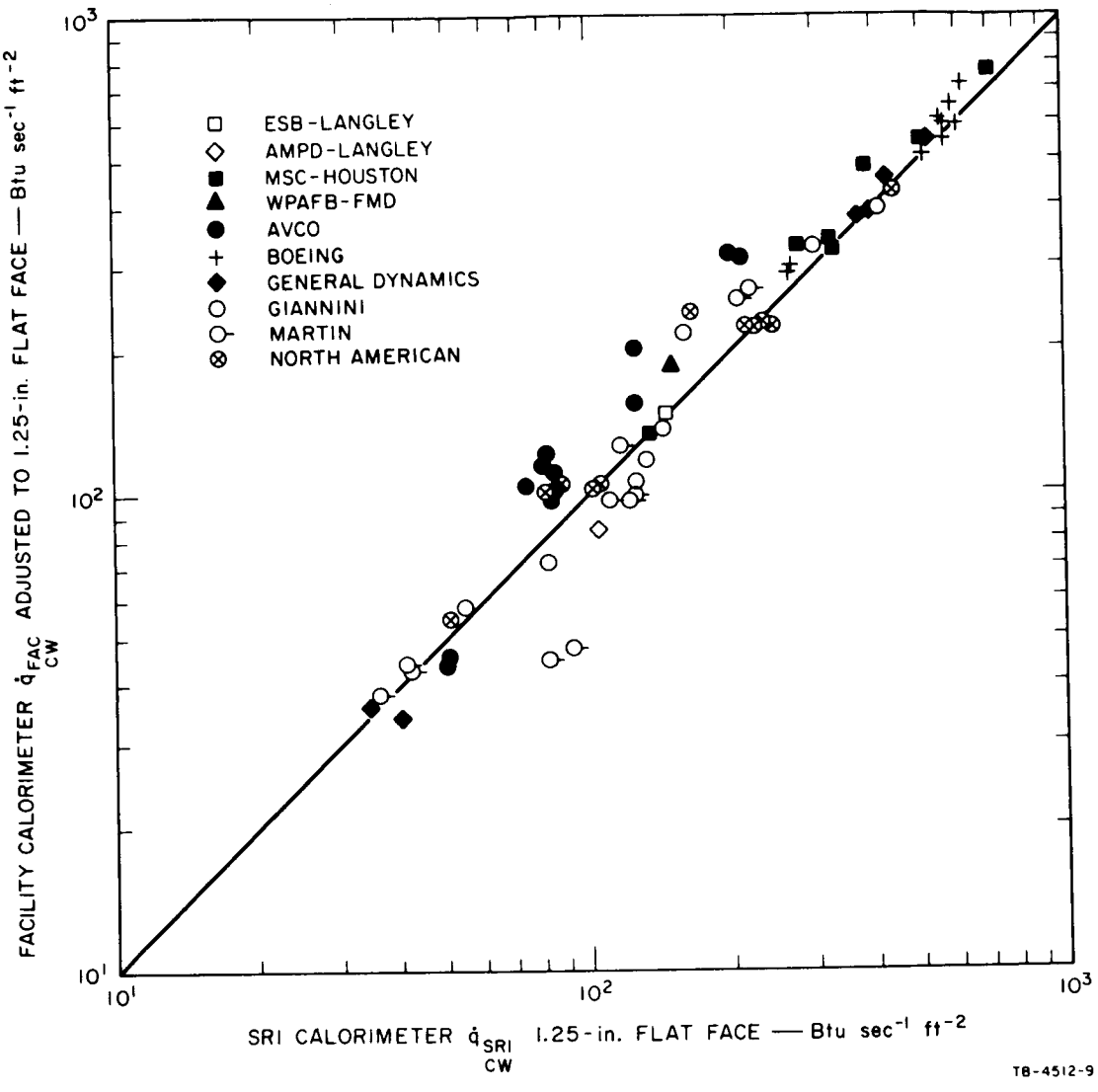

FIG. 20 COMPARISON OF FACILITY CALORIMETER WITH SRI CALORIMETER

Careful inspection of Fig. 20 indicates that more data lie above the correlation line than below, suggesting generally higher readings on the facility calorimeters. This is not surprising, since many of them had smaller sensing diameters than the SRI calorimeter.

These results seem to indicate that consistent data can be obtained by use of a standard calorimeter.

D. PREDICTION OF STAGNATION POINT ENTHALPIES

Prediction of the stagnation point enthalpy can be calculated directly from the over-all heat flux and stagnation pressure, using the relation of Fay-Riddell,[3] or by the sonic flow method proposed by Winovich,[1] which utilizes the mass gas flow, reservoir pressure, and nozzle throat area. Since much of this information was available in the majority of experimental runs, it was felt advisable to determine how well these calculated values for the enthalpy would compare with the value measured by the heat balance technique. The following sections make this comparison.

1. From SRI Heat Flux

The values for the enthalpy difference calculated from the stagnation pressure and cold wall heating rate for the SRI calorimeter are tabulated in Appendix C. These were obtained by using the following formula derived from the Fay-Riddell relation.

$$\Delta h^{calc}_{\substack{SRI \\ CW}} = 24 \dot{q}_{\substack{SRI \\ CW}} (R_{eff})^{1/2} (P_{t_2})^{-1/2} \quad . \tag{17}$$

This approximate formula is based upon air as the test gas and assumes an invarient Lewis No. = 1 and a Prandtl No. = 0.72. The value of R_{eff} was taken as 0.172 ft, based upon the 1.25-in.-diameter flat-faced configuration of the calorimeter and the 0.55 proportionality between hemispherical and flat-face shapes.

The calculated values shown in Appendix C are plotted in Fig. 21 against the enthalpy difference measured by the facilities, primarily using energy balance techniques. The only organizations not represented are Ames, which reported an enthalpy determined by the pressure rise method, and the Manned Spacecraft Center, whose subsonic plasma arc heater cannot be correlated through a Fay-Riddell type of relation.

The effect of "coring" at Boeing and General Electric is immediately apparent in the high calculated enthalpy values for a number of those runs. As would be expected, the calorimeter sensed a peak value of enthalpy rather than the average over the entire plasma stream, which is obtained by the energy balance measurement technique. Values were not calculated for General Dynamics, since the measurements were made on a

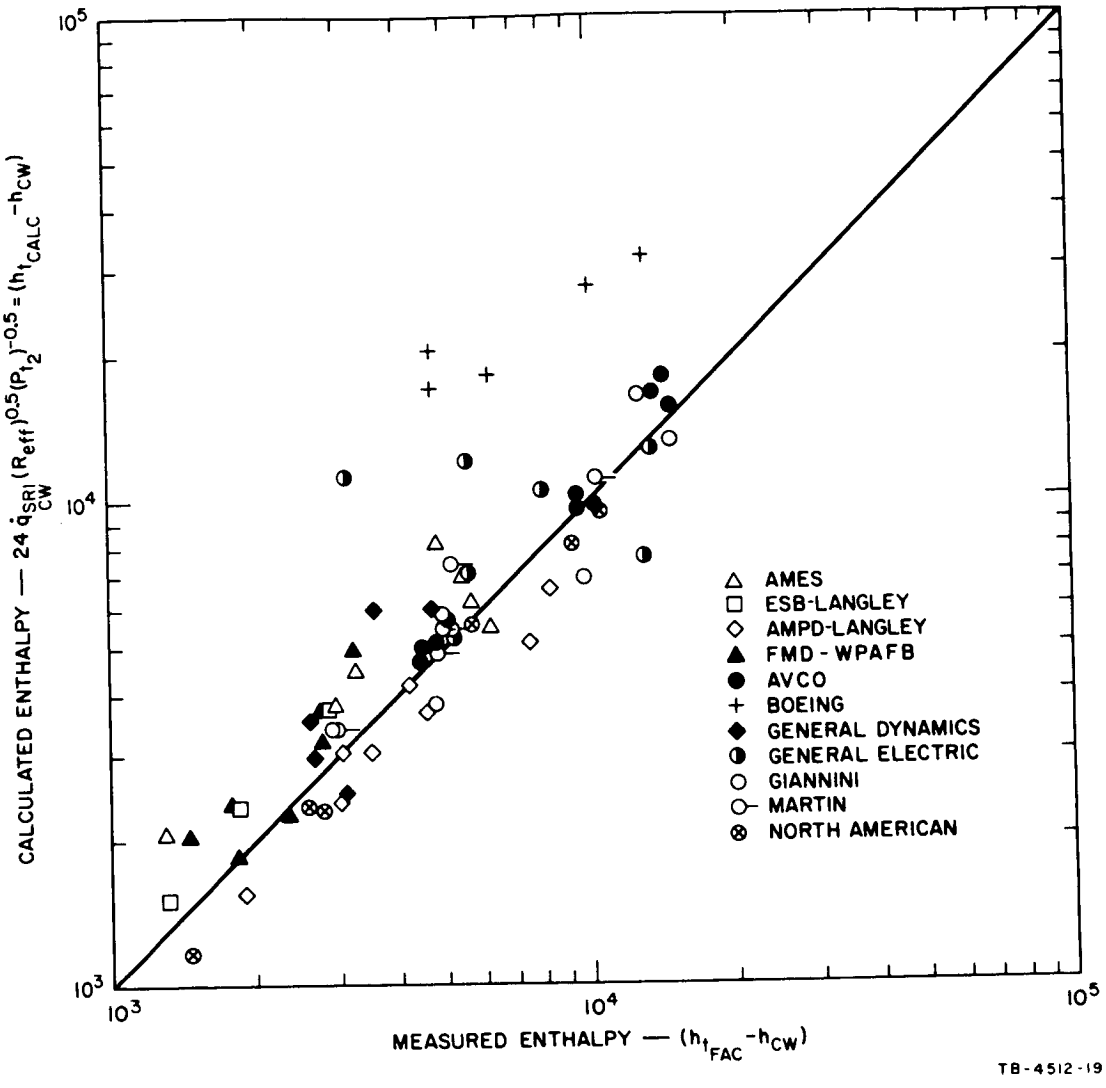

FIG. 21 ENTHALPY CALCULATED FROM HEATING RATE VERSUS ENTHALPY MEASURED BY THE FACILITY

different working fluid, namely nitrogen, and this affects the proportionality factor in the Fay-Riddell relation. It should also be pointed out that, as shown in Table VI, part of the data being correlated was not measured during the same run, for five of the facilities, namely Ames, AMPD—Langley, General Electric, North American, and ESB—Langley.

The correlation being tested in Fig. 21 is:

$$\Delta h_{FAC}^{meas} = \Delta h_{\substack{SRI \\ CW}}^{calc} \qquad (18)$$

so, from Eq. (6)

$$Y = \Delta h_{FAC}^{meas} \tag{19}$$

$$X = \Delta h_{CW}^{calc} = 24\dot{q}_{CW}^{SRI}(R_{eff})^{1/2}(P_{t_2})^{-1/2} \quad . \tag{20}$$

The percent standard deviation for this plot is, as might be expected, rather high, namely, 46%. Elimination of the Boeing and General Electric data, because of plasma "coring," from the calculation of the percent standard deviation, reduced P_σ to 18%. Further elimination of the data for facilities where they were not measured during the same run only changes the deviation to 19%.

2. From Facility Heat Flux

The enthalpy difference can also be calculated from the facility calorimeter heating rate and stagnation pressure. Where this information was available, the calculated values are shown in Appendix C. If these data were plotted in the same manner as the preceding figure, the percent standard deviation would be 22%, although this represents a considerably smaller sample of points. The above value of P_σ is based on exclusion of the Boeing data. The information from the Martin replicate runs was not considered in the correlation, since the triplicate sets showed such similar results. It is encouraging that such comparable values can be obtained in repeated runs.

It should be pointed out here that in the case of the enthalpy difference calculated from both the facility and the SRI calorimeters, there appeared to be no relation between the points that correlated poorly and those that had a shock pressure recovery ratio different from that expected (see Sec. VIIIB). This might suggest that, in cases where both pressures were measured directly during the run (for example, as with the Martin data), it is probable that the reservoir pressure is a less reliable value than the stagnation pressure.

3. By the Sonic Flow Method

The procedure for calculating the enthalpy difference by Winovich's sonic method,[1] was mentioned earlier, see Eq. (2). Where possible, such

a calculation was made; the results are tabulated in Appendix C. In comparing these data with the measured enthalpy difference, General Dynamics was left out because of its use of nitrogen as the plasma fluid and Manned Spacecraft Center because it is a subsonic facility. Boeing is not represented because no reservoir pressures were measured, due to instrumentation difficulties with the transducer during the experimental runs on this program.

The remainder of the data, when correlated, show a standard deviation of 54 percent. This is considerably worse than the other two enthalpy calculations and may be traced in part to questionable reservoir pressures in the Martin data (see Sec. VIIIB). If these runs are eliminated from the correlation, the standard deviation drops to 32%.

A comparison of the calculated sonic enthalpy with the enthalpy calculated from the SRI calorimeter heating rate is shown in Fig. 22. Boeing, General Electric, and General Dynamics are not represented in this plot for the reasons mentioned earlier. The standard deviation for this correlation, with the questionable Martin points eliminated, is 29%. It is apparent that this is a less suitable method of obtaining enthalpy than the energy balance procedure, at least insofar as it compares with the calculated enthalpy based upon the experienced heating rate measured by the SRI calorimeter, and the stagnation pressure.

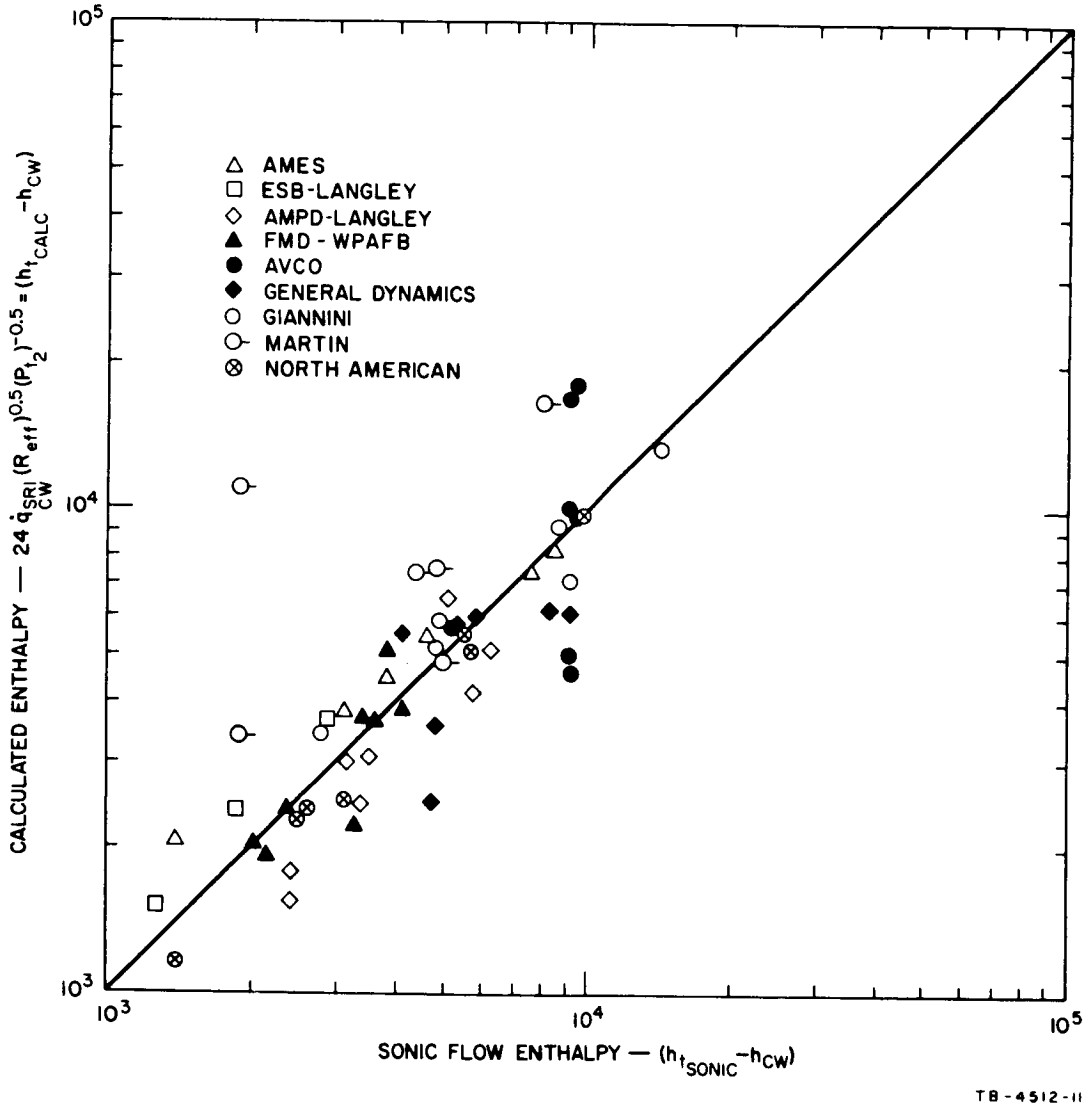

FIG. 22 ENTHALPY CALCULATED FROM HEATING RATE VERSUS SONIC FLOW ENTHALPY

IX ABLATION OF TEFLON

It is apparent from the previous section that the test conditions are best described by the heating rate and stagnation pressure. Not only were these comparable from facility to facility with less variation than measured enthalpies; they were also being measured in exactly the same position and environment in the plasma arc facility as was the model. For this reason the initial attempt to correlate the mass loss rate of Teflon was in terms of the heating rate and stagnation pressure

A. MASS LOSS RATE CORRELATION

Initially, the total mass loss rate, $\dot{m}_t$, was plotted against the heating rate as determined by the SRI calorimeter. This heating rate was used because the calorimeter had the same size, shape, and core diameter as the models, and, therefore, most accurately represented the enthalpy being experienced during the ablation runs. The appearance of that plot suggested a power function and attempts were made next to plot the following relation:

$$\dot{m}_t = a\left(q_{\substack{SRI \\ CW}}\right)^n \quad . \tag{21}$$

The results based upon early data received during the round-robin ablation program, when plotted on logarithmic coordinates, appeared to fall into two groups, each represented by an n value of two-thirds, but displaced from each other. The Boeing and AVCO data in the one group were obtained at stagnation pressures an order of magnitude lower than those for the North American data. For this reason it was next assumed that the relation might be a power function both in heating rate and stagnation pressure, as shown below.

$$\dot{m}_t = a\left(q_{\substack{SRI \\ CW}}\right)^n \left(P_{t_2}\right)^m \tag{22}$$

At this point it became apparent that a computer program was necessary to find the values of the constant and of the two exponents that would lead to the minimum standard deviation for the correlation. Such a program was available at the Institute in the form of a regression formula to solve the three unknown coefficients leading to the highest value of the multiple correlation coefficient. This program printed out the values of the coefficients along with their standard errors, the observed mass loss rate, the predicted mass loss rate based on the correlation shown in Eq. (22) above, and the variance estimate between these two.

In this case the correlation indicated by Eq. (6),

$$Y = X \tag{23}$$

considers

$$Y = \dot{m}_t \tag{24}$$

$$X = a\left(q_{\substack{SRI \\ CW}}\right)^n \left(P_{t_2}\right)^m \quad . \tag{25}$$

For this program

$$[\text{Variance Estimate}]^{1/2}/2.3 = \pm \log\left(\frac{Y}{X}\right)_\sigma = \sigma \quad , \tag{26}$$

but this can easily be converted to the percent standard deviation, P_σ, by Eqs. (9) and (10).

Use of the program on the results from the eight facilities that had appropriate data led to the following coefficients for Teflon:

$$a = 0.0058 \pm 20\%$$

$$n = 0.58 \pm 5.8\%$$

$$m = 0.25 \pm 7.3\%$$

with a percent standard deviation of

$$P_\sigma = +11\% \text{ and } -10\% \quad .$$

A plot of these results is shown in Fig. 23. Even though there is some error possible in the exponents, the correlation does spread over more than one order of magnitude in ablation rate and represents 41 sets of data from the eight facilities. The Boeing data fit into the correlation very well. This, plus the good correlation between the SRI and Boeing calorimeters, as shown on Fig. 20, indicates that both the ablation models and calorimeters were "seeing" the same test environment.

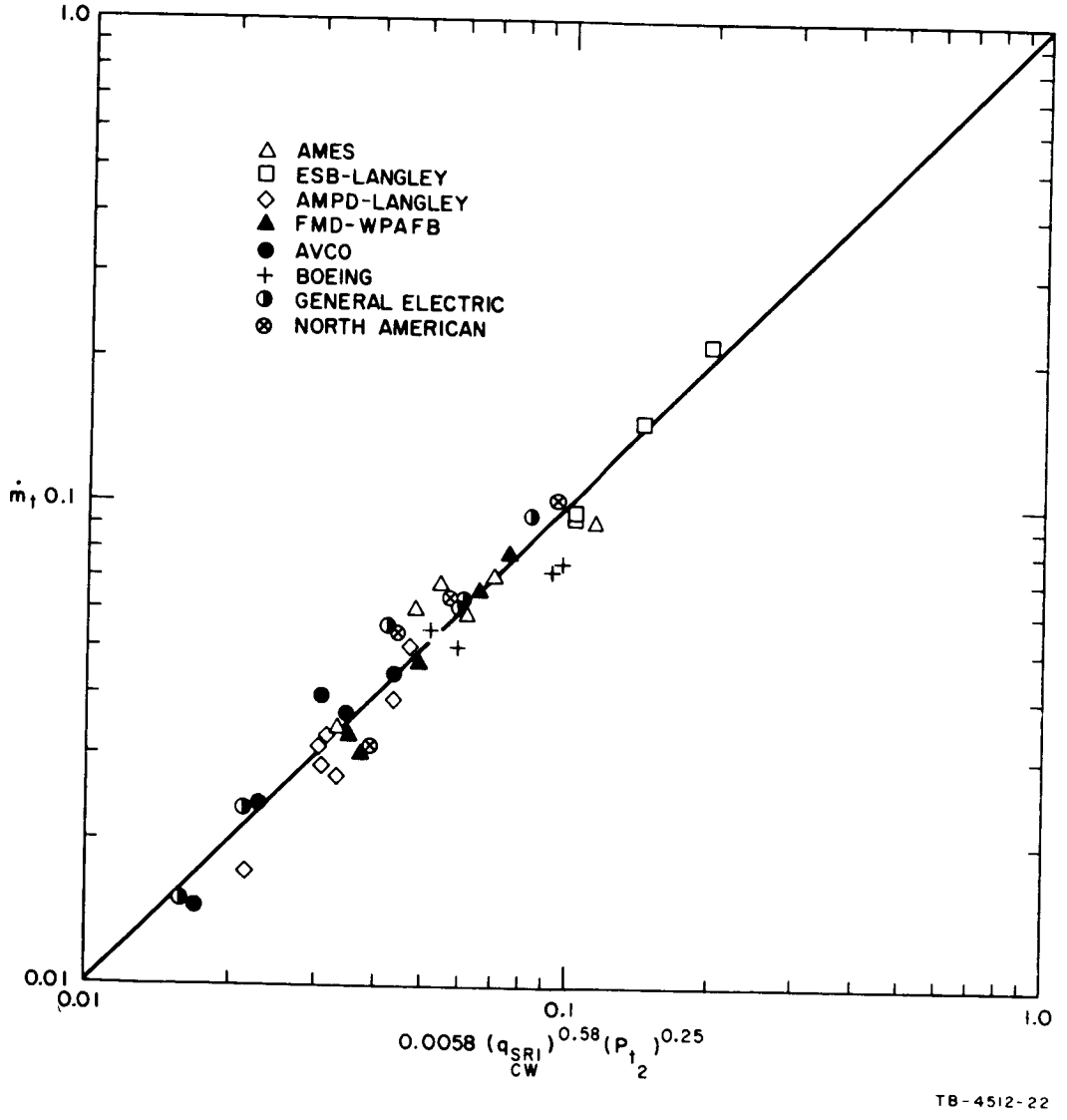

FIG. 23 MASS LOSS RATE CORRELATION FOR TEFLON
(SRI Calorimeter Cold Wall Heating Rate)

Of the four facilities not included in the correlation, General Dynamics was left out because the tests were run in nitrogen, and Manned Spacecraft Center was eliminated because the experiments were subsonic. The remaining two, Giannini and Martin, did not report SRI calorimeter values for the model runs, even though the calibration runs would have permitted estimating them. These runs have been used to predict what the values might have been, and they are tabulated in Appendix C with an appropriate footnote. Inclusion of this information in the correlation provides 52 sets of data and leads to the following values of the coefficients:

$$a = 0.0060 \pm 17\%$$

$$n = 0.57 \pm 5.0\%$$

$$m = 0.25 \pm 6.2\%$$

with a percent standard deviation of

$$P_{\sigma} = +10\% \text{ and } -9\% \quad .$$

The change in coefficients is almost negligible.

It would be of interest to compare the General Dynamics mass loss rates with those predicted from the correlation. Unfortunately, several of the runs had to be discarded because of nonuniform ablation due to a small plasma column and centering difficulties. One run did have all of the data necessary, and, using the first set of coefficients, the predicted mass loss rate was 0.0197 lb/ft^2 sec, compared with an observed value of 0.0259.

B. ALTERNATIVE CORRELATIONS

The above correlation involves a three-coefficient fit between the mass transfer rate, the SRI calorimeter cold wall heat transfer rate, and the stagnation pressure. It may be that there are other correlations between the mass transfer rate and the plasma arc conditions. The following sections consider some of the alternates.

1. Hot Wall Heating Rate

The heating rate from the SRI calorimeter used above was expressed on a cold wall basis. This could be converted to a hot wall heating rate, which might show a better correlation with a mass loss rate and stagnation pressure. The calculation of this value proceeded in the following manner.

a. The cold wall enthalpy potential was calculated from the SRI calorimeter cold wall heating rate and stagnation pressure through the Fay-Riddle relation Eq. (17).

b. The total enthalpy was obtained from this value by adding 150 Btu/lb, which is approximately the enthalpy content of the gas entering the arc reservoir; the latter is the cold wall enthalpy.

c. The sublimation temperature of the Teflon is read from the vapor pressure curve for this compound at the stagnation pressure for the experiment.

d. The hot wall enthalpy is calculated from this temperature and the heat content of air.

e. The enthalpy potential on a hot wall basis is determined by subtracting the hot wall enthalpy from the total enthalpy previously calculated.

f. The ratio of the hot wall enthalpy potential to the cold wall enthalpy potential is used to correct the cold wall heating rate to the hot wall heating rate.

Both the hot wall enthalpy potential and the hot wall heating rate, based on the SRI calorimeter, are tabulated in Appendix C. The latter heating rate and the stagnation pressures were used in the regression relation, with the mass loss rate of the Teflon models, to determine the values of the coefficients in a power function similar to that given in Eq. (22). The results are tabulated below:

$$a = 0.0076 \pm 17\%$$

$$n = 0.55 \pm 5.5\%$$

$$m = 0.27 \pm 6.3\%$$

with a percent standard deviation of

$$P_\sigma = +10\% \text{ and } -9\% \quad .$$

A plot of these data is given in Fig. 24 and it is almost identical to Fig. 23. It is apparent that there is a slight shift in the coefficients accompanied by a very small improvement in the percent standard deviation. It therefore is equally as good a correlation as the one in terms of the cold wall heating rate. It does have some disadvantage in the additional calculations required.

2. Measured Enthalpy Potential

The other environmental condition measured during the experimental runs was the enthalpy potential. The following correlation involving it was therefore checked.

$$\dot{m}_t = b(\Delta h_{\substack{meas \\ CW}})^u (P_{t_2})^v \tag{27}$$

Based on the information contained in Appendix C, the regression program led to the following values of the coefficients:

$$b = 0.0017 \pm 63\%$$

$$u = 0.59 \pm 10.8\%$$

$$v = 0.57 \pm 5.6\%$$

with a percent standard deviation of

$$P_\sigma = +21\% \text{ and } -17\% \quad .$$

A plot of this correlation is shown in Fig. 25. A comparison of this with Fig. 23, or comparison of the percent standard deviation with that found for the correlation involving the cold wall heating rate determined by the SRI calorimeter, shows that the measured enthalpy is not as satisfactory a correlation parameter. Elimination of the Boeing and General Electric data, because of "coring", does not improve the correlation appreciably.

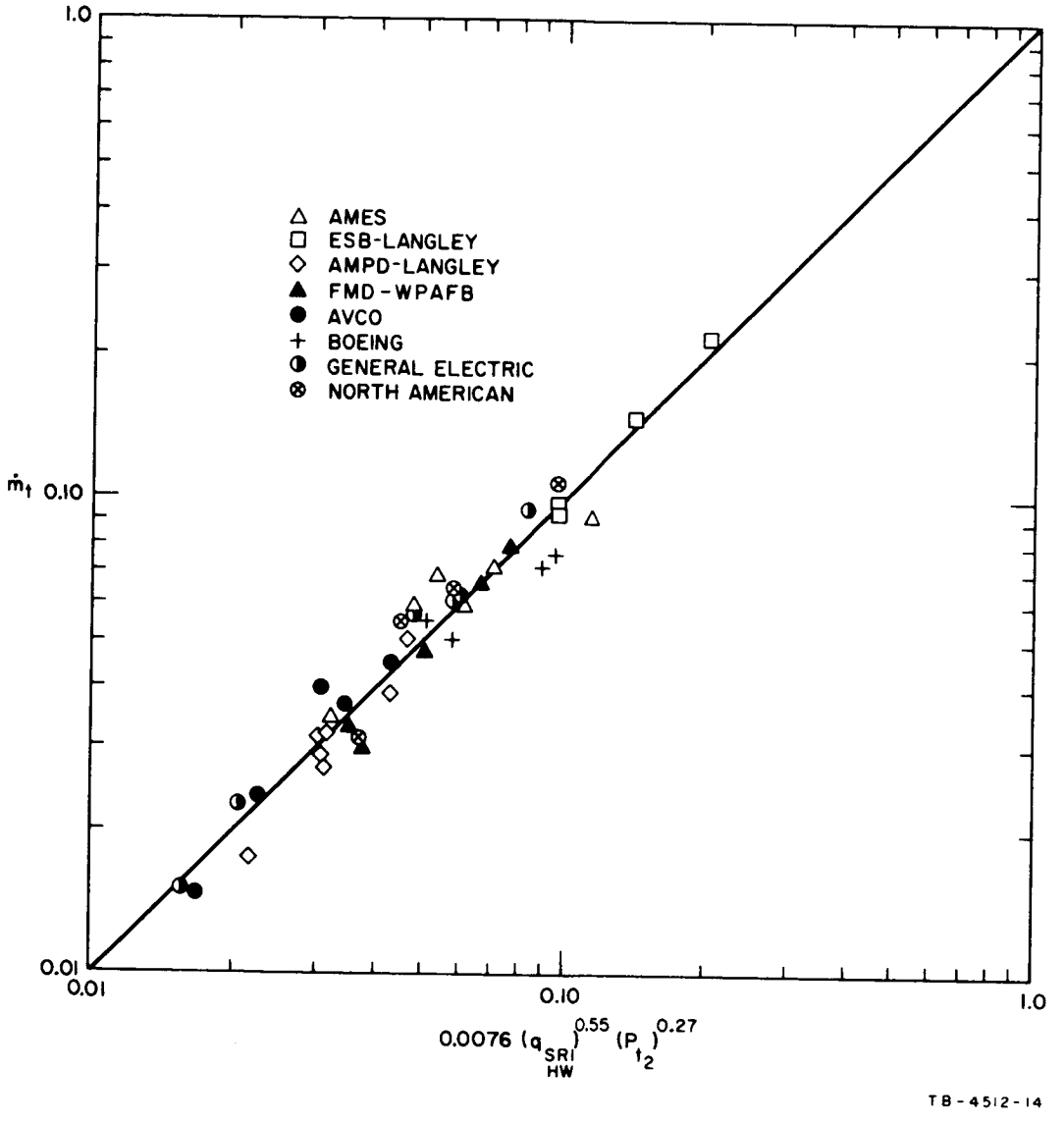

FIG. 24 MASS LOSS RATE CORRELATION FOR TEFLON
(SRI Calorimeter Hot Wall Heating Rate)

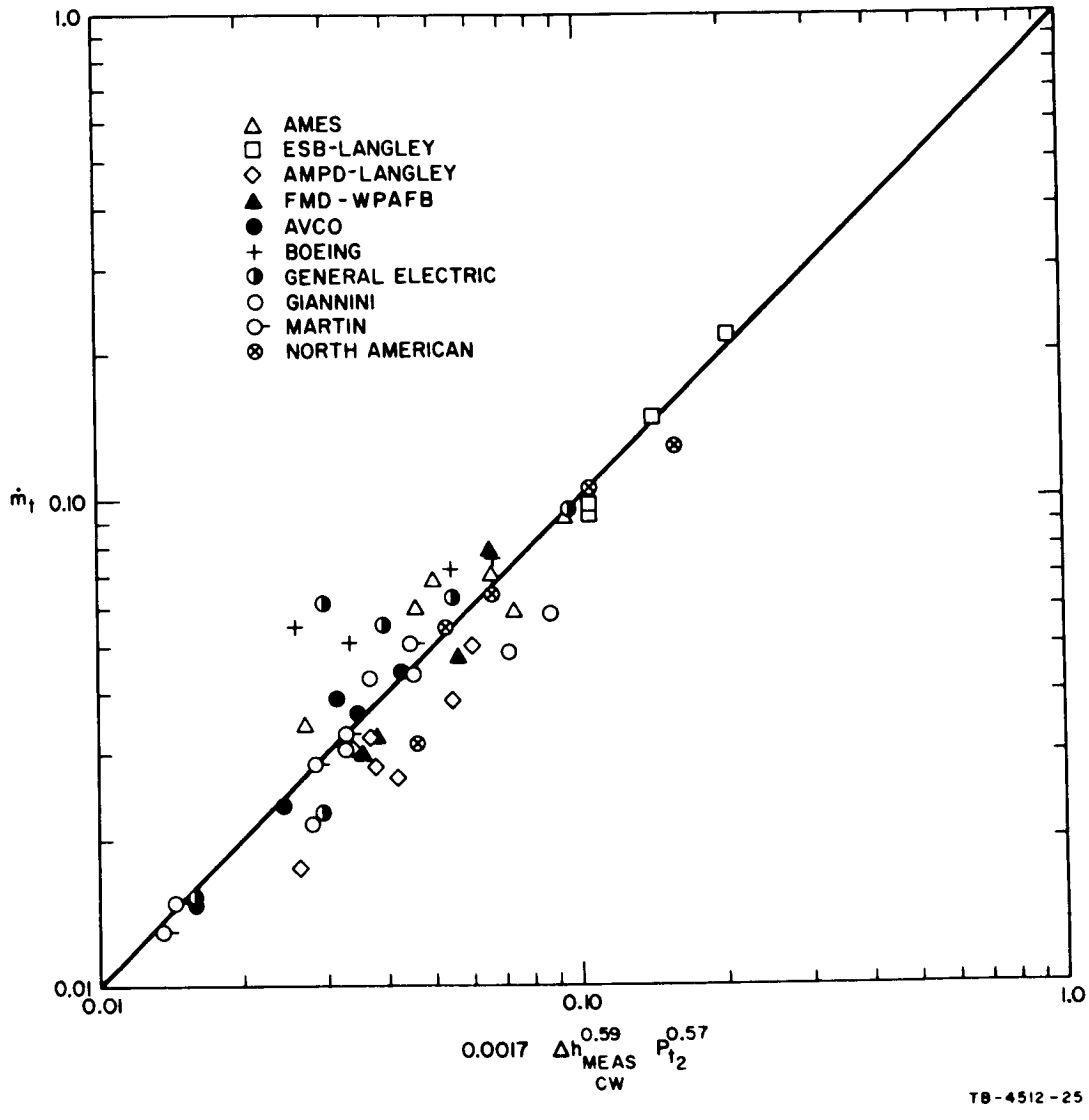

FIG. 25 MASS LOSS RATE CORRELATION FOR TEFLON
(Measured Cold Wall Enthalpy Potential)

3. Facility Cold Wall Heating Rate

It is, of course, possible that the facility calorimeter may best represent the conditions experienced by the ablation model, even though it may not have the same geometry and size. Therefore, for the data available in Appendix C, a correlation of the type shown in Eq. (22) was tried, using the facility calorimeter heating rate rather than that from the SRI calorimeter. The results from the regression program, based on 28 sets of data from the six facilities that obtained such information, are given below:

$$a = 0.011 \pm 23\%$$

$$n = 0.48 \pm 7.5\%$$

$$m = 0.29 \pm 6.2\%$$

with a percent standard deviation of

$$P_\sigma = +11\% \text{ and } -10\%^* \quad .$$

A plot of the data is given in Fig. 26. The deviation is the same order of magnitude as that for the SRI calorimeter heating rate. However, it intuitively seems more meaningful to have the calorimeter, pressure probe, and ablation model all have the same configuration and size in order to minimize experimental variability.

The round-robin results from Manned Spacecraft Center (see Appendix C), are plotted on Fig. 27, using the cold wall facility calorimeter correlation found for Teflon in supersonic arc facilities.

---

* Addition of the Martin replicate data to the computer program changes the coefficients to

$$a = 0.013 \pm 34\%$$

$$n = 0.44 \pm 11.5\%$$

$$m = 0.29 \pm 9.3\%$$

$$P_\sigma = +18\% \text{ and } -15\% \quad .$$

This tends to indicate that the Martin points are somewhat out of line with the other data.

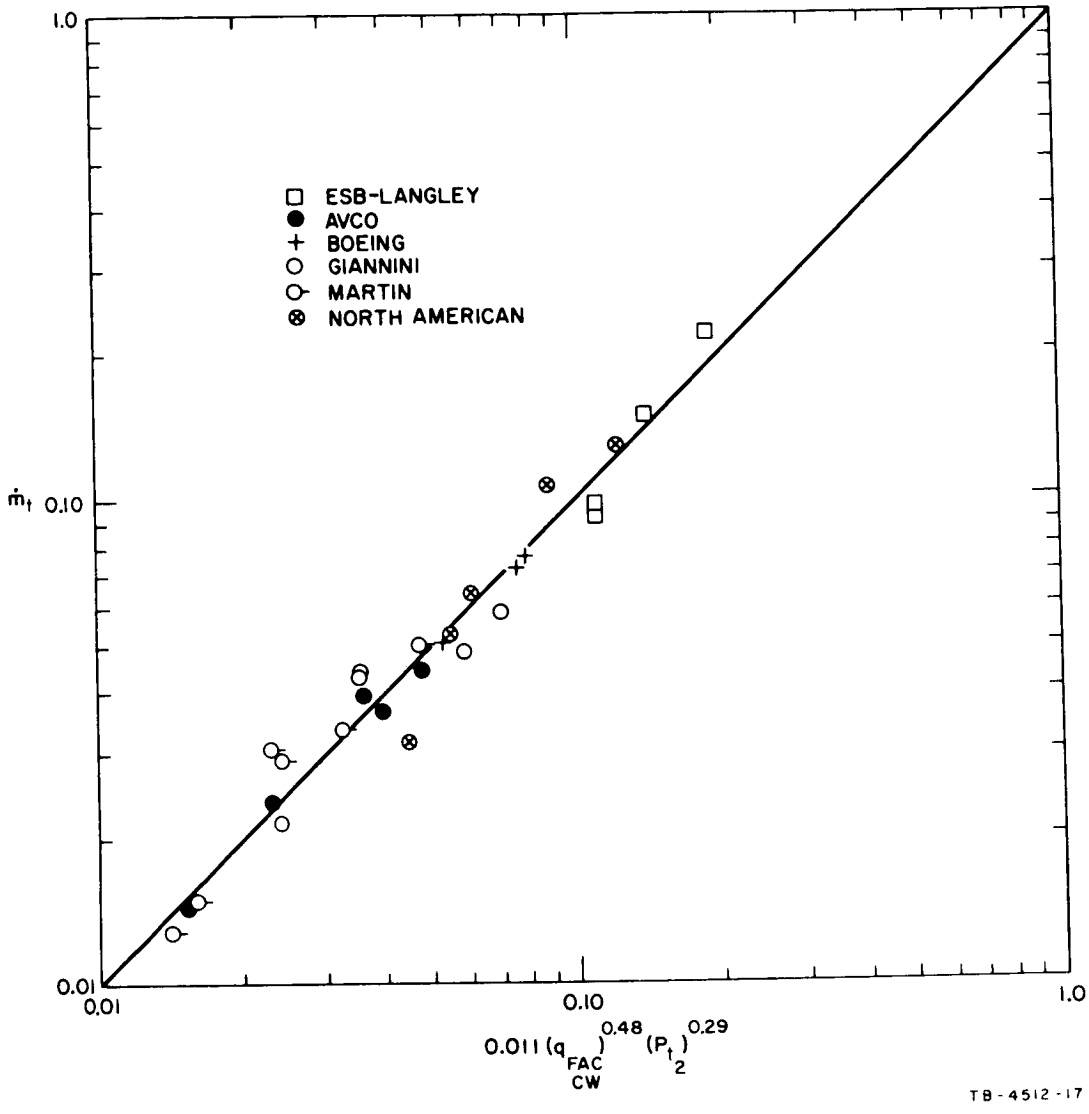

FIG. 26 MASS LOSS RATE CORRELATION FOR TEFLON
(Facility Calorimeter Cold Wall Heating Rate)

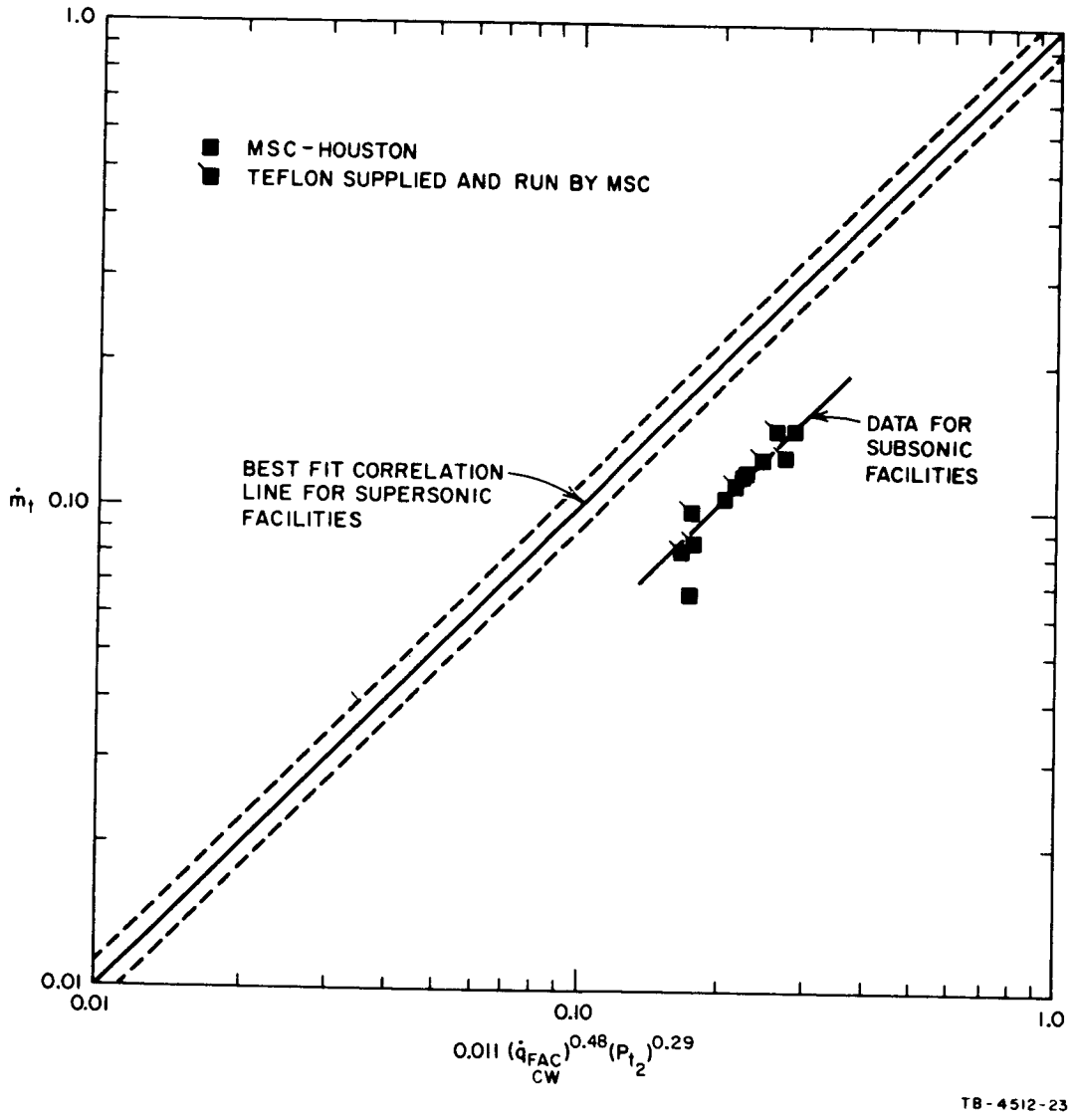

FIG. 27 MASS LOSS RATE CORRELATION FOR TEFLON
(Results from Subsonic Facilities)

The solid and dotted lines indicate the supersonic correlation and the percent standard deviation of the data. Note that the subsonic results appear to correlate among themselves with a lower intercept. A lower apparent stagnation pressure than the one atmosphere used, or a lower apparent heating rate (higher apparent model diameter), could bring these points on to the supersonic correlation line.

C. HEAT OF ABLATION CORRELATION

Common practice in this field of research is to calculate the heat of ablation from the heating rate and mass loss rate as shown below:

$$H_{eff} = \frac{\dot{q}_{\substack{SRI \\ HW}}}{\dot{m}_t} \tag{28}$$

1. Linear Relation

Georgiev, Hildalgo and Adams[9] have related the heat of ablation to the enthalpy potential by an energy balance at the surface of the model. The relation suggested is linear in form.

$$H_{eff} = \alpha + \beta \Delta h_{\substack{meas \\ HW}}$$

The coefficient α is derived to be the heat necessary to raise the material to the ablation temperature and decompose it, and β is defined as the transpiration shielding factor. Georgiev *et al.*[9] proposed theoretical values of

$$\alpha = 950 \text{ and } \beta = 0.44$$

but experimentally found that the data would fit

$$\alpha = 750 \text{ and } \beta = 0.44 \quad .$$

Chapman[10] found that his data fit

$$\alpha = 940 \text{ and } \beta = 0.39 \quad .$$

A linear plot of H_{eff} against the measured enthalpy potential, from data contained in Appendix C, is given in Fig. 28. Note that the enthalpy is on a cold wall basis. This will not affect the appearance of the plot since the hot wall enthalpy is, on the average, about 350 BTU lb^{-1} less for Teflon. This would therefore result in only a minor displacement of the points along the abscissa. The Chapman correlation is shown on the figure.

The spread of the data is not unexpected because of the wide scatter of measured enthalpy potentials. It can be reduced somewhat by using the hot wall enthalpy potential calculated from the heating rate as mentioned above. Such a plot is given in Fig. 29 with the Chapman correlation line.

2. Modified Linear Relation

Georgiev *et al*,[13] also proposed a correction to the term α when combustion of the Teflon occurs. Specifically he suggested that

$$H_{eff} = \frac{950}{1 + (2100/\Delta h_{HW})} + 0.44\Delta h_{HW} \quad . \tag{30}$$

This is, of course, linear at high enthalpy potentials but does go to zero at small values rather than to a finite intercept. This correlation line is also plotted on Fig. 29.

3. Logarithmic Relation

The data in Fig. 29 does not show the anticipated linear trend at higher enthalpy values. This is not unexpected, as can be shown by deriving a relation between the heat of ablation and enthalpy potential from the mass loss rate correlation based on the SRI calorimeter hot wall heating rate:

$$\dot{m}_t = 0.0076(\dot{q}_{\underset{HW}{SRI}})^{0.55}(P_{t_2})^{0.27} \quad . \tag{31}$$

Thus

$$H_{eff} = \frac{\dot{q}_{\underset{HW}{SRI}}}{\dot{m}_t} = 132(\dot{q}_{\underset{HW}{SRI}})^{0.45}(P_{t_2})^{-0.27} \quad . \tag{32}$$

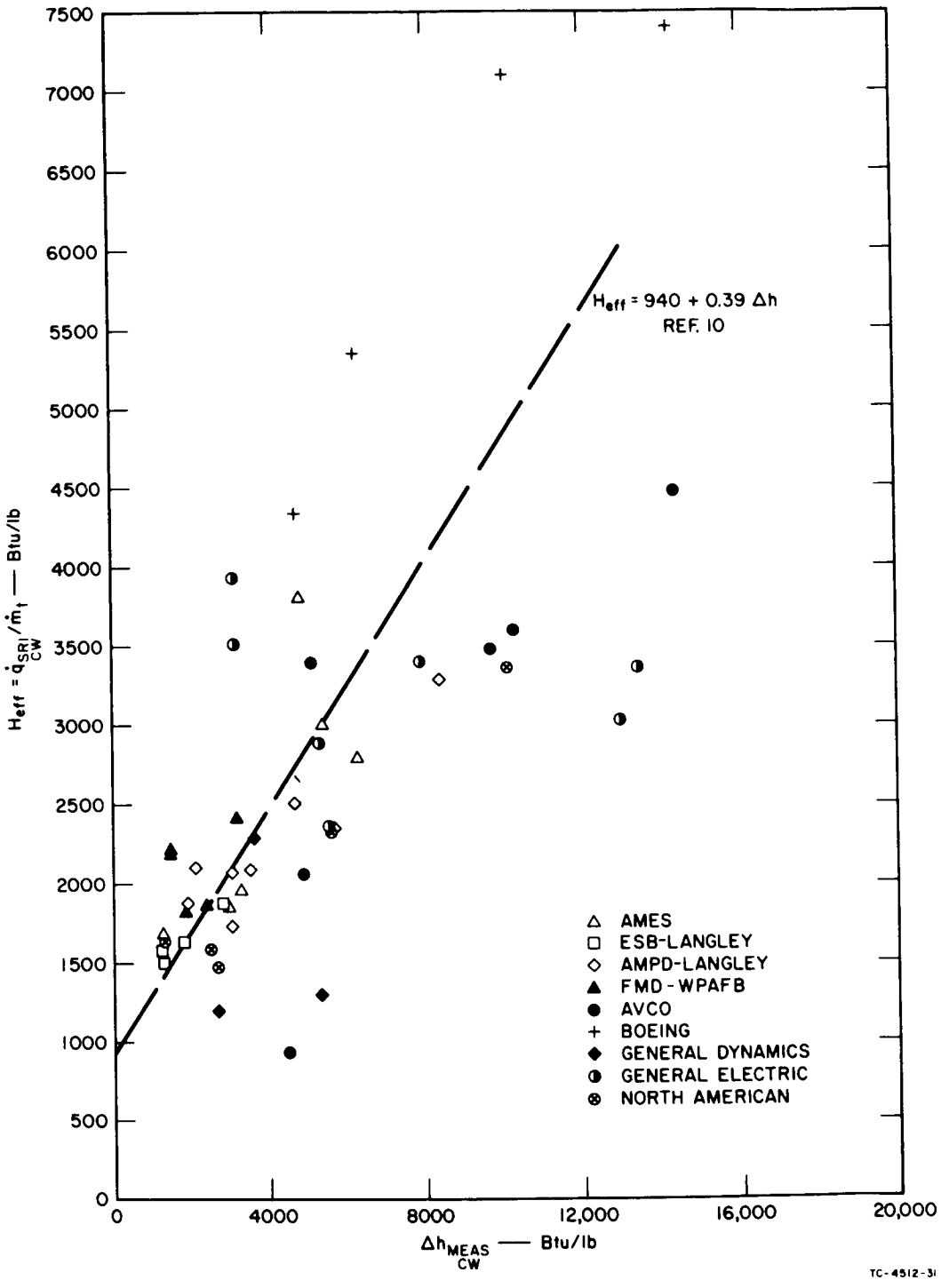

FIG. 28 HEAT OF ABLATION FOR TEFLON VERSUS ENTHALPY MEASURED BY THE FACILITY

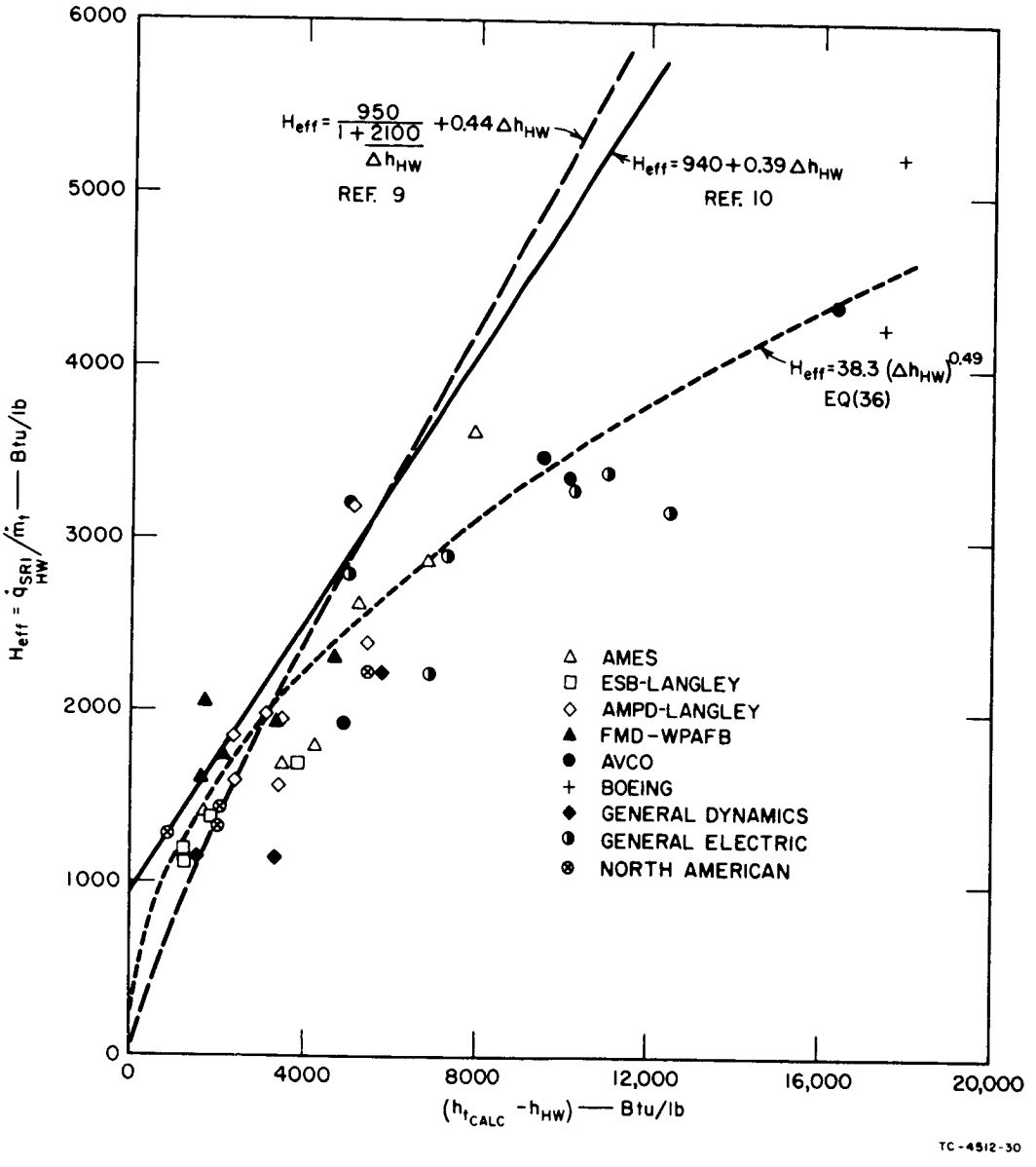

FIG. 29 HEAT OF ABLATION FOR TEFLON VERSUS ENTHALPY CALCULATED FROM HEATING RATE

The heating rate can be eliminated from the right hand side through the Fay-Riddell relation, Eq. (17), and, for the SRI model dimensions, Eq. (32) becomes

$$H_{eff} = 46.8(\Delta h_{\substack{calc \\ SRI \\ HW}})^{0.45}(P_{t_2})^{-0.04} \quad . \tag{33}$$

The interesting point is that this correlation is a power function rather than linear in form and is affected slightly by the stagnation pressure. Steg and Lew[11] found such an effect for ablation of Teflon.

4. Adjusted Logarithmic Relation

The effect of the stagnation pressure is quite small and it is therefore of interest to consider a mass loss rate correlation in which the exponents in Eq. (31) are related so that the stagnation pressure term vanishes when the correlation is put in the form of the heat of ablation as shown in Eq. (33). Taking into account the Fay-Riddell relation, simple algebra shows that when the correlation exponents are as shown

$$\dot{m}_t = c(q_{\substack{SRI \\ HW}})^n (P_{t_2})^{(1-n)/2} \tag{34}$$

the heat of ablation form becomes

$$H_{eff} = \frac{\dot{q}_{\substack{SRI \\ HW}}}{\dot{m}_t} = \frac{1}{c}\left[24(R_{eff})^{1/2}\right]^{m-1}(\Delta h_{\substack{calc \\ SRI \\ HW}})^{1-n} \quad . \tag{35}$$

A simple modification of the regression program permits computation of the two coefficients, c and n, and the results for the data contained in Appendix C are

$$c = 0.0085 \pm 17\%$$

$$n = 0.51 \pm 4.9\%$$

$$(1-n)/2 = 0.25 \pm 4.9\%$$

with a percent standard deviation for Eq. (34) of

$$P_{\sigma} = +11\% \text{ and } -10\%^{*} \quad .$$

A plot of the correlation indicated by Eq. (34) is shown in Fig. 30. Although the percent standard deviation for this, and for the earlier correlation with the hot wall heating rate where the exponents were uncontrolled, Eq. (31), are nearly the same, visual comparison of Fig. 30 with Fig. 24 shows that the initial correlation is slightly better.

However, assuming that the correlation with the adjusted exponents is a valid one, Eq. (33) then becomes

$$H_{eff} = \frac{\dot{q}_{\substack{SRI \\ HW}}}{\dot{m}_t} = 38.3(\Delta h_{\substack{calc \\ SRI \\ HW}})^{0.49} \qquad (36)$$

At the same time the percent standard deviation increases by 1/n fold to about 21%. The correlation indicated by Eq. (36) is shown as a dotted line on Fig. 29.

In dealing with Teflon it has also been a practice to plot ψ, the blockage factor, against B, the ratio of the enthalpy potential to the heat of ablation. These are defined as follows.

$$\psi = 940/(\dot{q}_{\substack{SRI \\ HW}}/\dot{m}_t) \qquad (37)$$

$$B = \Delta h_{\substack{calc \\ SRI \\ HW}} /(\dot{q}_{\substack{SRI \\ HW}}/m_t) \quad . \qquad (38)$$

Use of Eq. (36) to solve for ψ in terms of B leads to

$$\psi = 940(c)^{1/n}\,[24(R_{eff})^{1/2}]^{(1-n)/n} B^{(n-1)/n} \qquad (39)$$

---

* A relation similar to Eq. (34) but based on cold wall heating rates from the SRI calorimeter, lead to the coefficients

$$c = 0.0065 \pm 19\%$$
$$n = 0.55 \pm 5.1\%$$
$$(1-n)/2 = 0.23 \pm 5.1\%$$

with a percent standard deviation of

$$P_{\sigma} = +11\% \text{ and } -10\% \quad .$$

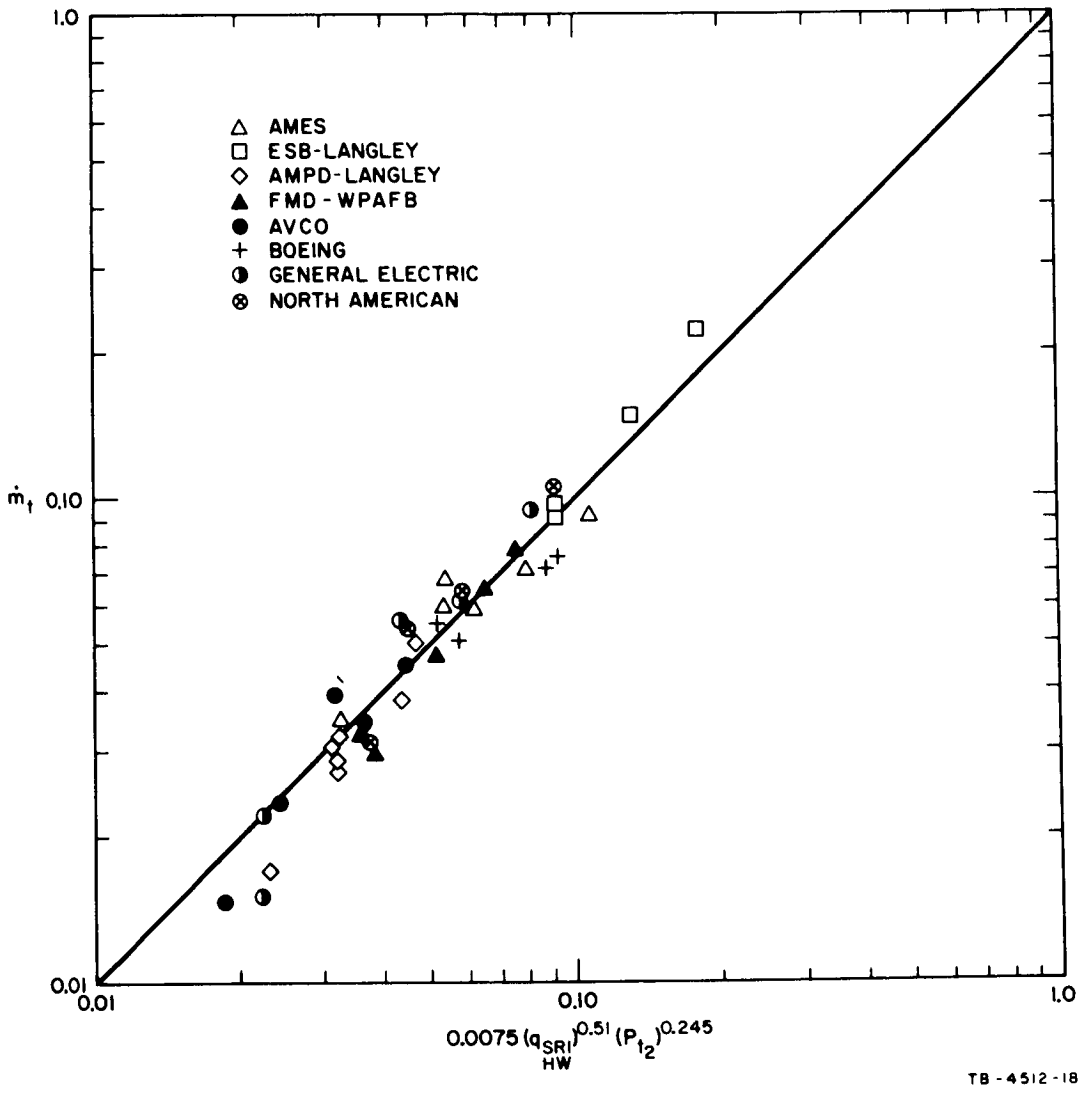

FIG. 30 MASS LOSS RATE CORRELATION FOR TEFLON
(Adjusted Stagnation Pressure Exponent)

and from the coefficients associated with Eq. (35)

$$\psi = 0.75\ B^{-0.96} \quad . \tag{40}$$

The data in Appendix C converted to the form of ψ and B are plotted in Fig. 31, and the correlation indicated by Eq. (40) is shown thereon as the dotted line. The Chapman and Georgiev correlations are also indicated on the figure. The asymptotic approach of the blockage factor to a low finite value has been experimentally observed by others.[12] Such behavior would be in agreement with the logarithmic correlation as opposed to the linear relation.

It is probable that the nonlinear form of the relation between heat of ablation and enthalpy was not noticed earlier because very few facilities were able to study a wide range of mass loss rates and enthalpies. In addition, the accuracy of the measured enthalpies used in these correlations left something to be desired. In fact, it will be noticed that in Fig. 31 the spread is quite large. This is to be expected since the spread will be at least twice (1/n) that shown in the heat of ablation plot, Fig. 29, which already has a percent standard deviation of 21%.

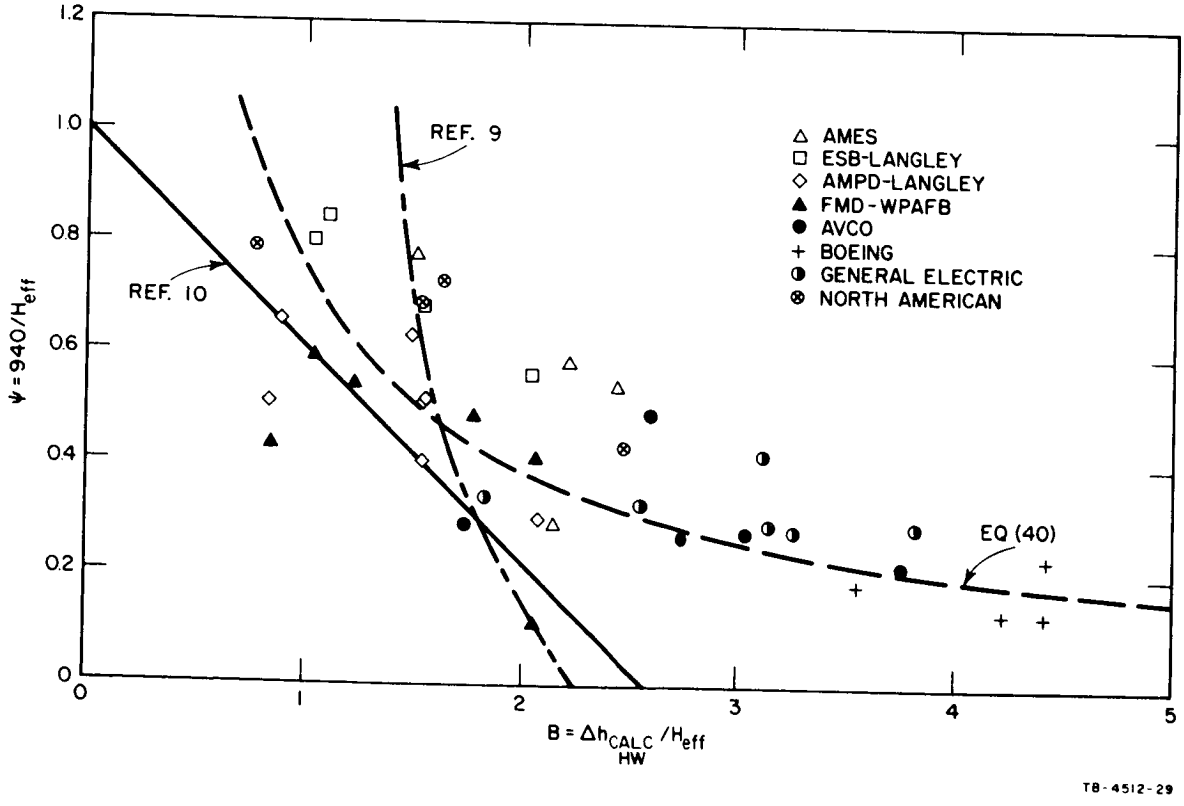

FIG. 31 CONVECTIVE BLOCKAGE OF TEFLON

D. ENTHALPY MEASUREMENT BY TEFLON ABLATION

The good correlation between the mass loss rate of Teflon, the cold wall heating rate, and the stagnation pressure suggests a secondary method of determining enthalpy. Elimination of the heating rate in Eq. (31) through use of the Fay-Riddell relation, [Eq. (17)] and rearrangement of terms leading to the following:

$$\Delta h_{CW} = 7.1 \times 10^4 (\dot{m}_t)^{1.72} (P_{t_2})^{-0.92} \quad . \tag{41}$$

This has a percent standard deviation of 19%, and is based on the SRI model dimensions. If such a Teflon model is used in an actual experimental run it should be possible to determine the enthalpy from the mass loss rate observed and the measured stagnation pressure, within the limits indicated.

E. COMPARISON OF MASS LOSS RATES BETWEEN FACILITIES

The mass loss rate correlation given in Eq. (22) and repeated below

$$\dot{m}_t = 0.0058 (\dot{q}_{CW}^{SRI})^{0.58} (P_{t_2})^{0.25} \tag{22}$$

can be used to compare ablation rates of Teflon between facilities in two ways. In the first, the specific data for a given facility can be corrected to a standard model configuration and size and to a standard heating rate and stagnation pressure. Thus for a

$$q_{CW} = 150 \text{ BTU/ft}^{-2}\text{sec}^{-1}$$

$$P_{t_2} = 0.1 \text{ atmos},$$

which is equivalent, for the present model size ($R_{eff} = 0.172$ ft), to

$$\Delta h_{CW} = 4{,}720 \text{ BTU/lb}^{-1},$$

the standard mass loss rate would be from Eq. (22)

$$(\dot{m}_t)_{Std} = 0.06 \text{ lb ft}^{-2}\text{sec}^{-1} \quad .$$

The results from any facility using the present Teflon model can then be converted to an adjusted standard value for that facility by

$$(\dot{m}_t)_{\substack{\text{Std}\\\text{FAC}}} = (\dot{m}_t)_{\text{FAC}} \left[150/(q_{CW})_{\text{FAC}} \right]^{0.58} \left[0.1/(P_{t_2})_{\text{FAC}} \right]^{0.25} \qquad (42)$$

as long as the heating rate has been adjusted to a 1.25-inch, flat-face basis. This adjusted value can then be compared to 0.06 lb ft^{-2} sec^{-1}.

The other comparison between facilities consists of comparing the results with the correlation line directly. Thus, two facilities operating at quite different heating rates and stagnation pressures could determine the relative goodness of fit of their results in terms of the correlation, and express this as a ratio of the measured to the predicted value.

A graphical indication of the operating regions for each facility is shown in Fig. 32. The envelopes shown on this plot for each facility are the minimum perimeter enclosures of the operating conditions (heating

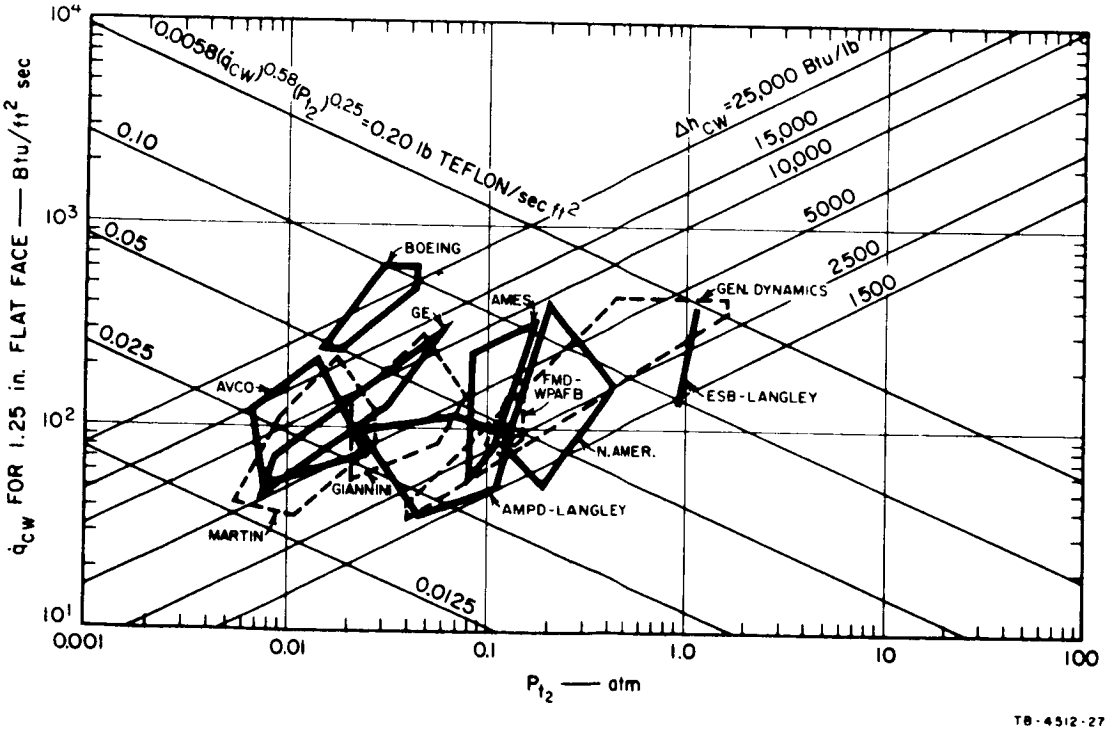

FIG. 32 TEST AREA COVERED BY EACH PARTICIPATING FACILITY IN TERMS OF HEATING RATE AND MODEL STAGNATION PRESSURE (Cross plots are lines of constant enthalpy potential and lines of constant mass loss rate of Teflon)

rate and stagnation pressure) used in the Teflon ablation runs. The ascending lines are for the constant enthalpies indicated and are calculated values based on the Fay-Riddell relation and the present model dimensions. The descending lines are for the indicated constant Teflon mass loss rates based on the ablation correlation, Eq. (22), found for the SRI calorimeter cold wall heating rate. The apparently high enthalpy conditions for the Boeing facility are due to the plasma arc "coring," which caused very high heating rates on the models.

It is obvious from this figure why few facilities can obtain comparative ablation rates. Only a few operate in the same heating rate (or enthalpy) and stagnation pressure regions, and, since both of these appear to be of importance in determining the mass loss rate, only these few might be expected to obtain comparable results directly.

All of the Teflon runs were made at exposure times of thirty seconds. At the lowest heating rate used, 33 BTU-ft^2/sec, this would be equivalent to a heat load of 1000 BTU/ft^2. These points correlated as well as those at higher heat loads.

X ABLATION OF PHENOLIC-NYLON

Ablation of phenolic-nylon is much more complicated than that of Teflon in that the former material heats up to its decomposition point and then begins to pyrolyze, forming low molecular weight gaseous fragments and a char. Initially these gaseous fragments are lost, but as the char begins to build up the gases are cracked in their passage through it and coke is deposited. The char ultimately becomes a porous carbon layer that acts as an insulator. At this point the decomposition proceeds in a steady state manner and the heat absorbed during this process becomes nearly constant.

A. STEADY STATE ABLATION

A series of runs were undertaken at each facility to determine the steady-state ablation characteristics of phenolic-nylon. This was generally a group of three models exposed under the same enthalpy and heating rate conditions but for varying time periods. The longest exposure was nominally chosen to be at a heat load of 6000 Btu/ft^2. Since the heat load was the product of the heating rate and exposure time, this time could be determined once the desired heating rate for the run was chosen. The medium exposure model was inserted for two-thirds of this time and the short exposure for one-third.

This set of models for each facility is so designated in Appendix C. The mass loss for each model is plotted against exposure time in Fig. 33. In most cases the related points can be connected by a straight line, indicating that a steady state mass loss rate had been reached by the minimum exposure time. At the same time, all of the lines have a positive intercept, showing that there is an initial but higher rate, unsteady-state period.

In view of the fact that the mass loss rate used in the correlations is obtained by dividing the total mass loss by the total exposure time, only the longest exposures will have mass loss rates near to the steady state rates indicated by the slopes of the lines on this plot. For this reason the medium- and short-exposure-time models were not used in the correlations.

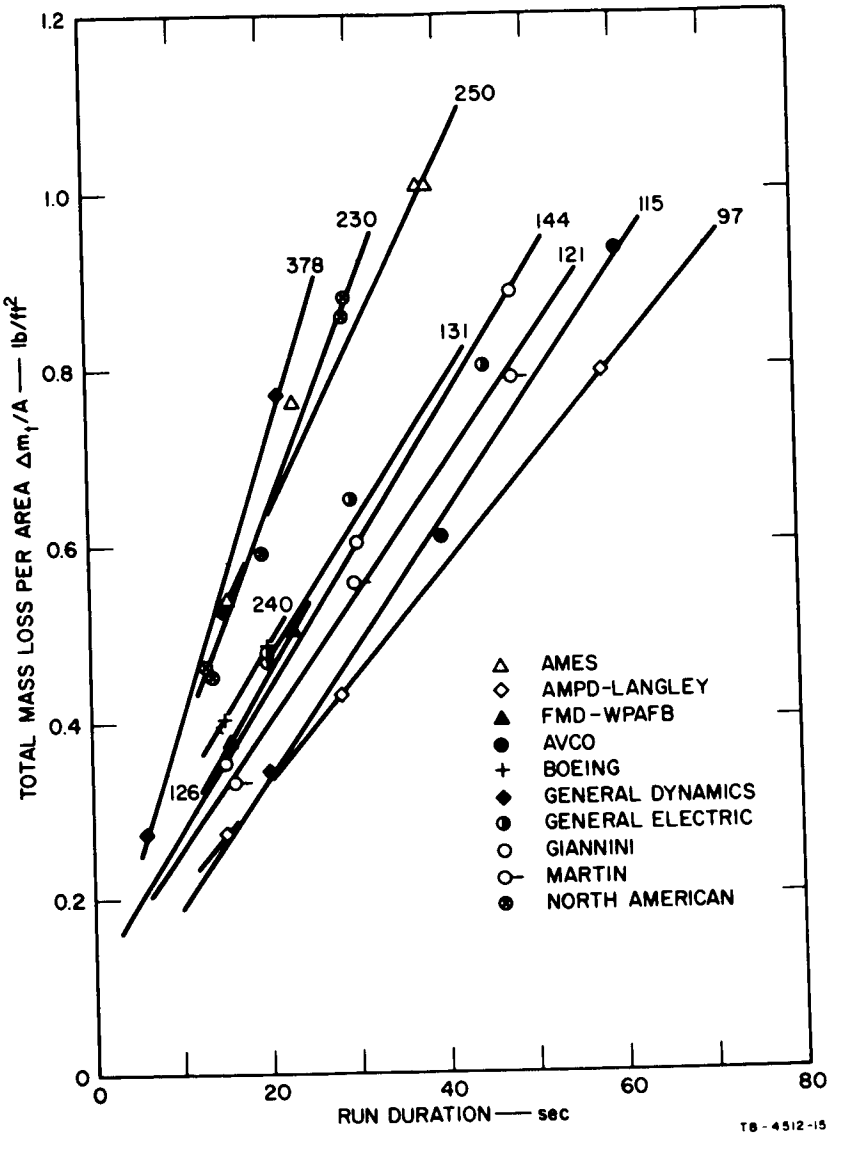

FIG. 33 MASS LOSS OF PHENOLIC–NYLON PER UNIT AREA AS A FUNCTION OF RUN DURATION (Heat Transfer Rate Indicated for Each Facility)

B. MASS LOSS RATE CORRELATION

The success in correlating the total mass loss rate of Teflon with the heating rate and stagnation pressure suggested an attempt of this type for the phenolic-nylon models. The form of the correlation would be similar to Eq. (22) and the data in Appendix C were used with the regression program to determine the coefficients. The results were:

$$a = 0.0017 \pm 21\%$$

$$n = 0.56 \pm 5.9\%$$

$$m = 0.13 \pm 14.6\%$$

with a percent standard deviation of

$$P_\sigma = +11\% \text{ and } -10\% \quad .$$

A plot of these data is shown in Fig. 34

As with the Teflon ablation correlation, General Dynamics, Manned Spacefract Center, Giannini, and Martin were excluded. If the estimated SRI calorimeter values for the last two facilities are considered in determining the coefficients for the correlation, the results are

$$a = 0.0018 \pm 18\%$$

$$n = 0.55 \pm 5.1\%$$

$$m = 0.13 \pm 12.5\%$$

with a percent standard deviation of

$$P_\sigma = +10\% \text{ and } -9\% \quad .$$

Again, the change in coefficients is negligible.

C. ALTERNATIVE CORRELATIONS

As with Teflon, there may be other correlations than the one between the mass transfer rate, the SRI calorimeter cold wall heat transfer rate, and the stagnation pressure. However, the use of a hot wall heating rate is much more difficult than in the Teflon case, because of problems in determining front surface temperatures. In addition, there are a number of mass loss rates that one can measure for phenolic-nylon. The following section considers some alternative correlations.

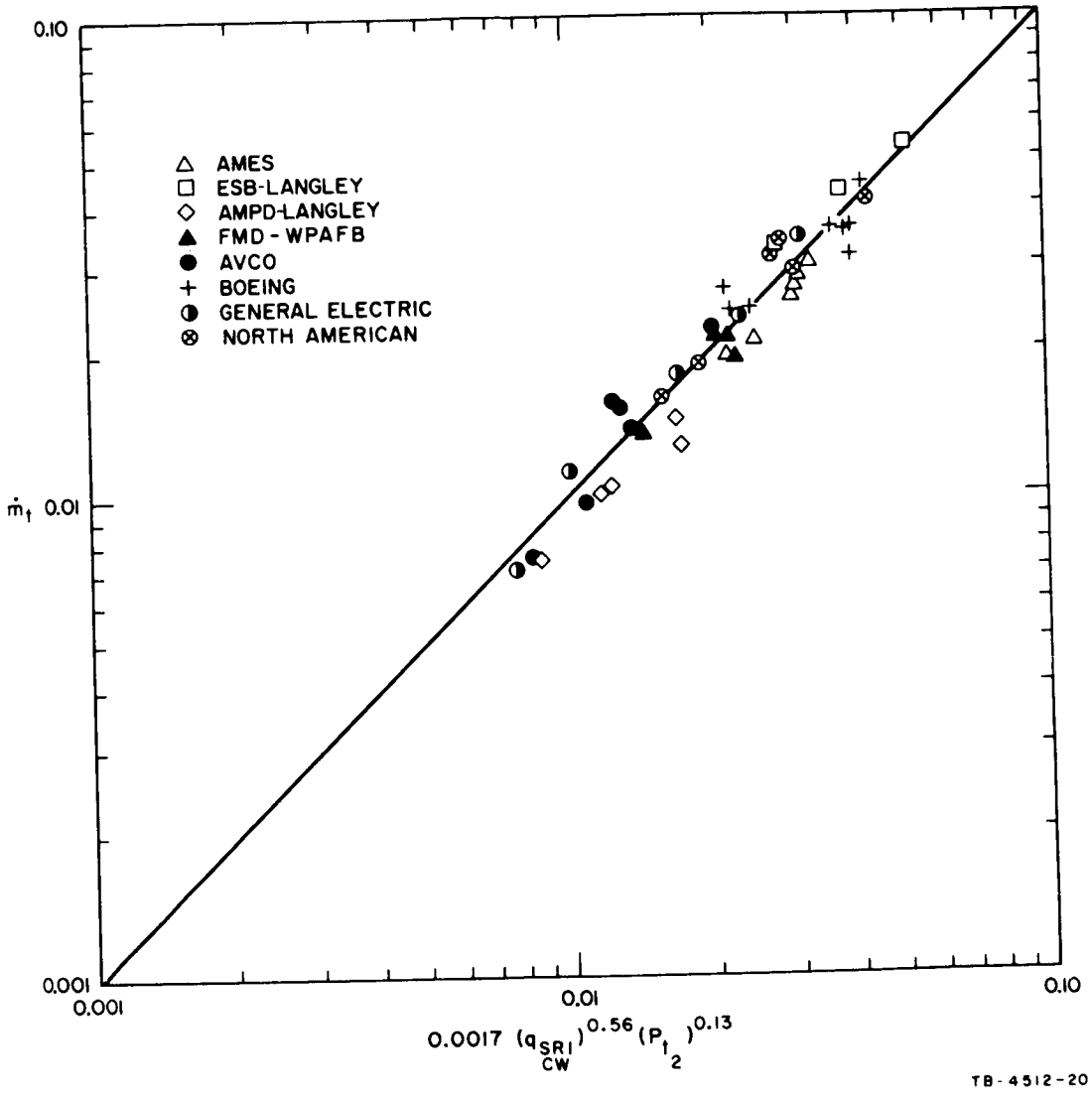

FIG. 34 MASS LOSS RATE CORRELATION FOR PHENOLIC-NYLON
(SRI Calorimeter Cold Wall Heating Rate)

1. Pyrolysis Rate

The pyrolysis rate is defined by Lundell *et al*,[13] as the sum of the vapor production and char production rates. The mass loss used in determining the rate is the difference in mass between the unablated model core and the post-run core with the char cap removed. This determination is somewhat subjective in that it requires determination of how much char must be removed.

A plot of the pyrolysis rate, $\dot{m}_p$, against the cold wall heating rate and stagnation pressure, using the previous set of exponents, is identical in appearance to Fig. 34, but with the intercept moved upward to a value of 0.0020. The spread of the data is the same and, therefore, there appears to be no advantage in using the pyrolysis rate rather than the total mass loss rate in the correlation, especially since the latter is simpler to determine.

2. Adjusted Exponents

Determination of the heat of ablation is less meaningful for phenolic-nylon than for Teflon because of the complex nature of the decomposition mechanism for charring ablators. It is therefore more difficult to relate this to enthalpy potentials and other environmental conditions. Nevertheless, it is of interest to determine how well the mass loss rate data might be correlated when the heating rate and stagnation pressure exponents are related as indicated in Eq. (34), so that the relation between the heat of ablation and enthalpy potential is independent of stagnation pressure. The correlation thus being considered is:

$$\dot{m}_t = c(q_{\substack{SRI \\ CW}})^n (P_{t_2})^{(1-n)/2} \quad . \tag{43}$$

Computations of these coefficients, based on the data in Appendix C, leads to:

$$c = 0.0013 \pm 25\%$$

$$n = 0.64 \pm 5.3\%$$

$$(1-n)/2 = 0.18 \pm 5.3\%$$

with a percent standard deviation of

$$P_\sigma = +14\% \text{ and } -12.3\% \quad .$$

These values are appreciably different from those obtained independent of related exponents and shown in Fig. 34. This and the higher percent standard deviation suggests that such a correlation is of little value.

3. Measured Enthalpy Potential

Replacement of the cold wall heating rate by the enthalpy potential provides another possible correlation as indicated in Eq. (27). Determination of the appropriate coefficient leads to

$$b = 0.0010 + 130\%$$

$$u = 0.49 \pm 22\%$$

$$v = 0.41 \pm 10\%$$

with a percent standard deviation of

$$P_{\sigma} - +30\% \text{ and } -23\% \quad .$$

A comparison of the percent standard deviation with that found for the correlation involving the cold wall heating rate determined by SRI calorimeter, namely, +11% and -10%, shows that the measured enthalpy is not a satisfactory correlation parameter. Even elimination of the Boeing and General Electric data because of "coring" does not have any major effect in improving the correlation.

4. Facility Cold Wall Heating Rate

The correlation involving the facility calorimeter rather than the SRI calorimeter can also be tried on the phenolic-nylon. Its form would be similar to Eq. (22).

$$\dot{m}_t = a(q_{\underset{CW}{FAC}})^n (P_{t_2})^m \quad . \tag{44}$$

Appendix C has 32 sets of data from six facilities which can be used to determine the coefficients. The results of the computer program are:

$$a = 0.0034 \pm 27\%$$

$$n = 0.46 \pm 5.9\%$$

$$m = 0.18 \pm 8.0\%$$

with a percent standard deviation of

$$P_{\sigma} = \pm 8\% \quad .$$

A plot of these data is shown in Fig. 35.

The Martin replicate data are not plotted since the other parts of the triplicate sets are so nearly the same in value that they would fall on the other points. If these replicate data are added to the computer program the coefficients become

$$a = 0.0039 \pm 27\%$$

$$n = 0.44 \pm 5.8\%$$

$$m = 0.18 \pm 7.7\%$$

with a percent standard deviation of

$$P_{\sigma} = +9\% \text{ and } -8\% \quad .$$

This indicates that the Martin points are slightly out of line with the other data. The facility correlation appears to be a good one although it would be advantageous to use calorimeters, pressure probes, and ablation models all of the same size and configuration.

The round-robin results from Manned Spacecraft Center (see Appendix C) can be compared with the facility correlation even though they are subsonic. These data are shown in Fig. 36. As before, the solid and dotted lines indicate the supersonic correlation and the percent standard deviation of the data.

D. CHAR BEHAVIOR

The char density was calculated for each of the phenolic-nylon models and is included in Appendix C. The char density was found to increase, generally, with higher heating rates and higher surface temperatures. This is equivalent to saying that the char density increases with higher mass loss rates. Also it was noted that there was a stagnation pressure effect since the subsonic data from Manned Spacecraft Center, and the relatively high pressure supersonic data from ESB-Langley, represented the high and low extremes in char density.

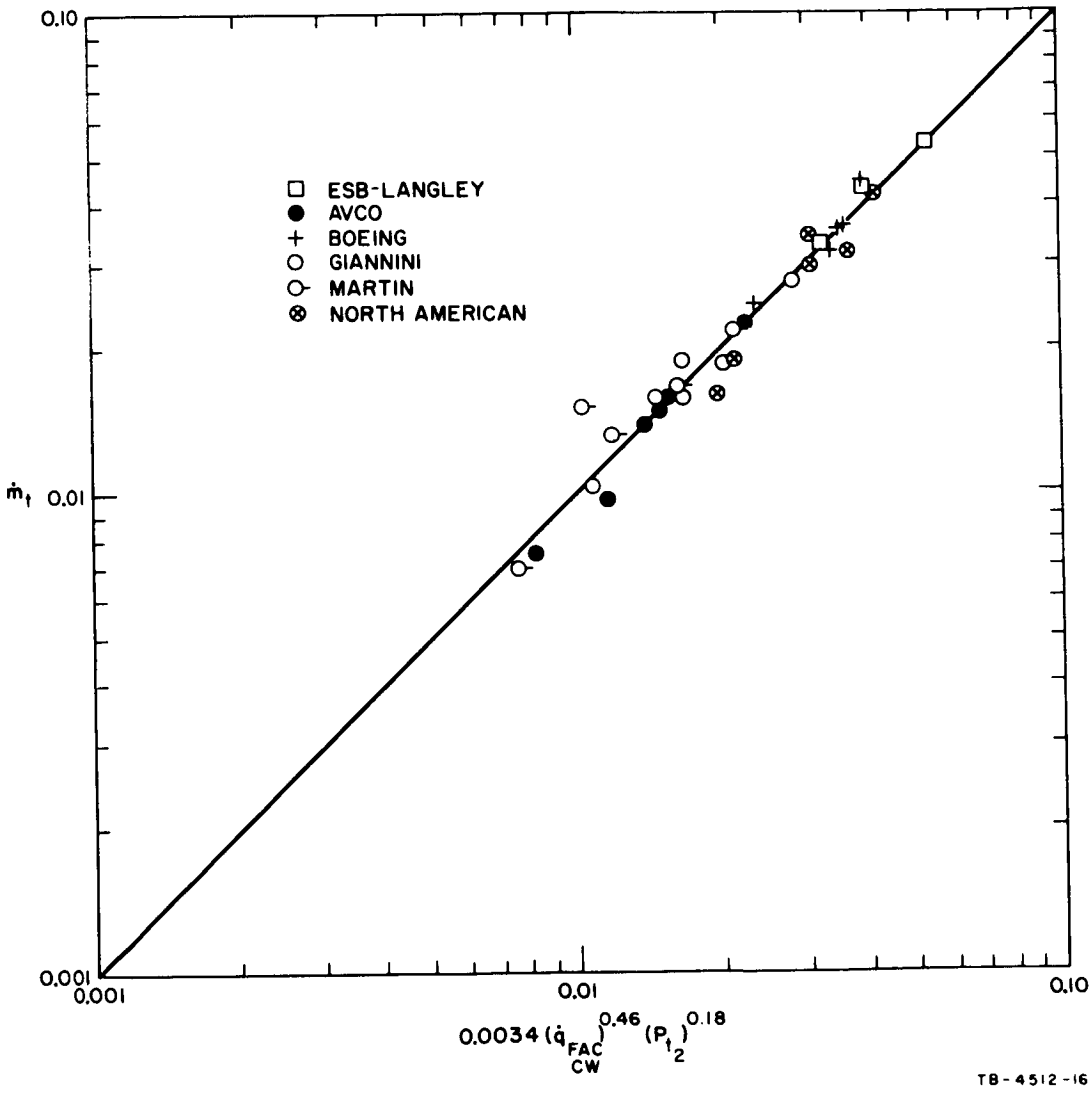

FIG. 35 MASS LOSS RATE CORRELATION FOR PHENOLIC-NYLON
(Facility Cold Wall Heating Rate)

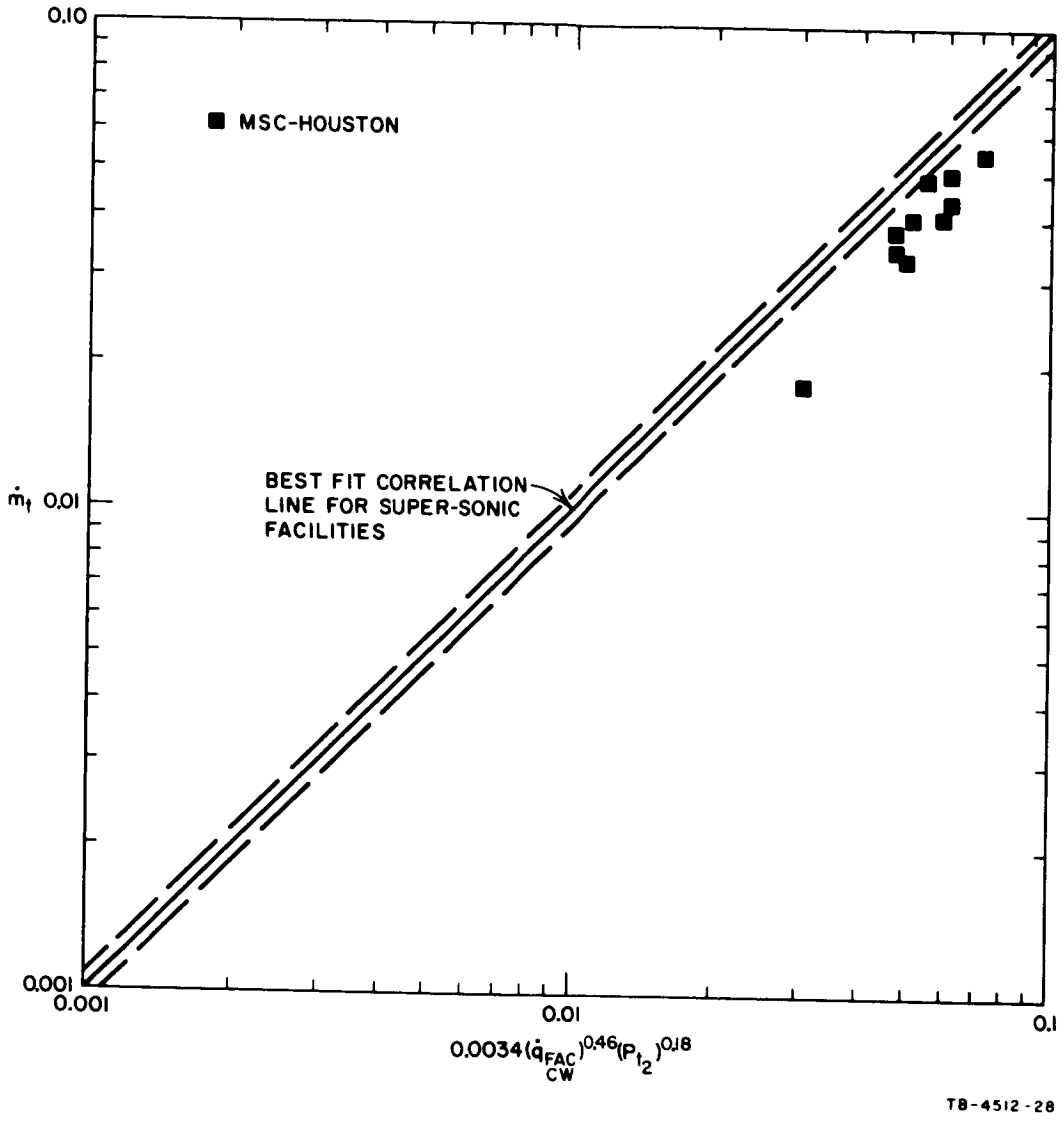

FIG. 36 MASS LOSS RATE CORRELATION FOR PHENOLIC-NYLON
(Results from Subsonic Facilities)

The analysis techniques that have been developed by Lundell[13] and others were used in an attempt to obtain tighter correlations on the phenolic-nylon results. These techniques are based on calculating mass loss rates for the various locations in the charring ablator.

The total mass loss rate ($\dot{m}_t$), as described previously, was from the relation:

$$\dot{m}_t = \frac{\Delta m}{At} \quad , \tag{45}$$

where Δm is the model core weight loss, A is core area, and t is run time. The char removal rate ($\dot{m}_{CR}$) was calculated with the relation:

$$\dot{m}_{CR} = \frac{\rho_{\underset{AV}{CR}} \Delta y_r}{t} \tag{46}$$

where $\rho_{\underset{AV}{CR}}$ is the average char density for each facility and Δy_{CR} is the char recession distance. The vapor production rate ($\dot{m}_V$) is then developed from:

$$\dot{m}_V = \dot{m}_t - \dot{m}_{CR}. \tag{47}$$

The char production rate ($\dot{m}_{CP}$) was calculated from:

$$\dot{m}_{CP} = \frac{\rho_{\underset{AV}{CR}} \Delta y_C}{t} \tag{48}$$

where Δy_C is the char thickness remaining on the model core.

The pyrolysis rate, $\dot{m}_p$, is from the relation

$$\dot{m}_p = \dot{m}_V + \dot{m}_{CP} \quad . \tag{49}$$

The above values were calculated for each phenolic-nylon model and are included in Appendix C. The pyrolysis rate ($\dot{m}_p$) was used in place of the total mass loss rate in various correlations, such as versus front surface temperature, but no reduction in data spread was realized.

A plot of the ratio ($\dot{m}_v/\dot{m}_p$) for various heating rates is included in Fig. 37 for the interest of materials evaluation groups. The ratio decreased with increasing heat flux and followed a pattern similar to the char density with the high pressure ESB-Langley results and the Manned Spacecraft Center subsonic results representing the extremes.

No other meaningful correlations were found between char parameters and environmental conditions.

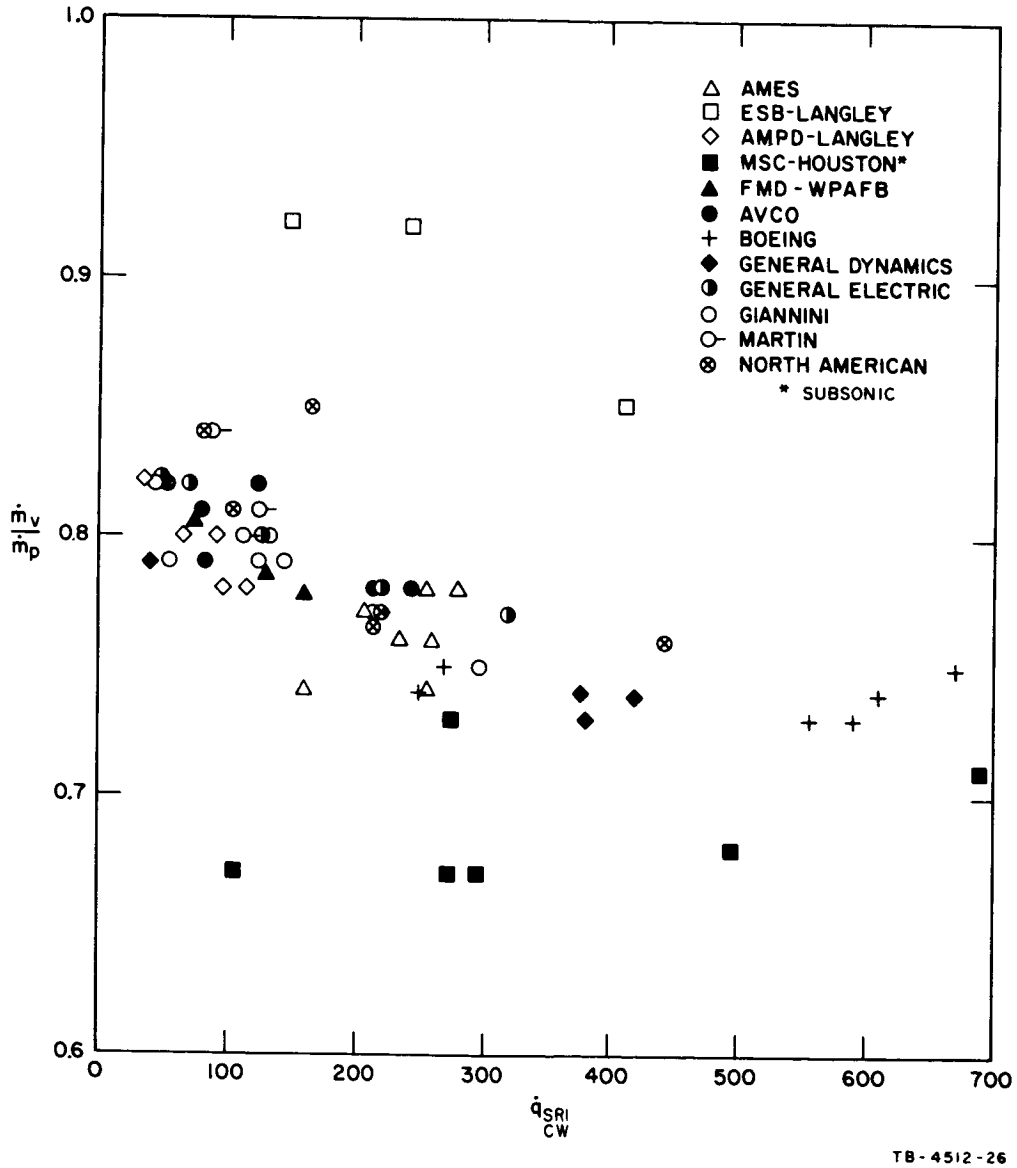

FIG. 37 RATIO OF PHENOLIC-NYLON VAPOR TO PYROLYSIS MASS LOSS RATE VERSUS HEAT TRANSFER RATE

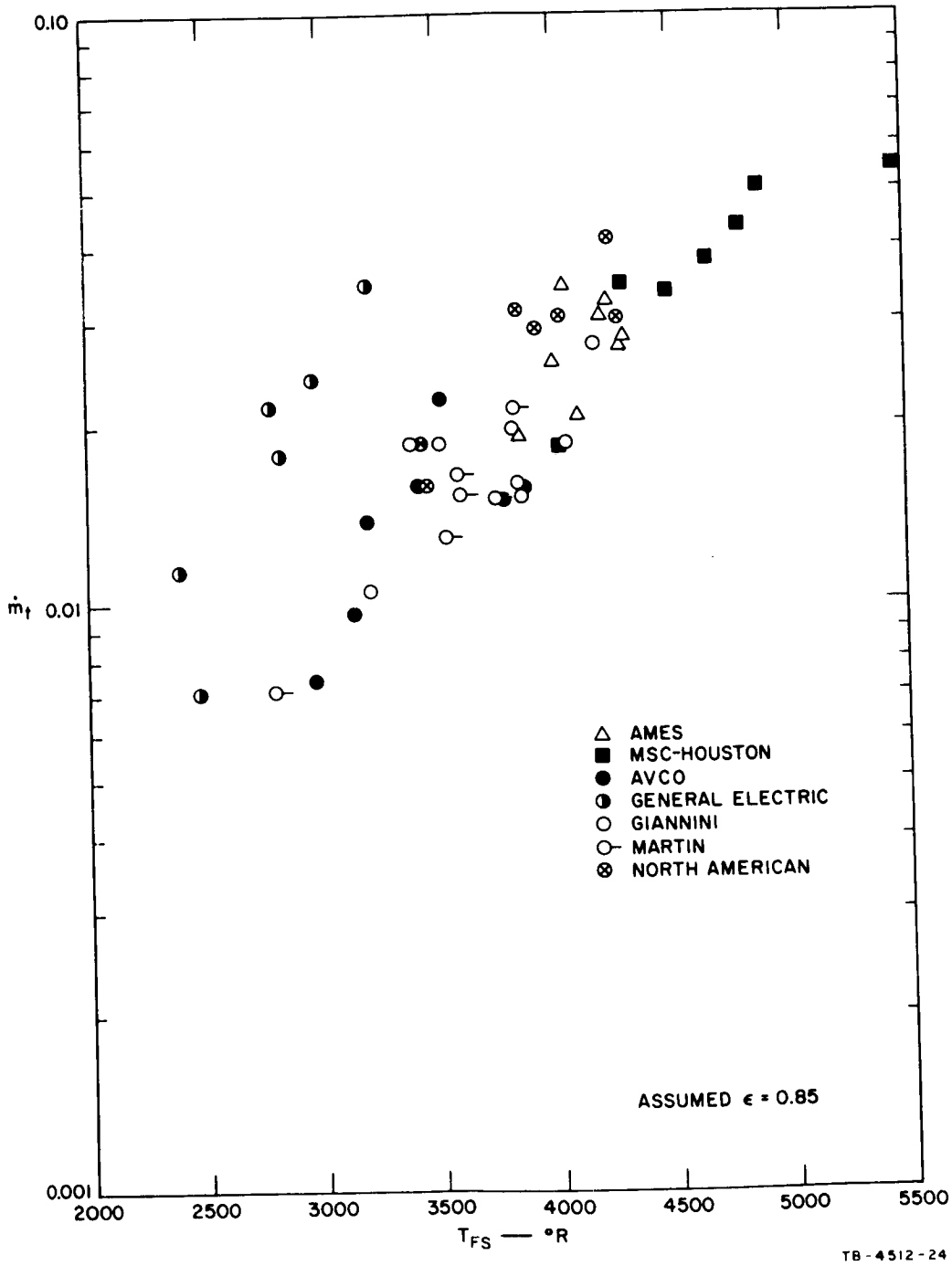

FIG. 38 EFFECT OF FRONT SURFACE TEMPERATURE ON THE MASS LOSS RATE OF PHENOLIC-NYLON

E. FRONT SURFACE TEMPERATURE

The reported front surface temperatures of the ablating phenolic-nylon models were adjusted to an assumed emissivity of 0.85 and corrected to absolute temperature in °Rankin. These data are included in Appendix C and are also correlated with the mass loss rate of the phenolic-nylon in Fig. 38. This graph indicates a reasonably good agreement in results for all facilities, with the exception of the data from General Electric where a different technique is used. In addition, when each facility is evaluated separately, there is less variation than for all groups viewed collectively. This indicates a fairly good precision within a facility, with possible differences in calibration techniques contributing to the group-to-group deviation.

The front surface temperature of the ablating Teflon was also received from five facilities and is included in Appendix B. These data, however, were not correlated because of the wide variation in results and the general concensus that such values are difficult to measure on Teflon.

F. BACK SURFACE TEMPERATURE RISE

The model back surface temperature was monitored at most facilities during an ablation run, and also as the model equilibrated in temperature after the run was completed. As a result, two back surface temperature rises are recorded in Appendix B: (1) the temperature rise at arc cutoff, and (2) the maximum equilibrium temperature rise after run completion. Numerous attempts were made to correlate the back surface temperature rise with various relations involving such variables as heating rate, run time, and core weight. These correlations gave extreme variations, both in facility-to-facility results and also within each group. It is believed that these variations resulted from: (1) a long core length that resulted in a low temperature response during the run, (2) side heating through the metal back plate on the model, and (3) the various methods used for mounting and holding the models.

REFERENCES

1. Winovich, W., NASA TN D2132, "On the Equilibrium Sonic-Flow Method for Evaluating Electric-Arc Air-Heater Performance," March, 1964

2. Hiester, N. K. and C. F. Clark, NASA Contractor Report NASA CR-99, "Relative Operating Capabilities of Selected Electric-Arc Reentry Environment Simulators," September, 1964

3. Fay, J. A., and F. R. Riddell, "Theory of Stagnation Point Heat Transfer in Disassociated Air," J. Aero. Sci. 25, 73-85 (1958)

4. Lees, L., "Laminar Heat Transfer Over Blunt Nosed Bodies at Hypersonic Flight Speeds," Jet Propulsion, 26, 259-69 (1956)

5. Yoshikawa, K., and E. Katzen, NASA TN D693, "Charts for Air-Flow Properties in Equilibrium and Frozen Flows in Hypervelocity Nozzles," April 1961

6. Jorgensen, L. and G. Baum, NASA TN D1333, "Charts for Equilibrium Flow Properties of Air in Hypervelocity Nozzles," September 1962

7. Stoney, W. E., and J. T. Markly, NACA TN4300, "Heat Transfer and Pressure Measurements on Flat-Faced Cylinders at a Mach No. of 2," July 1958

8. Goulard, R., "On Catalytic Recombination Rates in Hypersonic Stagnation Heat Transfer," Jet Propulsion, 28, 737-45, (1958)

9. Georgiev, S., H. Hildalgo, and M. Adams, AVCO Report 65, "On Ablating Heat Shields for Satellite Recovery," July 1959

10. Chapman, A., NASA TND 1520, "An Experimental Investigation of Several Ablation Materials in an Electric Arc-Heated Air Jet," April 1963

11. Steg, L. and H. Lew, "Hypersonic Ablation" May 1962, General Electric Space Sciences Laboratory Report R 62 SD 55

12. Vojvodich, N. and R. Pope, "The Influence of Ablation on Stagnation Region Convective Heating for Dissociated and Partially Ionized Boundary Layer Flows," Proceedings of the 1965 Heat Transfer and Fluid Mechanics Institute, University of California, Los Angeles, California, June 21-23, 1965.

13. Lundell, J., R. Wakefield, and J. Jones, "Experimental Investigation of a Charring Ablative Material Exposed to Combined Convective and Radiative Heating in Oxidizing and Nonoxidizing Environments," AIAA Publication CP9, Entry Technology Conference, Williamsburg and Hampton, Virginia, October 12-14, 1964

APPENDIX A

FACILITY INFORMATION AND INSTRUMENTATION USED FOR NASA ROUND-ROBIN ABLATION TESTS

APPENDIX A

FACILITY INFORMATION AND INSTRUMENTATION USED FOR NASA ROUND-ROBIN ABLATION TESTS

Appendix A tabulates, by facility, a description of each plasma arc jet heater. The tables first describe the arc heater and power supply, then nozzle and test chamber dimensions, as well as the vacuum system and insertion capability. The section of the table on instrumentation describes the instruments or procedures used to measure the parameters indicated.

The facilities are tabulated in the following order.

A- 1 Gas Dynamics Branch—Ames Research Center—NASA

A- 2 Entry Structures Branch—Langley Research Center—NASA

A- 3 Applied Materials and Physics Division—Langley Research Center—NASA

A- 4 Manned Spacecraft Center—NASA

A- 5 Flight Mechanics Division—Wright Patterson Air Force Base

A- 6 AVCO Corporation

A- 7 Boeing Company

A- 8 General Dynamics

A- 9 General Electric Corporation, Space Technology Center

A-10 Giannini Scientific Corporation

A-11 Martin Company

A-12 North American Aviation Incorporated

Appendix A

FACILITY INFORMATION AND INSTRUMENTATION USED FOR NASA ROUND-ROBIN ABLATION TESTS

	A-1	A-2	A-3	A-4
Facility	NASA-Ames Research Center	NASA-Langley Research Center Entry Structures Branch	NASA-Langley Research Center Applied Materials & Physics Div.	NASA-Manned Spacecraft Center
Location	Moffett Field, California	Langley Station, Hampton, Va.	Langley Station, Hampton, Va.	Houston, Texas
Tunnel Designation	Ames Entry Heating Simulator	Structures 2.5-Mach AC Arc Tunnel	6.6-in. Hypersonic Arc Heated Tunnel	MSC 1-Megawatt Arc Jet-Subsonic
Facility Personnel	B. H. Wick W. Winovich J. Chin	R. D. Ross R. D. Brown	G. M. Stokes R. Midden	D. H. Greenshields D. J. Tillian
Arc Heater - Design	NASA-Ames Design Magnetically Driven Arc	NASA-Langley Design 3 Phase, A-C	NASA-Langley Design Rotating Arc	Modified Giannini
- Electrode Material	Copper	Copper cathode and anode	Copper cathode and anode	Copper
- Stabilization	Magnetic field, 3500 gauss	Magnetic field, 2000 gauss	Magnetic field	Magnetic field and gas vortex
- Input Power Max.	1000 KW DC	3700 KW AC	1700 KW DC	1000 KW DC
Min.	150 KW DC	350 KW AC	900 KW DC	--
- Plenum Press., atm.	0.35 to 3.0	3 to 5	1.36 to 10.0	1 to 3
- Gas Flow Rates, pps	0.005 to 0.04	to 0.45	0 02 to 0.34	0.02 to 0.05
Power Supply - Type	DC Motor Generator	AC, 3 phase, 2400v	DC Batteries-1440-2.2v each	DC-Silicon Rectifiers-Saturable Core, Reactor Control 1500 KW
- Make			Exide	
- Max. amp.	3300 @ 300v	5000	6000	2000
Nozzle-Throat Diam., D_t, in.	0.742	1.04	0.538	Subsonic
- Exit Diam., D_e, in.	2.67	2.00	6.6	3.0
- D_t to D_e, in.	7.5	6.5	76	1.5
Nozzle Expansion Sect.	Contoured - Free Jet	Conical	--	--
D_e to Model Face, in.	1.156	1.5	1.37	1.5
Test Chamber-Diam., in.	31	8	24	None
- Length, ft	4	2.5	8	--
- Cooling	None	None	None	--
Vacumm System - Type	8200-c.f. sphere pumped down to 1 mm Hg	High pressure air ejector	12,000-c.f. sphere pumped down with Roots Blower	None
Capacity-cfm		0.25 lb air at 0.1 atm	1,400 cfm	--
Min. press. at no flow	1.0 mm Hg	--	0.50 mm Hg	--
Multiple Insertion Capability	2	1	2	2
Tunnel Instrumentation Input Power - volts	General Electric Volt Meter to C.E.C.	Wattmeter-Westinghouse-Hall effect transducer to Mosely recorder and Beckman magnetic tape recorder	Voltage divider to C.E.C. recorder	Nobotrol transducers to Bristol recorder and to Systems Engineering Lab. digital system
- amp.	General Electric Ammeter to C.E.C.	Current transformer to Easterline Angus recorder—indicate only	Mv shunt to transductors to C.E.C. recorder	Mv shunt to Bristol recorder

[illegible] - Water Flow	(NOTE: photographic record is continuously made of all indicating instruments such as volts, amps., and pressures)	Potter turbine meter to Fisher-Porter frequency converter to Beckman tape recorder	Potter turbine meter to Cox frequency meter to C.E.C. recorder	Hydropoise flow transducer to frequency converter and recorder. Analog to digital magnetic tape record of most test variables
- Temperature Rise	Not measured - Enthalpy measured by pressure rise method	Ch-Al thermocouples to Beckman tape recorder	Ch-Al thermocouples to C.E.C. recorder	
Enthalpy Probe	--	--	--	Enthalpy from Greyrad total enthalpy probe
Test Gas - Composition	Air	Air	Air	Nitrogen plus oxygen to equal air
- Flow rate	Venturi meters, Foxboro press. transducer, Wallace-Tierman gage	Orifice plates, Barton differential press. transducer to indicator and Beckman tape recorder	Std. orifice, press. transducers to C.E.C. recorder	Choked orifices, electrical press. transducers
- Temperature	Thermocouple monitor	Air Temperature to arc is monitored	Thermocouples ahead of orifice	---
Pressures - Plenum Pressure	Wallace-Tiernan 0-30 psia Statham transducer to CEC	Statham transducer to Brown recorder and Beckman	Transducer to CEC recorder	Subsonic - Not measured
- Nozzle exit press.	Not measured	Not measured	Not measured	Subsonic - Not measured
- Test chamber press.	McLeod gage	Statham Transducer to Beckman	Hasting thermopile	Subsonic - Not measured
- Model stagnation press.	Statham transducer 0-3 psia to CEC	Statham Transducer to Beckman	Statham Transducer to CEC recorder	Statham Press. Transducer
Model Temperature - Front surface	Radiometer No. 1 Pbs Detector 7950 to 8450 Å Radiometer No. 2 Pbs Detector 8100 to 8900 Å	Not measured	Not measured	Pyro optical pyrometer and Barnes R4D radiometer
Back Surface	Ch-Al to Brown Recorder	Ch-Al to Beckman, Constant temperature hot junction near tunnel	Ch-Al to CEC recorder	Ch-Al to tape recorder
SRI Calorimeter	SRI Calorimeter to CEC Recorder	SRI Calorimeter to Beckman tape recorder	SRI Calorimeter to CEC Recorder	
Facility Calorimeter - Type	Used SRI Calorimeter only	Transient, thin-shell (0.030-in.) wall thickness-Langley Design	Transient, thin-shell (0.080-in.) wall thickness-Langley Design	Hy-Cal Engineering asymptotic steady state
- Shape		Hemisphere	Hemisphere	Flat Face
- Surface Material		Stainless Steel	Stainless Steel	Constantan plus carbon black
- Shroud Diam., in.		1.5	2.0	1.0 in. plus 1.25 in. S.S. Shroud
- Sensing Diam., in.		1.5 Multiple Couples	2.0 Multiple Couples	0.15 in.
Run Time	Exposure time automatically controlled, models protected with water-cooled shield	Patch panel for varying run time with automatic model withdrawal	From C.E.C. recorder	Microswitch on sting to tape recorder
Camera	Kodak Cine Special 16 mm	Not run	Not run	Milliken

Appendix A Continued

	A-5	A-6	A-7	A-8
Facility	Wright-Patterson Air Force Base, Flight Mech. Div.	AVCO Corporation	Boeing Company	General Dynamics
Location	Dayton, Ohio	Wilmington, Mass.	Seattle, Washington	Fort Worth, Texas
Tunnel Designation	4-Mw Electro-Gas Dynamic Facility	Orbital Vehicle Reentry Simulators (OVERS)	Mini-Arc Model A in 1-2 Mw Altitude Chamber	Hyperthermal Research Facility
Facility Personnel	D. Zonars J. C. Beachler	R. R. John H. E. Hoercher M. G. Metzger	W. K. Klose J. C. Baker H. R. Givens	R. A. Stevens A. P. Madsen G. H. Hull
Arc Heater - Design	WPAFB design—similar to Linde N4000	AVCO design	Boeing design	Vidya design, concentric electrode
- Electrode Material	Copper and silver copper alloy	Thoriated tungsten cathode, copper anode	Tungsten cathode, copper anode	Copper
- Stabilization	Magnetic field plus gas vortex	Gas Vortex stabilization	Gas Stabilization at low mass flows (0.008 lb/sec), magnetic stabilization at higher flows	Magnetic
- Input Power Max.	2016 KW DC during these tests	500 KW DC	500 KW DC	1800 KW DC
Min.	1049 KW DC during these tests	15	65	250
- Plenum Press., atm	23.1 to 117 during these tests	0.013 to 0.13	0.10 to 0.50	0.5 to 34
- Gas Flow Rates, pps	0.08 to 1.0	0.0007 to 0.006	0.002 to 0.50	0.01 to 0.20
Power Supply - Type	DC, solid state rectifiers, Saturable reactor control	DC, silicon rectifiers	Four AC to DC generators, 840 KW @ 460v	Silicon rectifiers
- Make	A. O. Smith	Perkin	Reliance	General Dynamics
- Max. amp.	4000 @ 1000v; 1000 @ 5000v	2500 at 40-60v	800	4500
Nozzle Throat Diam., D_t, in.	0.375 in. $\leq$ 36 atm P_{t1} 0.165 in. $\geq$ 117 atm P_{t1}	1.0	0.70	0.50
- Exit Diam., D_e, in.	9.5	3.0	3.0	1.34
- D_t to D_e, in.	46.7	6.0	6.2	8.0
Nozzle Expansion Sect.	Contoured - Free Jet	Contoured - Free Jet	Contoured - Free Jet	Conical - Free Jet
D_e to Model Face, in.	0.375	3.62	2.50	Test in 2nd rhombus of supersonic nozzle
Test Chamber-Diam., in.	Free jet	24	28	52-in. cubic section
- Length, ft	1.5 ft to diffuser inlet plane	20	1.0 ft to diffuser inlet	4.3 ft to diffuser inlet
- Cooling	Water cooled	Water cooled	Water cooled	None on jacket heat exchanger after test chamber
Vacuum System - Type	Roots blowers plus Kinney and Allis Chalmers pumps	Vacuum tank approx. 36,000 cf pumped down to 0.5 mm Hg	Four-stage steam ejector	Five-stage steam ejector
- Capacity cfm	41,000 cfm @ 0.4 mm Hg	Throttling valve to control test chamber press.	0.04 lb/sec	10 lb/sec max.
		0.5 mm Hg	1.5 mm Hg	4 mm Hg

Multiple Insertion Capability	3	4	4	4
Tunnel Instrumentation				
Input Power - volts	Magnetics Inc. to Brown Recorder	Weston MO 273 to CEC and Magnetic tape recorder	Voltage Divider to Esterline-Angus Recorder	Voltage Divider to Brown Recorder
- amp	Magnetics Inc. to Brown Recorder	Weston MO 273 to CEC and Magnetic tape recorder	Shunt to Esterline-Angus Recorder	Shunt to Brown Recorder
Power Loss - Water Flow	Potter Turbine Flow Meters	Fisher Porter Rotameter	Potter Turbine Meters to Dymec Counter	Venturi - Flow Dyne V 32 1200 Wiancko Press. Transducer P2760 5-element thermopile
- Temp. Rise	Iron-Constantan Thermo-couples	Mercury thermometers and thermopile to CEC and magnetic tape	Differential thermocouples to LN Speedomax H recorder	
Enthalpy Probe	WPAFB Design	---	---	Greyrad Enthalpy Probe
Test Gas - Composition	Air	Nitrogen + oxygen to equal air	Nitrogen + oxygen to equal air	Nitrogen only for these tests
- Flow Rate	Hagan Flow Sections with ring balance readout of orifice ΔP	Standard orifice plates-Heise gages	Choked nozzles, Heise gages	Critical flow nozzles Wiancko Pressure Transducer P2701
- Temperature	---	---	---	---
Pressures - Plenum Pressure	Statham Transducer Bristol Recorder	Wallace and Tiernan gage	Not measured	Wiancko Transducer P2701
- Nozzle exit press.	Kaman Nuclear, Statham and CEC transducers	Not measured	Dynisco transducer to Speed-omax H	Not measured
- Test chamber press.	C.V.C. Magnevac	Wallace and Tiernan gage	Dynisco transducer to Speed-omax H	Wiancko Transducer P2701
- Model stagnation press.	Statham transducer	Micromanometer Infrared Devel. indicating and to Sanborn recorder	1.25-in.-diam. water-cooled pilot, Statham transducer to Speedomax H	Wiancko Transducer P2701
Model Temperature - Front Surface	Not measured for these tests	Micro-Optical Pyrometer Mo-95	Pyro 650 - Instrument Devel. Lab.	Optical pyrometer
- Back Surface	Ch-Al to MH 1612 Visicorder	Ch-Al to CEC and magnetic tape ice junction at tunnel	Ch-Al to Visicorder 1012	---
SRI Calorimeter	SRI cal. to MH 1612 Visi-corder	SRI cal. to CEC + magnetic tape	SRI cal. to Visicorder 1012	---
Facility Calorimeter				
- Type	Steady state - WPAFB design	Transient - AVCO design	Steady state - Boeing Design-water temp. rise	Transient - Gen. Dynamics design
- Shape	Hemisphere	Flat Face	Hemisphere	Flat Face
- Surface Material	Silver - Chemically cleaned	Copper	Platinum plating on copper	Copper slug - graphite shroud
- Shroud diam., in.	0.50	1.25	2.00	0.75, 1.9, and 1.25 in.
- Sensing diam., in.	0.50	0.375	0.74	Slug Diam. / Shroud Diam. = 0.5
Run Time	Visicorder time reference	Stop watch + CEC time reference	Stop watch	Facility timer Electronic timer Recorder time reference
Camera	---	Arriflex 16	---	Not run

Appendix A Concluded

	A-9	A-10	A-11	A-12
Facility	General Electric Corp.	Giannini Scientific Corp	Martin Company	North American Incorporated
Location	Valley Forge, Penna.	Santa Ana, California	Baltimore, Maryland	Los Angeles, California
Tunnel Designation	Hypersonic Arc Tunnel	Plasma Arc Hyperthermal Test Facility - High Enthalpy Facility	200-KW Plasma Tunnel Facility	1-Mw Hyperthermal Electric-Arc Tunnel
Facility Personnel	M. J. Engle J. W. Metzger	S. L. Grindle	A. Guido G. Guenterberg	J. W. Van Camp T. T. Yokoi
Arc Heater - Design	G.E. Design - Tandem Gerdien	Giannini Design	Giannini MK 4	Thermal Dynamics
- Electrode Material	Graphite	Tungsten cathode-copper anode	Thoriated tungsten cathode Copper anode	Thoriated tungsten cathode Copper anode
- Stabilization	Electrical ballast and gas stabilization	Gas vortex stabilization	Gas vortex stabilization	Gas vortex stabilization
- Input Power Max	500 KW DC	1000 KW DC	200 KW DC	650 KW DC
Min	75	35	10	65
Plenum Press. atm	1.0 to 1.6	0.02 to 0.36	0.005 to 0.20	0.35 to 5.5
Gas Flow Rates, pps	0.001 to 0.0020	0.0005 to 0.010	0.001 to 0.010	0.02 to 0.2
Power Supply - Type	Mercury Rectifier	25-40 KW AC to DC Selenium Rectifiers	320 KW AC to DC Selenium Rectifiers	8-125 KW AC to DC Silicon Rectifiers
- Make	---	Miller	Miller	A. O. Smith
- Max. amp	2200	3000	3000	2500
Nozzle-Throat Diam., D_t, in.	0.156	1.0	0.50 and 1.0	0.70
- Exit Diam., D_e, in.	1.19 and 5.0	3.0	1.50 and 3.0	2.50
- D_t to D_e, in.	2.76 and 13.5	6.18	3.0 and 6.0	11.0
- Nozzle Expansion Sect.	Conical, Free Jet	Contoured, Free Jet	Contoured, Free Jet	Contoured, Free Jet
D_e to Model Face, in.	0.625	2.12	1.50	0.50
Test Chamber-Diam., in.	12	30	30	48
- Length, ft	Approx. 10	6	8	8
- Cooling	None	Water-Cooled	None	Water-Cooled jacket plus exit heat exchanger
Vacuum System - Type	Stokes Pump plus Roots Blower	Kinney Pumps	Roots Blower plus Beach Russ vacuum pumps	5 Kinney vacuum pumps (KD 850)
- Capacity, cfm	5000 cfm	9000 cfm	3300 cfm	4200 cfm
- Min. Press. at no flow	0.025 mm Hg	0.2 mm Hg	0.03 mm Hg	---
Multiple Insertion Capability	1	3	3	2
Tunnel Instrumentation				
- Input Power	Enthalpy measured with total			
- volts	Enthalpy Calorimeter, G.E. design, measures heat content of entire gas stream	Westinghouse PX 161	Sensitive Research Inst CEW 74	Greibach Instrument Corp Mo 700
- amp		Westinghouse PX 161	Sensitive Research Inst. CEW 74, Westinghouse shunt	Greibach Instrument Corp Mo 700

- Power Loss, water flow	Fisher Porter Rotameter (gas flow)	Hydropoise Turbine Meter to Erie Electronic Counter	Potter Turbine Meters to frequency converter to Digetec Readout	Potter Turbine Meter
- Temperature Rise	Ch-Al thermocouples to Midwest Instrument Oscillograph	I-C couples to Brown Multi-point recorder	Pt. resistance thermometers Zener diode voltage supply	I-C couples to MHD panel
Enthalpy Probe	See Above	---	---	---
Test Gas - Composition	Air	Nitrogen + oxygen to equal air	Nitrogen + oxygen to equal air	Nitrogen + oxygen to equal air
- Flow Rate	Fisher Porter Rotameters	Standard orifice plates to Heise gage	Critical flow orifices - Heise gages	Quantomics Turbine Meters Digital to analogue converter readout
- Temperature	Thermocouples to Midwest Inst. Oscillograph	---	Gas temperature controlled to 90°F	Pt-Rh couples
Pressures - Plenum Press.	Computrain Transducer to Midwest	Wallace and Tiernan	Merriam Hg Manometer	Wallace and Tiernan
- Nozzle Exit Press.	Not run	Wallace and Tiernan	Trans Sonics - Equi-Bar Meter and Transducers	Consolidated Vacuum Corp.
- Test Chamber Press.	Not run	Wallace and Tiernan	Trans Sonics - Equi-Bar Meter and Transducers	Consolidated Vacuum Corp.
- Model stagnation press.	Oil and Hg Manometers	Wallace and Tiernan diff. press. gage, Statham press. Transducer to Texas Inst. Recorder	Trans Sonics - Equi-Bar	Merriam Hg Manometer SRI Pitot - Baldwin Transducer to Brown Recorder
Model Temperature - Front Surface	G.E. Design, two-color pyrometer, 4800 and 7500 angstroms	Leeds and Northrup optical pyrometer	Instrument Devel Lab. Pyro 650 L-N Total Radiation Pyrometer Mo 8891	Thermodot TD-9H optical pyrometer to Brown Recorder
- Back Surface	Ch-Al to Midwest Inst. Oscillograph	Ch-Al to Texas Inst. F4W Recorder	Ch-Al to Bristol Recorder All couples referenced to 150°F controlled junction	Ch-Al to Brown Recorder
SRI Calorimeter	SRI cal. to Midwest Inst. Oscillograph	SRI cal. to Texas Inst. F4W Recorder, 150 Fºcold junction	SRI cal. to Bristol Recorder	SRI cal. to Brown 1/4-sec Recorder
Facility Calorimeter - Type	Transient - G.E. Design-other slug shapes were also used	Steady State Giannini Design-Water Temp. Rise	Steady State Martin Design Heat Meter Type Two couples separated axially	Steady State - Thermal Dynamics Design-Water Temp. Rise
- Shape	Flat Face	Hemisphere	Flat Face	Hemisphere
- Surface Material	Copper	Copper	Copper	Copper
- Shroud Diam., in.	1.25	2	1.0	0.5
- Sensing Diam., in.	0.25 diam. x 0.25 long copper slug surrounded with 0.125-in. thick plastic	2	0.375	0.5
Run Time	Industrial Timer - Automatic shutoff and sting withdrawal	Stopwatch plus electric timer with switch on sting	Bayside Timers, Inc. with switch on sting, automatic shutoff	Standard Timer with switch on sting
Camera - Type	Not run	Bolex H-16 Movie Camera	Giannini Scientific-Flight Research Div. Model IV-E 35 mm multiple exposures	Mitchell 16 mm movie camera

APPENDIX B

TUNNEL CALIBRATION AND TEST DATA

APPENDIX B

TUNNEL CALIBRATION AND TEST DATA

This appendix consists of separate tables containing the data supplied by each participating facility, plus information on the ablation models determined at Stanford Research Institute. The latter data constitute the last five columns of the tables. The headings of the tables are not completely uniform since individual organizations reported their data somewhat differently.

One other note of interest is the assignment of calibration run numbers by the Institute so that these runs could be identified in other tabulations. Other remarks applicable to the specific columns are indicated in the footnotes to the tables.

The order of the tables is as follows.

	MODEL NO.	TOTAL ENTHALPY h_t (Btu lb^{-1})	HEAT TRANSFER RATE $\dot{q}_{cw}$ (Btu sec^{-1} ft^{-2})	MODEL STAGNATION PRESSURE P_{t_2} (atm)	PLENUM PRESSURE P_{t_1} (atm)	GAS FLOW RATE W (lb sec^{-1})
			SRI CALORIMETER	SRI PITOT PROBE		
		(1)		(2)		
Teflon Models	T96	5,500	212	0.0844	0.418	0.0114
	T97	6,400	162	0.0878	0.435	0.0112
	T98	1,400	58	0.0794	0.393	0.0180
	T99	3,400	132	0.0862	0.427	0.0143
	T100	4,900	347	0.177	1.37	0.0376
	T103	3,100	110	0.0824	0.408	0.0142
Phenolic-Nylon Models	P7A2	5,400	212	0.0838	0.415	0.0113
	P7A3	6,300	163	0.0834	0.413	0.0105
	P7A4	5,200	256	0.164	0.810	0.0227
	P7A5	5,000	236	0.159	0.789	0.0217
	P7A6	4,900	235	0.157	0.776	0.0217
	P7A7	5,850	251	0.159	0.789	0.0191
	P7B1	5,200	261	0.162	0.803	0.0206
	P7B2	4,650	281	0.171	1.34	0.0374

(1) Enthalpy calculated by pressure rise method. Ref: TND 2132.
(2) Obtained from ratio of stagnation pressure to total pressure measured with SRI pitot probe for similar conditions
(3) Temperature data from radiometer No. 1 was believed to be more reliable and was used for all correlations.

	MODEL NO.	TOTAL ENTHALPY h_t (Btu lb^{-1})				HEAT TRANSFER RATE $\dot{q}_{cw}$ (Btu sec^{-1} ft^{-2})		MODEL STAGNATION PRESSURE P_{t_2} (atm)
						CALORIMETER		FACILITY PITOT PROB
						Facility	SRI	
		(1)	(2)	(3)	(4)	(5)	(6)	
Teflon Models	T26	1,910	2,100	2,000	1,900	209	245	1.05
	T27	2,955	3,000	3,050	2,750	360	410	1.18
	T28	1,365	1,450	1,270	1,370	136	145	0.92
	T29	1,380	1,450	1,270	1,380	136	145	0.92
Phenolic-Nylon Models	P6A2	1,400	1,450	1,270	1,370	136	145	0.92
	P6A7	3,195	3,000	3,050	2,750	360	410	1.18
	P6B1	--	2,100	--	--	209	245	1.05

(1) Enthalpy by heat balance method.
(2) Enthalpy by sonic throat method. Ref: TND 1333.
(3) Enthalpy calculated from facility calorimeter.
(4) Enthalpy from pressure rise method Ref: TND 2132.
(5) Facility thin shell transient calorimeter, 1.5-in. hemisphere adjusted by SRI to 1.25-in. flat face $\dot{q}_{FF} = 0.55\ \dot{q}_{FAC}\ (1.5/1.25)^{0.5}$ measured during calibration runs.
(6) SRI calorimeter measured during calibration run.

NOTE: Facility had single insertion capability so data on each variable were obtained during separate runs.

Table B-1

TUNNEL CALIBRATION AND TEST DATA REPORTED BY AMES RESEARCH CENTER—NASA
Ref: Data on Ames Test 51, Runs 55 to 75

FRONT SURFACE TEMPERATURE T_{FS} $\epsilon = 0.85$ (°F)		MAXIMUM EQUILIBRIUM TEMPERATURE RISE AFTER RUN COMPLETION (°F)	RUN TIME t (sec)	CORE WEIGHT LOSS (g)	CORE CHAR WEIGHT (g)	RECESSION (in.)	CHAR THICKNESS (in.)	PYROLYSIS ZONE (in.)
Rad. No. 1	Rad. No. 2							
		98	30.9	2.102		0.178		
		95	31.9	1.786		0.152		
		--	30.2	1.006		0.081		
		101	28.6	1.876		0.159		
		138	40.0	3.523		0.314		
		91	30.1	1.725		0.138		
(3)								
3,640	4,040	64	61.1	1.224	0.332	0.087	0.148	0.070
3,390	3,710	152	41.4	0.769	0.190	0.027	0.113	0.055
3,840	4,140	186	38.4	1.040	0.307	0.078	0.122	0.055
3,770	4,090	156	23.2	0.736	0.231	0.032	0.110	0.045
3,590	3,970	121	15.6	0.521	0.143	0.022	0.073	0.030
3,540	3,880	157	27.6	0.684	0.199	0.032	0.099	0.045
3,830	4,140	186	38.6	1.023	0.317	0.063	0.136	0.060
3,740	4,080	198	30.3	0.900	0.245	0.064	0.105	0.050

Table B-2

TUNNEL CALIBRATION AND TEST DATA REPORTED BY ENTRY STRUCTURE BRANCH-LANGLEY RESEARCH CENTER—NASA
Ref: Letter Report on Runs 30 to 39

ARC CHAMBER PRESSURE P_{t_1} (atm)	GAS FLOW RATE W (lb sec^{-1})	RUN TIME t (sec)	CORE WEIGHT LOSS (g)	CORE CHAR WEIGHT (g)	RECESSION (in.)	CHAR THICKNESS	PYROLYSIS ZONE (in.)
3.28	0.254	20	2.875		0.256		
3.69	0.254	20	4.213		0.371		
2.87	0.254	19.6	1.806		0.151		
2.87	0.257	30	2.909		0.259		
2.87	0.257	40	1.287	0.080	0.158	0.050	0.030
3.69	0.254	20	1.033	0.149	0.105	0.077	0.035
3.28	--	40	1.659	0.102	0.212	0.055	0.030

	MODEL NO.	TOTAL ENTHALPY h_t (Btu lb^{-1})		HEAT TRANSFER RATE $\dot{q}_{cw}$		MODEL STAGNATION PRESSURE P_{t_2} (atm)	PLENUM PRESSURE P_{t_1} (atm)
				CALORIMETER		SRI Pitot Probe	
				Facility	SRI		
		(1)	(2)			(3)	
Teflon Models	T1	3,686	3,650		68	0.0483	3.83
	T4	2,056	2,550		51	0.110	9.30
	T5	2,216	2,550		37	0.0434	3.70
	T6	5,815	5,150		93	--	3.52
	T7	3,150	3,600		88	0.1302	10.50
	T8	3,187	3,300		65	0.0454	3.60
	T11	8,503	5,300		94	0.020	1.52
	T61	4,782	6,600		98	0.069	5.86
Phenolic-Nylon Models	P2A4	2,218	2,500		37	0.0431	3.67
	P2A5	5,012	4,900		97	--	3.47
	P4B3	4,382	6,000		113	0.069	5.86
	P5B1	7,670	6,400		77	0.0221	1.75
	P5B3	6,031	5,300		93	--	3.54
	P5B4	4,900	4,900		102	--	3.50
	P5B5	3,478	3,650		67	0.0495	3.93
	P5B6	3,586	3,500		63	0.0490	3.90
	P5B7	2,985	3,400		91	0.1262	10.10
	SRI Calib. Run No.			(4)			
Tunnel Calibration Runs	3C1	5,430	4,900	95	106	--	3.54
	3C2	3,731	3,300		67	0.0454	3.60
	3C3	2,300	2,700		36	0.0442	3.76
	3C4	2,035	2,650		51	0.110	9.30
	3C5	2,721	2,500		84	0.1302	10.50
	3C6	5,025	5,300		91	0.0480	4.10
	3C7	7,143	6,600		86	0.0228	1.74

(1) Enthalpy by heat balance method.
(2) Enthalpy by sonic flow method. TND 2132
(3) Based on results obtained with SRI pitot pressure probe in tunnel calibration runs.
(4) Facility thin shell calorimeter, 2-in.-diameter hemisphere adjusted to 1.25-in. flat face.

$$\dot{q}_{FF} = 0.55\, \dot{q}_{FAC}\, (2.0/1.25)^{0.5}$$

Table B-3

TUNNEL CALIBRATION AND TEST DATA REPORTED BY AMPD-LANGLEY RESEARCH CENTER—NASA

Ref: Data on Runs 288 to 334 in 20-in. HAHT

GAS FLOW RATE $\dot{W}$ (lb sec^{-1})	BACK SURFACE TEMPERATURE RISE AT ARC CUTOFF (^{o}F)	RUN TIME t (sec)	CORE WEIGHT LOSS (g)	CORE CHAR WEIGHT (g)	RECESSION (in.)	CHAR THICKNESS (in.)	PYROLYSIS ZONE (in.)
0.0656	2	31.0	0.972		0.087		
0.1817	3	29.3	0.764		0.067		
0.0732	4	31.5	0.529		0.048		
0.052	10	28.9	1.102		0.096		
0.179	9	30.2	1.473		0.129		
0.0644	2	30.8	0.932		0.083		
0.0225	2	31.0	0.858		0.075		
0.0789	5	37.0	1.388		0.122		
0.0727	67	136.8	0.974	0.191	0.041	0.111	0.060
0.0525	6	28.5	0.415	0.114	0.011	0.062	0.042
0.0825	--	32.6	0.402	0.105	0.015	0.058	0.040
0.023	--	16.6	0.321	0.076	0.012	0.042	0.033
0.052	20	58.6	0.769	0.200	0.024	0.106	0.053
0.053	2	15.1	0.265	0.074	0.008	0.038	0.025
0.0672	46	98.1	0.992	0.220	0.052	0.120	0.062
0.0677	42	99.1	0.975	0.210	0.043	0.119	0.065
0.1778	22	65.4	0.916	0.212	0.045	0.112	0.056
0.0535							
0.0645							
0.0730							
0.1801							
0.2081							
0.0598							
0.0234							

	MODEL NO.	TOTAL ENTHALPY h_t (Btu lb^{-1})	HEAT TRANSFER RATE $\dot{q}_{cw}$ (Btu sec^{-1} ft^{-2})			MODEL STAGNATION PRESSURE P_{t_2} (atm)
			CALORIMETER			FACILITY PITOT PROBE
			Facility		SRI	
		(1)	(2)			
Teflon Models	T47	5,000	300			1.0
	T48	8,818	525			1.0
	T51	12,449	807			1.0
	T53	5,493	436			1.0
	T54	7,500	528			1.0
Phenolic-Nylon Models	P4B2	7,701	540			1.0
	P4B4	6,037	478			1.0
	P4B5	7,527	534			1.0
	P4B6	5,064	316			1.0
	P4B7	5,424	413			1.0
	P8B2	5,800	295			1.0
	P8B4	4,510	115			1.0
	P8B5	5,800	295			1.0
	P8B6	5,876	300			1.0
	P9A3	12,068	746			1.0
	P9A4	5,281	350			1.0
Teflon Models (4)	1	13,273	783			1.0
	2	4,266	300			1.0
	3	5,001	280			1.0
	4	8,378	529			1.0
	5	13,146	657			1.0
	6	5,864	320			1.0
	7	7,419	506			1.0
	8	13,043	793			1.0
	SRI Calib. Run No.			(5)	(6)	
Calorimeter Calibration Runs	4C1	4,830	315	331		1.0
	4C2	6,568	470	463		1.0
	4C3	11,638	652	616		1.0
	4C4	5,223	330		331	1.0
	4C5	7,505	497		381	1.0
	4C6	13,300	778		698	1.0
	4C7	5,486	337		275	1.0
	4C8	5,760		280	283	1.0
	4C9	5,380		323	296	1.0
	4C10	5,440		307	181	1.0
	4C11	5,025	137		134	1.0
	4C12	6,525	345		325	1.0
	4C13	11,681	550		504	1.0

(1) Enthalpy by heat balance method
(2) Facility Hy-Cal asymptotic calorimeter
(3) Measured by MSC, Houston
(4) Teflon models furnished by MSC-similar dimensions as SRI model

Table B-4

TUNNEL CALIBRATION AND TEST DATA REPORTED BY MANNED SPACECRAFT CENTER, HOUSTON—NASA

Ref: Report ES3, September 3, 1964

FRONT SURFACE TEMPERATURE T_{Fs} (°F)	RUN TIME t (sec)	CORE WEIGHT LOSS (g)	CORE CHAR WEIGHT (g)	RECESSION (in.)	CHAR THICKNESS (in.)	PYROLYSIS ZONE (in.)	MODEL DISTANCE FROM NOZZLE EXIT (in.)
(ϵ = 1.0) (7)							
900	31.3	1.995		0.184			1.5
400	29.4	3.290		0.305			1.5
--	30.0	4.221		0.389			1.5
1,500	31.7	3.200		0.296			1.5
1,900	29.4	3.329		0.303			1.5
(ϵ = 0.8) (8)							
4,430	12.8	0.623	0.275	0.028	0.104	0.050	1.5
5,070	30.2	1.184	0.456	0.085	0.160	0.083	1.5
4,342	30.3	1.271	0.483	0.092	0.192	0.075	1.5
4,025	22.0	0.728	0.324	0.030	0.127	0.070	1.5
--	4.6	0.213	0.079	0.004	0.037	0.020	1.5
4,218	32.7	0.973	0.456	0.057	0.156	0.075	1.5
3,552	31.9	0.570	0.248	+0.004	0.108	0.080	1.5
3,820	15.0	0.504	0.243	0.019	0.090	0.045	1.5
3,733	10.0	1.227	0.270	0.061	0.163	0.082	1.5
5,025	20.0	1.059	0.407	0.073	0.145	0.055	1.5
--	8.5	0.345 (3)	0.129	0.005	0.062	0.030	1.5
	18.1	2.28					2.0
	34.2	3.27					2.0
	28.8	2.29					1.5
	29.8	3.39					1.5
	29.2	3.59					1.5
	31.9	2.61					1.5
	31.0	3.39					1.5
	27.8	3.95					1.5
							1.5
							1.5
							1.5
							1.5
							1.5
							1.5
							1.5
							1.5
							1.5
							1.5
							1.5
							1.5

(5) Heat transfer data determined on MSC slug calorimeter similar to SRI design
(6) Heat transfer data determined on SRI calorimeter
(7) Measured with radiometer
(8) Measured with optical pyrometer

	MODEL NO.	TOTAL ENTHALPY h_t (Btu lb^{-1})		HEAT TRANSFER RATE $\dot{q}_{cw}$ (Btu sec^{-1} ft^{-2})		MODEL STAGNATION PRESSURE P_{t_2} (atm)		PLENUM PRESSURE P_{t_1} (atm)
				CALORIMETER		PITOT PROBE		
				Facility	SRI	Facility	SRI	
		(1)	(2)		(3)			
Teflon Models	T33(9)	1,597	2,177		64.7	0.0996		116.5
	T34	2,500	2,403		88	0.1493		35.9
	T35	1,971	2,034		59.2	0.0962		23.1
	T36	3,281	5,137		190.2	0.1434		35.7
	T37(9)	--	3,811		144	0.152		35.4
Phenolic-Nylon Models	P1A2	4,994	13,533		651.4	0.2338		16.75
	P1A4	2,908	3,854		143.4	0.1481		34.0
	P1A6	2,978	4,018		152.6	0.1531		36.0
	P1A7	2,945	3,337		126.3	0.1547		35.9
	P1A8	2,794	3,367		126.3	0.1513		35.4
	P6B4	1,827	2,538		76.3	0.0999		117.0
	P1A5	--	4,346		269.3	0.4059		43.5
	SRI Calib. Run No.			(4)				
Tunnel Calibration Runs	5C1	1,760	2,327	98.5	86.5(5)	0.1448		35.4
	5C2	2,950	3,962	164.0	150.0(5)	0.1520		35.4
	5C3	2,880	3,937	189.0	149.0(3)	0.1520		35.6
	5C4	2,820	3,648	202.5	136.5(6)	0.1495		35.6
	5C5	1,760	--	--	--	0.1369	0.1377	35.9
	5C6	4,562	15,511	--	660.8(5)	0.1828		19.6
	5C7	4,900	11,491	598.4(5)	488.0(3)	0.1828		19.1
	5C8	--	3,984	249.3(7)	242.2(3)	0.3914		41.5

(1) Enthalpy by heat balance method.

(2) Enthalpy calculated from SRI heat transfer data.

(3) SRI calorimeter with nickel surface identical to SRI calorimeter furnished all other facilities.

(4) Facility calorimeter, silver surface, 1-in.-diameter hemisphere, results adjusted by SRI to equal 1.25-in.-diameter flat face with relation $\dot{q}_{FF} = 0.55\ \dot{q}_{FAC}\ (1.0/1.25)^{0.5}$.

(5) SRI design calorimeter, silver surface.

(6) SRI design calorimeter, silicon monoxide surface.

(7) SRI design calorimeter, copper surface.

(8) No heat shield on aft end of ablation model.

(9) Model T33 was designated T33A in WPAFB data and T37 was designated T33 in WPAFB data.

Table B-5

TUNNEL CALIBRATION AND TEST DATA REPORTED BY FLIGHT MECHANICS DIVISION, WRIGHT-PATTERSON AIR FORCE BASE.

Ref: Data on Runs FDM 4 to 17

GAS FLOW RATE W (lb sec^{-1})	BACK SURFACE TEMPERATURE RISE AT ARC CUTOFF (^{o}F)	RUN TIME t (sec)	D_t (in.)	CORE WEIGHT LOSS (g)	CORE CHAR WEIGHT (g)	RECESSION (in.)	CHAR THICKNESS (in.)	PYROLYSIS ZONE (in.)
0.220	0.18	28.80	0.165	0.837		0.074		
0.297	0	28.73	0.375	1.384		0.120		
0.223	2.20	30.82	0.375	0.968		0.085		
0.282	0	30.23	0.375	2.181		0.193		
0.285	10.07	29.28	0.375	1.821		0.161		
0.280	396.0(8)	53.93	0.375	2.015	0.555	0.159	0.189	0.070
0.277	1.76	27.28	0.375	0.559	0.139	0.022	0.076	0.054
0.297	4.17	40.34	0.375	0.743	0.200	0.037	0.096	0.072
0.298	0.88	23.36	0.375	0.484	0.128	0.019	0.065	0.052
0.298	0.44	16.19	0.375	0.362	0.092	0.013	0.048	0.036
0.211	6.15	58.93	0.165	0.759	0.148	0.039	0.086	0.082
--	3.52	22.56	0.375	0.696	0.170	0.030	0.097	0.045
0.325			0.375					
0.285			0.375					
0.273			0.375					
0.272			0.375					
0.281			0.375					
0.233			0.375					
0.235			0.375					
--								

	MODEL NO.	TOTAL ENTHALPY h_t (Btu lb^{-1})	HEAT TRANSFER RATE $\dot{q}_{cw}$ (Btu sec^{-1} ft^{-2})		MODEL STAGNATION PRESSURE P_{t_2} (atm)	PLENUM PRESSURE P_{t_1} (atm)	NOZZLE EXIT PRESSURE P_e (atm)	GAS FLOW RATE W (lb sec^{-1})
			CALORIMETER		SRI PITOT PROBE			
			Facility	SRI				
		(1)	(2)		(3)			
Teflon Models	T18	4,600	104	74	0.0250	0.121	0.0010	0 0050
	T14	5,000	122	82	0.0255	0.137	0.00092	0.0057
	T17	14,500	322	200	0.0140	0.0697	0.00145	0.0029
	T16	9,800	202	127	0.0150	0.0841	0.00120	0.0035
	T15	10,400	102	85	0.0075	0.0378	0.00105	0.0015
	T13	5,200	44	50	0.0075	0.0426	0.00066	0.0022
Phenolic-Nylon Models	P2B1	4,700	116	80	0.025	0.137	0.00092	0.0057
	P2B3	5,100	112	84	0.025	0.135	0.00079	0.0057
	P2B4	5,100	117	84	0.0255	0.137	0.00079	0.0057
	P2B2	14.500	317	215	0.014	0.0697	0.00145	0.0029
	P2B5	10,100	100	84	0.0075	0.0371	0.00105	0.0015
	P2B6	15,000	155	125	0.0066	0.0341	0.00120	0.0014
	P2B7	4,900	47	51	0.0075	0.0429	0.00066	0.0022

(1) Enthalpy measured by energy balance method.

(2) AVCO design transient type calorimeter, 1.25-in.-diameter flat face shape, 0.375 heated diameter, copper surface.

(3) 1.25-in.-diameter uncooled SRI pitot probe used for all stagnation pressure measurements.

	MODEL NO.	TOTAL ENTHALPY h_t (Btu lb^{-1})	HEAT TRANSFER RATE $\dot{q}_{cw}$ (Btu sec^{-1} ft^{-2})			MODEL STAGNATION PRESSURE P_{t_2} (atm)	NOZZLE EXIT PRESSURE P_e (atm)	TEST CHAMBER PRESSURE P_c (atm)
			CALORIMETER			FACILITY PITOT RROBE		
			Facility		SRI			
		(1)	(2)	(3)		(4)		
Teflon Models	T40	6,360	419	291	269	0.022	0.0030	0.0025
	T41	4,850	--	--	238	0.018	0.0034	0.0027
	T45	14,480	793	551	568	0. 031	0.0033	0.0027
	T46	10,230	735	511	511	0.031	0.0034	0.0029
Phenolic-Nylon Models	P1B5	4,000	--	--	467	0.041	0.0045	--
	P1B3	4,830	--	--	246	0.015	0.0034	0 0026
	P1B6	4,810	--	--	235	0.017	0.0035	0.0031
	P1B1	14,530	852	592	570	--	0.0033	0.0029
	P1B2	4,590	1,035	719	617	0.045	0.0061	0.0048
	P1B4	10,350	945	656	590	0.034	0.0039	0.0031
	P1B7	5,050	871	605	559	0. 035	0.0052	0.0043
	P3B4	6,390	431	299	270	0.023	0.0031	0.0027
	P3B5	14,180	850	591	612	0.030	--	--

(1) Enthalpy measured by energy balance method.

(2) Boeing calorimeter 2.0-in.-diameter hemispherical shape, 0.74-in. heated diameter, steady state type, water temperature ris
platimum-plated surface on copper.

(3) Boeing calorimeter data reduced by SRI to 1.25-in.-diameter flat face. $\dot{q}_{FF} = 0.55\, \dot{q}_{FAC}\, (2.0/1.25)^{0.5}$.

(4) Boeing pitot probe, 1.25-in.-diameter water-cooled copper probe.

Table B-6

TUNNEL CALIBRATION AND TEST DATA REPORTED BY AVCO CORPORATION

Ref: AVCO Report Prepared Under Purchase Order B-54320 US, 6 May 1964

FRONT SURFACE TEMPERATURE T_{FS} (°F)	BACK SURFACE TEMPERATURE RISE AT ARC CUTOFF (°F)	MAXIMUM EQUILIBRIUM TEMPERATURE RISE AFTER RUN COMPLETION (°F)	RUN TIME t (sec)	CORE WEIGHT LOSS (g)	CORE CHAR WEIGHT (g)	RECESSION (in.)	CHAR THICKNESS (in.)	PYROLYSIS ZONE (in.)
	3.3	130	30	2.265		0.190		
	2.	100	30	1.149		0.103		
	9.	--	30	1.291		0.111		
	5.	134	30	1.056		0.088		
	4.	110	30	0.683		0.070		
	0.	86	30	0.425		0.035		
3,350	5.	--	60	0.902	0.178	0.060	0.107	0.055
3,260	--	--	40	0.588	0.127	0.029	0.075	0.050
2,920	0.	82	20	0.332	0.080	0.050	0.050	0.015
3,010	1.5	--	20	0.428	0.119	0.010	0.068	0.035
2,640	1.3	--	60	0.560	0.133	0.010	0.084	0.065
2,700	2.5	154	40	0.536	0.116	0.018	0.071	0.030
2,480	--	--	120	0.867	0.176	0.031	0.105	0.087

Table B-7

TUNNEL CALIBRATION AND TEST DATA REPORTED BY BOEING COMPANY

Ref: Boeing Document D2-23402, June 30, 1964

GAS FLOW RATE W (lb sec^{-1})	BACK SURFACE TEMPERATURE RISE AT ARC CUTOFF (°F)	MAXIMUM EQUILIBRIUM TEMPERATURE RISE AFTER RUN COMPLETION (°F)	RUN TIME t (sec)	CORE WEIGHT LOSS (g)	CORE CHAR WEIGHT (g)	RECESSION (in.)	CHAR THICKNESS (in.)	PYROLYSIS ZONE (in.)
0.0065	7.5	116	30	1.458		0.132		
0.0095	7	127	30	1.598		0.139		
0.0040	9	121	30	2.204		0.199		
0.0053	9	125	30	2.061		0.186		
0.020	1	--	9	0.307	0.107	0.009	0.047	0.038
0.0095	24	102	20	0.469	0.159	0.009	0.080	0.040
0.0095	3	105	15	0.390	0.130	0.007	0.065	0.035
0.0040	2	109	13	0.477	0.131	0.013	0.078	0.035
0.020	3.5	103	9	0.388	0.119	0.008	0.063	0.045
0.0069	1.5	105	12	0.418	0.161	0.007	0.079	0.035
0.014	3.0	117	13	0.447	0.162	0.011	0.080	0.040
0.0065	3.5	130	21	0.504	0.145	0.011	0.082	0.045
0.0040	--	--	13	0.394	0.109	0.005	0.070	0.025

	MODEL NO.	TOTAL ENTHALPY h_t (Btu lb^{-1})	HEAT TRANSFER RATE $\dot{q}_{cw}$ (Btu sec^{-1} ft^{-2})				MODEL STAGNATION PRESSURE P_{t_2} (atm)	
			CALORIMETER				PITOT PROBE	
			Facility			SRI	Facility	SRI
		(1)	(2)	(3)	(4)		(5)	
Teflon Models	T49	4,900		398			0.421	
	T50	3,880	--	--	--		0.490	
	T52	5,500	47		36	34		0.037
	T56	2,800				434		1.43
	T86	3,700		535		451		0.56
	T44	15,000			245		0.72	
Phenolic-Nylon Models	P6A5	4,900		387			0.394	
	P6A6	2,800				381		1.63
	P6B2	4,900		372			0.388	
	P8B1	3,700		461		425		0.557
	P8B3	4,900		376			0.400	
	P9B3	5,500	44		33	40		0.037
	P7B4	17,000			318		0.84	
	SRI Calib. Run No.							
Tunnel Calibration Runs	8C1	4,900		394		397	0.422	
	8C2	4,900		384		370		0.367
	8C3	3,700		550		519		0.77
	8C4	3,300		--		317		1.63

(1) Total enthalpy by heat balance method.

(2) Facility calorimeter 0.75-in.-diameter flat face adjusted by GD to 1.25-in. flat face $\dot{q}_{1.25} = \dot{q}_{0.75}\,(0.75/1.0)^{0.5}$ sensing diameter 0.375 in.

(3) Facility calorimeter 1-in.-diameter flat face adjusted by GD to 1.25-in. flat face $\dot{q}_{1.25} = \dot{q}_{1.0}\,(1.0/1.25)^{0.5}$, sensing diameter 0.5 in.

(4) Facility calorimeter 1.25-in.-diameter, sensing diameter 0.625 in.

(5) Facility pitot probe 1-in. diameter.

NOTE: All above tests were made with nitrogen gas. Models T56 and T86 were asymmetric possibly due to small jet diameter.

Table B-8

TUNNEL CALIBRATION AND TEST DATA REPORTED BY GENERAL DYNAMICS
Ref: GD/FW Test No. HRF 64-2-1

ARC CHAMBER PRESSURE P_{t_1} (atm)	GAS FLOW RATE W (lb sec^{-1})	BACK SURFACE TEMPERATURE RISE AT ARC CUTOFF (°F)	RUN TIME t (sec)	CORE WEIGHT LOSS (g)	CORE CHAR WEIGHT (g)	RECESSION (in.)	CHAR THICKNESS (in.)	PYROLYSIS ZONE DEPTH (in.)
3.23	0.0333	> 1,075	8.40	1.279		0.117		
3.26	0.0326	--	10.70	3.886		0.347		
0.54	0.00385	--	25.08	0.628		0.056		
13.96	0.180	--	9.18	3.208		0.290		
6.80	0.0808	--	15.12	2.868		0.240		
6.51	0.00318	--	34.43	2.007		0.180		
3.2	0.0332	> 1,075	6.05	0.326	0.089	0.002	0.053	0.022
15.0	0.109	--	11.28	2.173	0.055	0.240	0.023	0.033
3.26	0.0332	--	21.60	0.760	0.299	0.037	0.115	0.055
6.76	0.0800	--	20.46	0.868	0.308	0.013	0.137	0.080
3.26	0.0333	--	15.12	0.546	0.204	0.016	0.085	0.048
0.54	0.00385	--	63.0	0.586	0.119	0.023	0.067	0.052
7.14	0.00316	--	24.21	0.606	0.226	0.014	0.112	0.050
3.17	0.0329							
3.29	0.0331							
6.74	0.0843							
15.0	0.193							

	MODEL NO.	TOTAL ENTHALPY h_t (Btu lb^{-1})	HEAT TRANSFER RATE $\dot{q}_{cw}$ (Btu sec^{-1} ft^{-2})	MODEL STAGNATION PRESSURE P_{t_2} (atm)	PLENUM PRESSURE P_{t_1} (atm)	GAS FLOW RATE $\dot{W}$ ($lb\ sec^{-1}$)	FRONT SURFACE TEMPERATURE T_{FS} (°F)
			SRI CALORIMETER	SRI PITOT PROBE			
		(1)	(2)	(3)			(8)
Teflon Models	T62	13,550	320	0.0630	1.61	0.00150	2,040
	T63	3,210	215	0.0370	1.17	0.00175	1,900
	T64	3,180	215	0.0370	1.14	0.00175	--
	T65	13,120	69	0.00825	1.60	0.00150	1,650
	T66	8,000	214	0.0411	1.23	0.00150	1,880
	T70	5,660	131	0.0331	1.08	0.00140	1,770
	T75	5,400	44.7	0.00720	1.09	0.00140	1,640
Phenolic-Nylon Models	P5A2	5,690	131	0.0331	1.08	0.00140	2,330
	P5A3	13,440	320	0.0630	1.59	0.00150	2,750
	P5A5	5,660	131	0.0331	1.08	0.00140	2,370
	P5A6	8,120	214	0.0411	1.24	0.00150	2,510
	P5A7	5,700	131	0.0331	1.09	0.00140	--
	P8A2	5,770	131	0.0331	1.08	0.00140	2,310
	P8A3	5,600	44.7	0.00720	1.13	0.00140	2,030
	P8A4	13,120	69.0	0.00825	1.60	0.00150	1,940
	SRI Calib. Run No.	(4)					
Pre-Test Calibration Runs	9C1	13,080			1.58	0.00150	
	9C2	13,170			1.58	0.00152	
	9C3	12,900			1.57	0.00152	
	9C4	13,170			1.58	0.00150	
	9C5	8,290			1.26	0.00148	
	9C6	8,350			1.26	0.00152	
	9C7	8,600			1.22	0.00150	
	9C8	5,660			1.08	0.00140	
	9C9	5,580			1.08	0.00140	
	9C10	5,480			1.11	0.00144	
	9C11	5,720			1.09	0.00140	
	9C12	3,250			1.14	0.00176	
	9C13	3,250			1.14	0.00174	
		(5)	(6)				
	9C14	13,000	330		1.63		
	9C15	13,000	324		1.62		
	9C16	8,500	212		1.27		
	9C17	8,500	215		1.27		
	9C18	5,000	133		1.10		
	9C19	5,000	129		1.10		
	9C20	3,000	217		1.14		
	9C21	3,000	214		1.16		
	9C22	13,000	75.3		1.63		
	9C23	13,000	64.0		1.63		
	9C24	13,000	67.2		1.62		
	9C25	5,000	44.5		1.09		
	9C26	5,000	44.9		1.10		
		(1)		(7)			
	9C27	5,650		0.0331	1.08	0.00140	
	9C28	13,130		0.0630	1.60	0.00150	
	9C29	8,700		0.0411	1.22	0.00150	
	9C30	3,110		0.0370	1.10	0.00175	
	9C31	13,080		0.00825	1.61	0.00150	
	9C32	5,590		0.00720	1.10	0.00140	

(1) Enthalpy calculated from pre-test calibration with total calorimeter and the relation:

$$\frac{h}{h_r} = \frac{PE^{0.5}W_r^{0.5}}{P_r E_r^{0.5} W^{0.5}}$$

where h = enthalpy, P = plenum pressure, E = power, W = air mass flow and subscript r refers to pre-test total calorimeter runs.

(2) Heating rate averaged from pre-test SRI calorimeter runs.

(3) Stagnation pressures from pre-test SRI pitot probe runs.

Table B-9

NEL CALIBRATION AND TEST DATA REPORTED BY GENERAL ELECTRIC SPACE TECHNOLOGY CENTER

Ref: G.E. Round Robin Ablation Final Report, 30 September 1964

BACK SURFACE TEMPERATURE RISE AT ARC CUTOFF (°F)	MAXIMUM EQUILIBRIUM TEMPERATURE RISE AFTER RUN COMPLETION	RUN TIME t (sec)	NOZZLE EXIT DIAMETER D_e (in.)	CORE WEIGHT LOSS (g)	CORE CHAR WEIGHT (g)	RECESSION (in.)	CHAR THICKNESS (in.)	PYROLYSIS ZONE (in.)
7	146	30.0	1.19	2.756		0.244		
3	55	25.2	1.19	1.488		0.140		
0	24	12.0	1.19	0.633		0.055		
0	66	31.6	5.00	0.695		0.060		
7	124	32.2	1.19	1.955		0.172		
0	44	30.0	1.19	1.611		0.142		
4	40	36.0	5.00	0.522		0.045		
1	64	29.9	1.19	0.630	0.147	0.033	0.078	0.036
1	111	22.0	1.19	0.738	0.267	0.047	0.107	0.045
7	98	45.0	1.19	0.776	0.160	0.045	0.088	0.055
4	110	33.1	1.19	0.763	0.197	0.041	0.105	0.050
0	54	20.0	1.19	0.466	0.114	0.018	0.061	0.045
1	56	20.0	1.19	0.456	0.105	0.019	0.077	0.045
30	173	120.0	5.00	0.823	0.157	0.039	0.092	0.110
11	178	75.0	5.00	0.818	0.148	0.051	0.088	0.080
			1.19					
			1.19					
			1.19					
			1.19					
			1.19					
			1.19					
			1.19					
			1.19					
			1.19					
			1.19					
			1.19					
			1.19					
			1.19					
			1.19					
			1.19					
			1.19					
			1.19					
			1.19					
			1.19					
			1.19					
			1.19					
			1.19					
			5.00					
			5.00					
			5.00					
			5.00					
			1.19					
			1.19					
			1.19					
			1.19					
			5.00					
			5.00					

(4) Enthalpy determined by total calorimetry.
(5) Nominal enthalpy from results under (4).
(6) Heating rate determined on SRI transient calorimeter.
(7) Stagnation pressure determined on SRI pitot probe.
(8) Two-color optical pyrometer emissivity factor assumed to cancel out.

	MODEL NO.	TOTAL ENTHALPY h_t (Btu lb^{-1})	HEAT TRANSFER RATE $\dot{q}_{cw}$ (Btu sec^{-1} ft^{-2})			MODEL STAGNATION PRESSURE P_{t_2} (atm)		PLENUM PRESSURE P_{t_1} (atm)	NOZZLE EXIT PRESSURE P_e (atm)
			CALORIMETER			PITOT PROBE			
			Facility		SRI	Facility	SRI		
		(1)	(2)			(3)			
Teflon Models	T20	5,105	275.6			0.047		0.230	0.00450
	T23	15,110	857.9			0.048		0.311	0.00520
	T24	10,025	563.4			0.052		0.279	0.00500
	T21	3,035	186.5			0.057		0.270	0.00550
	T22	4,965	152.4			0.021		0.082	0.00166
Phenolic-Nylon Models	P3A2	5,000	276.5			0.046		0.230	0.00460
	P3A3	4,855	274.9			0.046		0.229	0.00440
	P3B3	15,050	854.8			0.048		0.311	0.00515
	P3B1	10,035	303.3			0.021		0.080	0.00146
	P3A5	4,978	352.4			0.078		0.361	0.00718
	P3A6	5,010	354.4			0.077		0.360	0.00715
	P3A7	4,975	353.4			0.078		0.362	0.00728
	P3B2	5,010	150.8			0.020		0.083	0.00165
				(4)					
Tunnel Calibration Runs for Model Nos.	T20	4,920	274.8	106.9	127.7	0.046		0.229	0.0045
	P3A2	4,955				0.043	0.0446	0.230	0.0046
	P3A3	5,005	275.2	107.1	125.7	0.047		0.230	0.0045
	T23	14,955	855.3	332.7	296.4	0.049		0.310	0.00515
	P3B3	15,875	855.5			0.048	0.0491	0.311	0.00520
	T24	9,985	561.4	218.4	160.7	0.051		0.277	0.00499
	T21	2,985	184.9	71.9	81.8	0.058		0.268	0.00548
	P3A5 P3A6, P3A7	5,005	351.2	136.6	144.5	0.077		0.361	0.00725
	T22	5,025	151.4	58.9	55.1	0.020		0.083	0.00166
	P3B2	5,000	152.5			0.020	0.020	0.085	0.00169
	P3B1	9,974	302.8	117.8	133.9	0.021		0.079	0.00142
		10,054	301.8			0.021	0.021	0.079	0.00144

(1) Enthalpy measured by energy balance method.

(2) Giannini calorimeter - 0.625-in.-diameter, hemispherical steady state type, water temperature rise - copper surface.

(3) Giannini pitot probe - water cooled - 0.625-in.-diameter.

(4) Giannini calorimeter reduced by GSC to 1.25-in.-diameter flat face $\dot{q}_{FF} = 0.55\ \dot{q}_{FAC}\ (0.625/1.25)^{0.5}$.

Table B-10

TUNNEL CALIBRATION AND TEST DATA REPORTED BY GIANNINI SCIENTIFIC CORPORATION

Ref: Giannini Report No. ITR-024-B54319, February 1964

GAS FLOW RATE W ($lb\ sec^{-1}$)	FRONT SURFACE TEMPERATURE T_{FS} $\epsilon = 1$ (^{o}F)	BACK SURFACE TEMPERATURE RISE AT ARC CUTOFF (^{o}F)	MAXIMUM EQUILIBRIUM TEMPERATURE RISE AFTER RUN COMPLETION (^{o}F)	RUN TIME t (sec)	CORE WEIGHT LOSS (g)	CORE CHAR WEIGHT (g)	RECESSION (in.)	CHAR THICKNESS (in.)	PYROLYSIS ZONE (in.)
0.01237	2,420	5	148	30	1.272		0.106		
0.01062	2,860	15	175	30	1.700		0.145		
0.01150	2,660	7	141	30	1.403		0.119		
0.01750	2,390	10	60	30	1.242		0.099		
0.00437	2,150	3	140	30	0.625		0.051		
0.01237	3,000	5	140	30	0.540	0.134	0.014	0.078	0.055
0.01237	3,350	62	275	60	0.912	0.237	0.027	0.132	0.065
0.01062	3,650	6	295	20	0.527	0.171	0.012	0.088	0.040
0.00338	3,350	21	216	60	0.882	0.214	0.034	0.123	0.075
0.0191	3,510	33	--	48	0.855	0.255	0.035	0.121	0.065
0.0191	3,300	15	--	30	0.580	0.166	0.011	0.093	0.050
0.0191	2,880	3	255	15	0.341	0.084	0.007	0.047	0.030
0.00437	2,700	134	275	120	1.189	0.214	0.044	0.138	0.120
	SRI Calib. Run No.								
0.01237	10C1								
0.01237	10C2								
0.01237	10C3								
0.01062	10C4								
0.01062	10C5								
0.01150	10C6								
0.01750	10C7								
0.01910	10C8								
0.00437	10C9								
0.00437	10C10								
0.00338	10C11								
0.00338	10C12								

	MODEL NO.	TOTAL ENTHALPY h_t (Btu lb^{-1})	HEAT TRANSFER RATE $\dot{q}_{cw}$ (Btu sec^{-1} ft^{-2})		MODEL STAGNATION PRESSURE P_{t_2} (atm)		PLENUM PRESSURE P_{t_1} (atm)	NOZZLE EXIT PRESSURE P_e (atm)	TEST CHAMBER PRESSURE P_c (atm)
			CALORIMETER		PITOT PROBE				
			Facility	SRI	Facility	SRI			
		(1)	(2)		(3)				
Teflon Models	T72	5,086	95		0.0271		0.1355	0.00195	0.00191
	T74	5,220	94		0.0271		0.1355	0.00195	0.00191
	T76	4,926	94		0.0267		0.1355	0.00195	0.00191
	T67	12,510	268		0.0178		0.0915	0.00208	0.00184
	T68	12,250	260		0.0180		0.0830	0.00202	0.00184
	T71	12,410	268		0.0179		0.0804	0.00199	0.00184
	T79	3,013	38		0.0111		0.0817	0.00169	0.00147
	T82	3,050	38		0.0112		0.0817	0.00171	0.00150
	T84	3,073	39		0.0111		0.0830	0.00171	0.00150
	T81	10,435	95		0.00974		0.0197	0.00100	0.00100
	T83	10,233	93		0.00980		0.0197	0.00100	0.00100
	T87	10,137	96		0.00974		0.0197	0.00100	0.00100
	T77	4,910	45		0.0282		0.2145	0.00294	0.00284
	T78	5,070	45		0.0275		0.2120	0.00292	0.00284
	T88	5,265	44		0.00552		0.0105	0.000526	0.000566
	T80	5,220	45		0.00539		0.0118	0.000513	0.000513
Phenolic-Nylon Models	P9B4	4,994	100		0.0272		0.1340	0.00200	0.00191
	P9B5	4,780	99		0.0270		0.1340	0.00193	0.00191
	P9B6	5,051	100		0.0275		0.1340	0.00194	0.00191
	P2A6	11,610	262		0.01815		0.0813	0.00201	0.00184
	P2A7	12,560	266		0.01802		0.0803	0.00200	0.00184
	P3B6	11,680	268		0.01802		0.0803	0.00201	0.00184
	P10A4	10,219	93		0.00970		0.0201	0.000975	0.000975
	P10A3	9,875	95		0.00960		0.0198	0.000974	0.000986
	P10A5	9,500	96		0.00960		0.0204	0.00100	0.00100
	P7B6	5,020	129		0.0240		0.1138	0.00156	0.00117
	P8A5	5,253	132		0.0244		0.1131	0.00154	0.00117
	P8A6	5,033	132		0.0242		0.1139	0.00155	0.00117
	P8A7	4,988	132		0.0242		0.1139	0.00155	0.00117
	P9A5	5,180	132		0.0244		0.1151	0.00154	0.00117
	P9A6	4,738	132		0.0244		0.1146	0.00154	0.00117
	P9A7	4,861	137		0.0246		0.1143	0.00155	0.00117
	P9B1	4,980	129		0.0245		0.1150	0.00155	0.00117
	P9B2	5,094	132		0.0245		0.1143	0.00155	0.00117
	P9B7	5,170	47		0.0276		0.2120	0.00291	0.00283
	P10A2	5,110	45		0.0276		0.2120	0.00292	0.00284
	P10A6	5,200	45		0.00539		0.0118	0.000525	0.000525
	P9A2	4,780	45		0.00552		0.0132	0.000514	0.000500

Table B-11

TUNNEL CALIBRATION AND TEST DATA REPORTED BY MARTIN COMPANY

Ref: Martin Company Report ER13598

GAS FLOW RATE W (lb sec^{-1})	FRONT SURFACE TEMPERATURE T_{FS} ϵ = 1 ($^{\circ}$F)	BACK SURFACE TEMPERATURE RISE AT ARC CUTOFF ($^{\circ}$F)	MAXIMUM EQUILIBRIUM TEMPERATURE RISE AFTER RUN COMPLETION ($^{\circ}$F)	RUN TIME t (sec)	NOZZLE EXIT DIAMETER D_e (in.)	CORE WEIGHT LOSS (g)	CHAR WEIGHT (g)	RECESSION (in.)	CHAR THICKNESS (in.)	PYROLYSIS ZONE (in.)
0.00175	2,210	2	247	30	1.5	0.966		0.084		
0.00175	2,230	2	140	30	1.5	0.941		0.082		
0.00175	2,215	1	200	30	1.5	1.026		0.090		
0.00100	2,260	-	--	30	1.5	1.460		0.132		
0.00100	--	9	256	30	1.5	1.453		0.126		
0.00100	2,650	2	272	30	1.5	1.461		0.134		
0.00600	2,035	-	--	30	3.0	0.430		0.033		
0.00600	2,035	-	--	30	3.0	0.408		0.032		
0.00600	2,030	-	--	30	3.0	0.418		0.033		
0.00150	2,550	2	245	30	3.0	0.838		0.070		
0.00150	2,380	-	--	30	3.0	0.803		0.068		
0.00150	2,435	2	300	30	3.0	0.817		0.068		
0.00275	2,220	2	252	30	1.5	0.894		0.078		
0.00275	2,545	4	206	30	1.5	2.106		0.176		
0.001125	2,065	-	--	30	3.0	0.375		0.027		
0.001125	2,060	-	--	30	3.0	0.388		0.032		
0.00175	3,330	4	227	60	1.5	0.914	0.198	0.044	0.109	0.060
0.00175	3,170	4	271	60	1.5	0.868	0.195	0.047	0.101	0.062
0.00175	2,910	4	252	60	1.5	0.906	0.184	0.056	0.100	0.052
0.00100	3,420	3	252	24	1.5	0.503	0.131	0.018	0.077	0.033
0.00100	--	-	--	24	1.5	0.500	0.131	0.018	0.072	0.040
0.00100	3,320	2	225	24	1.5	0.491	0.133	0.012	0.076	0.035
0.00150	3,240	4	250	60	3.0	0.763	0.180	0.029	0.103	0.068
0.00150	3,000	0	212	60	3.0	0.736	0.175	0.034	0.094	0.065
0.00150	2,975	2	230	60	3.0	0.739	0.165	0.032	0.093	0.055
0.00150	3,200	0	313	48	1.5	0.764	0.166	0.047	0.091	0.053
0.00150	3,150	0	294	48	1.5	0.771	0.178	0.047	0.096	0.055
0.00150	3,020	5	311	48	1.5	0.772	0.165	0.060	0.085	0.050
0.00150	2,970	2	260	30	1.5	0.551	0.119	0.034	0.062	0.035
0.00150	2,710	5	231	30	1.5	0.535	0.133	0.027	0.070	0.040
0.00150	3,020	-	--	30	1.5	0.545	0.119	0.028	0.068	0.033
0.00150	2,830	8	275	15	1.5	0.319	0.076	0.012	0.043	0.024
0.00150	3,030	0	265	15	1.5	0.319	0.071	0.012	0.043	0.025
0.00150	2,835	0	255	15	1.5	0.304	0.081	0.009	0.044	0.030
0.00275	3,135	-	--	120	1.5	1.750	0.333	0.145	0.160	0.071
0.00292	3,440	22	280	120	1.5	1.764	0.325	0.153	0.154	0.060
0.00112	2,340	42	367	120	3.0	0.810	0.178	0.033	0.095	0.065
0.00112	2,370	-	360	120	3.0	0.837	0.165	0.037	0.091	0.070

	MODEL NO.	TOTAL ENTHALPY h_t (Btu lb^{-1})	HEAT TRANSFER RATE $\dot{q}_{cw}$ (Btu sec^{-1} ft^{-2})				MODEL STAGNATION PRESSURE P_{t_2} (atm)		PLENUM PRESSURE P_{t_1} (atm)	NOZZLE EXIT PRESSURE P_e (atm)	TEST CHAMBER PRESSURE P_c (atm)
			CALORIMETER				PITOT PROBE				
			Facility			SRI	Facility	SRI			
		(1)	(2)		(4)		(3)				
Pre-Test and Post-Test Tunnel Calibration Runs	SS-15g	5,040			99		0.0271		0.1355	0.00195	0.00191
	SRI Cal.	4,783	97			123	0.0271		0.1361	0.00195	0.00191
	SRI Cal.	5,171	100			126	0.0275		0.1370	0.00194	0.00191
	SRI Pitot	5,150	99				0.0276	0.0259	0.1370	0.00191	0.00188
	SS-7g	12,430			268		0.01780		0.0915	0.00208	0.00184
	SRI Cal.	12,108	268			221	0.01788		0.0867	0.00208	0.00184
	SRI Cal.	11,630	260			210	0.01814		0.0803	0.00201	0.00184
	SRI Pitot	12,580	268				0.01789	0.01868	0.0855	0.00200	0.00184
	SS-19g	2,988			38		0.0111		0.0804	0.00170	0.00149
	SRI Cal.	3,050	38			36	0.0111		0.0817	0.00167	0.00147
	SS-13g	10,426			96		0.00974		0.0191	0.00100	0.00100
	SRI Cal.	9,987	97			111	0.00968		0.0201	0.000987	0.000987
	SRI Cal.	9,513	97			118	0.00974		0.0191	0.000994	0.000994
	SRI Cal.	5,122	128			117	0.0240		0.1131	0.00158	0.00117
	SS-14g	4,857			44		0.0276		0.2100	0.00287	0.00283
	SRI Cal.	5,269	45			82	0.0263		0.2100	0.00287	0.00283
	SRI Cal.	5,244	48			93	0.0276		0.2120	0.00291	0.00283
	SS-17g	5,244			45		0.00552		0.0118	0.000526	0.000526
	SRI Cal.	5,220	45			42	0.00539		0.0118	0.000525	0.000513
	SRI Cal.	5,020	44			41	0.00539		0.0118	0.000525	0.000525

(1) Enthalpy measured by energy balance method.

(2) Martin steady state calorimeter, 1-in.-diameter flat face, 0.375-in. diameter sensing area, copper surface, heat meter type calorimeter — calibrated with calorimeter described under (4) thus data is adjusted to 1.25 in flat face.

(3) Martin pitot probe, 0.625-in. diameter, water-cooled.

(4) Martin transient calorimeters, 0.25-in.-diameter copper slug 0.25-in. long set in phenolic flat face model 1.25-in. diameter. These calorimeters were used to calibrate the Martin steady state calor meter described under (2).

Table B-11 *Concluded*

GAS FLOW RATE W ($lb\ sec^{-1}$)	SRI CALIBRATED RUN NO.	BACK SURFACE TEMPERATURE RISE AT ARC CUTOFF (°F)	MAXIMUM EQUILIBRIUM TEMPERATURE RISE AFTER RUN COMPLETION (°F)	RUN TIME (t) (sec)	NOZZLE EXIT DIAMETER D_e (in.)	CORE WEIGHT LOSS (g)	CHAR WEIGHT (g)	RECESSION (in.)	CHAR THICKNESS (in.)	PYROLYSIS ZONE (in.)
0.00175	11C1				1.5					
0.00175	11C2				1.5					
0.00175	11C3				1.5					
0.00175	11C4				1.5					
0.00100	11C5				1.5					
0.00100	11C6				1.5					
0.00100	11C7				1.5					
0.00100	11C8				1.5					
0.0060	11C9				3.0					
0.0060	11C10				3.0					
0.0015	11C11				3.0					
0.0015	11C12				3.0					
0.0015	11C13				3.0					
0.0015	11C14				1.5					
0.00275	11C15				1.5					
0.00275	11C16				1.5					
0.00275	11C17				1.5					
0.001125	11C18				3.0					
0.001125	11C19				3.0					
0.001125	11C20				3.0					

	MODEL NO.	TOTAL ENTHALPY h_t (Btu lb^{-1})				HEAT TRANSFER RATE $\dot{q}_{cw}$ (Btu sec^{-1} ft^{-2})		MODEL STAGNATION PRESSURE P_{t_2} (atm)		PLENUM PRESSURE P_{t_1} (atm)	NOZZLE EXIT PRESSURE P_e (atm)
						CALORIMETER		PITOT PROBE			
						Facility	SRI	Facility	SRI		
		(1)	(2)	(3)	(4)	(5)		(6)			
Teflon Models	T55	2,503	2,680	2,600	2,580	105	102.5	0.192		1.293	0.0138
	T57	5,558	5,210	5,900	5,670	226	248	0.190		1.285	0.0132
	T58	2,692	2,820	2,600	2,770	103	81	0.120		0.812	0.0076
	T59	1,390	1,550	1,400	1,450	54	51	0.194		1.300	0.0133
	T60	10,507	10,000	--	10,450	434	--	0.202		1.198	0.0092
Phenolic-Nylon Models	P3A4	5,329	5,940	5,200	5,550	226	217	0.191		1.288	0.0099
	P4A2	2 479	2,780	2,680	2,600	106	105.5	0.193		1.307	0.0138
	P4A3	5,400	5,980	5,800	5,615	227	243	0.190		1.285	0.0132
	P4A4	5,534	5,900	5,300	5,700	228	223	0.190		1.287	0.0099
	P4A5	5,784	5,900	5,600	5,789	231	235	0.190		1.285	0.0099
	P4A6	5,770	5,900	5,400	5,770	230	226	0.190		1.285	0.0099
	P4A7	2,710	2,820	2,700	2,770	105	83.6	0.120		0.812	0.0074
	P6B7	10,165	10,000	10,200	10,165	431	442	0.205		1.215	0.0092
	P6B6	3,122	3,320	2,800	3,190	244	166	0.424		2.960	0.0210
				(7)		(8)		(9)			
Pre-Test Tunnel Calibration For Model Nos.	T55, P4A2	3,185	2,860	3,200	3,096	127.8		0.194		1.320	0.0099
	T57, P4A3 P4A4 P4A5, P4A6 P3A4	5,663	5,900	5,400	5,663	224		0.186		1.285	0.0097
	T58 P4A7	2,599	2,780	3,200	2,730	100		0.117		0.808	0.0066
	T59	1,341	1,500	1,540	1,450	55.1		0.187		1.286	0.0121
	T60 P6B7	10,465	10,000	9,400	10,130	382		0.166		1.221	0.0089
	P6B6	2,947	3,500	3,700	3,330	219		0.408		2.790	0.0195
									(10)		
Post-Test Tunnel Calibration For Model Nos.	T55, P4A2	2,791	2,930	2,550			100		0.196	1.327	0.0105
	T57, P4A3	5,365	5,940	5,850			234		0.189	1.291	0.0094
	P4A4, P4A5	5,513	5,960	6,100			263		0.192	1.286	0.0105
	P4A6, P3A4	5,410	5,960	5,200			220		0.191	1.285	0.0131
	T58, P4A7	2,570	3,000	2,800			87.7		0.120	0.814	0.0079
	T59	1,358	1,570	2,000			77		0.194	1,300	0.0142
	T60, P6B7	9,761	10,000	8,000			365		0.206	1.215	0.0089
	P6B6	3,095	3,300	3,100			185		0.424	2.960	0.0210

(1) Enthalpy by heat balance method.

(2) Enthalpy by sonic throat method. Equilibrium flow, P_{t_o} 1 atm, (Ref: NASA TND 1333) $A^* = 3.1 \times 10^{-3}$ ft^2.

(3) Enthalpy calculated from $\dot{q}_{cw_{SRI}}$ and Fay-Riddell equation.

(4) Mean enthalpy from (1), (2) and (3) above.

(5) Calculated from pre-test calibration data on NA calorimeter corrected to 1.25-in. flat face and for enthalpy and stagnatio

(6) Calculated stagnation pressures from pre-test and post-test calibration runs.

(7) Enthalpy calculated from $\dot{q}_{cw_{FAC}}$ and Fay-Riddell equation.

(8) North American calorimeter, 0.5-in.-diameter hemispherical shape, steady state water temperature rise type, copper surfac data reduced by NAA to 1.25-in.-diameter flat face as follows: $\dot{q}_{FF} = 0.55\dot{q}_{FAC}(0.5/1.25)^{0.5}$.

(9) North American pitot probe, 0.5-in. diameter, water-cooled.

(10) SRI uncooled pitot probe, 1.25-in. diameter.

Table B-12

TUNNEL CALIBRATION AND TEST DATA REPORTED BY NORTH AMERICAN AVIATION, INCORPORATED

Ref: North American Report No. NA-64-733 Test PT 15

TEST CHAMBER PRESSURE P_c (atm)	GAS FLOW RATE W (lb sec^{-1})	FRONT SURFACE TEMPERATURE T_{FS} $\epsilon = 1$ (°F)	BACK SURFACE TEMPERATURE RISE AT ARC CUTOFF (°F)	MAXIMUM EQUILIBRIUM TEMPERATURE RISE AFTER RUN COMPLETION (°F)	RUN TIME t (sec)	CORE WEIGHT LOSS (g)	CORE CHAR WEIGHT (g)	RECESSION (in.)	CHAR THICKNESS (in.)	PYROLYSIS ZONE (in.)
0.0116	0.0485	2,400	16	130	29.6	1.840		0.158		
0.0105	0.0366	2,700	14	164	30.0	3.075		0.266		
0.0092	0.0299	2,300	8	112	30.0	1.587		0.138		
0.0153	0.0601	2,240	6	110	30.2	0.913		0,077		
0.0088	0.0284	3,000	26	182	30.2	3.752		0.330		
0.0104	0.0365	3,320	2	96	13.4	0.442	0.123	0.015	0.066	0.035
0.0132	0.0485	2,900	12	172	51.6	0.931	0.178	0.060	0.097	0.072
0.0099	0,0365	3,410	22	132	29.0	0.831	0.229	0.045	0.108	0.070
0.0103	0.0367	3,500	9	146	19.5	0.574	0.173	0.017	0.092	0.035
0.0103	0.0366	3,350	-	-	13.0	0.450	0.124	0.015	0.066	0.042
0.0103	0.0366	3,500	4	152	29.2	0.856	0.237	0.057	0.102	0.060
0.0091	0.0299	2,920	38	202	80.2	1.232	0.184	0.101	0.105	0.055
0.0089	0.0287	3,700	5	114	17.2	0.691	0.255	0.037	0.102	0.045
0.0264	0.102	3,320	8	162	34.0	1.043	0.143	0.098	0.077	0.050
		SRI Calib. Run No.								
0.0106	0.0483	12C1								
0.0092	0.0366	12C2								
0.0081	0.0297	12C3								
0.0141	0.0601	12C4								
0.0080	0.0284	12C5								
0.0260	0.0952	12C6								
0.0125	0.0482	12C7								
0.0103	0.0365	12C8								
0.0105	0.0365	12C9								
0.0145	0.0365	12C10								
0.0088	0.0293	12C11								
0.0165	0.0597	12C12								
0.0085	0.0281	12C13								
0.0260	0.1035	12C14								

	MODEL NO.	TOTAL ENTHALPY (Btu lb^{-1})	HEAT TRANSFER RATE $\dot{q}_{c_{w_1}}$ (Btu sec^{-1} ft^{-2})	MODEL STAGNATION PRESSURE P_{t_2} (atm)	PLENUM PRESSURE P_{t_1} (atm)
			SRI CALORIMETER	SRI PITOT PROBE	
		(1)		(2)	
Phenolic-Nylon Models	P1A1	5,380	302	0.191	0.944
	P2A1	5,300	216	0.189	0.935
	P3A1	5,050	278	0.184	0.913
	P4A1	5,300	257	0.189	0.935
	P5A1	5,300	274	0.189	0.937
	P6A1	5,150	260	0.186	0.922
	P7A1	4,920	280	0.182	0.904
	P8A1	5,200	280	0.187	0.927
	P9A1	5,100	265	0.185	0.918
	P10A1	5,050	210	0.184	0.909
	P11A1	5,300	290	0.189	0.937

(1) Enthalpy calculated by pressure rise sonic flow method. Ref: TND 2132

(2) Obtained from ratio of stagnation pressure to total pressure measured with SRI pitot probe for similar conditions.

Table B-13

TUNNEL CONDITIONS FOR PHENOLIC NYLON QUALITY CONTROL TESTS

Reported by Ames Research Center—NASA

GAS FLOW RATE W ($lb\ sec^{-1}$)	FRONT SURFACE TEMPERATURE T_{FS} $\epsilon = 0.85$ ($^{\circ}F$)	MAXIMUM EQUILIBRIUM TEMPERATURE RISE AFTER RUN COMPLETION ($^{\circ}F$)	RUN TIME (sec)	CORE WEIGHT LOSS (lb) x 10^3	CORE CHAR WEIGHT (lb) x 10^4	RECESSION (ft) x 10^3	CHAR THICKNESS (ft) x 10^3	PYROLYSIS ZONE (ft) x 10^2
0.0249	4,240	208	39.8	2.4107	6.847	7.3	9.67	1.40
0.0254	3,990	153	39.1	2.4198	6.357	7.9	9.50	1.32
0.0252	4,190	188	39.4	2.3668	6.723	7.8	9.75	1.35
0.0252	4,140	187	40.8	2.3860	6.388	7.5	9.42	1.35
0.0249	4,215	189	39.5	2.4770	6.789	8.2	9.75	1.41
0.0253	4,140	190	39.8	2.4822	6.463	7.9	9.75	1.40
0.0253	4,190	192	39.9	2.3953	6.635	7.3	9.80	1.48
0.0252	4,240	187	39.2	2.3022	6.789	7.4	9.67	1.41
0.0252	4,160	192	39.5	2.4500	7.005	7.6	10.0	1.45
0.0253	3,940	181	43.1	2.4546	6.776	8.0	10.1	1.43
0.0251	4,240	190	39.7	2.4261	6.842	6.3	10.3	1.49

APPENDIX C

SUMMARY OF CORRELATION DATA

APPENDIX C

SUMMARY OF CORRELATION DATA

This appendix tabulates information derived from the measurements listed in Appendix B. It is therefore the source of the information interpreted and correlated in the report. The order in which the facilities are listed is the same as for Appendixes A and B, namely

C- 1 Gas Dynamics—Ames Research Center—NASA

C- 2 Entry Structures Branch—Langley Research Center—NASA

C- 3 Applied Materials and Physics Division—Langley Research Center—NASA

C- 4 Manned Spacecraft Center—NASA

C- 5 Flight Mechanics Division—Wright-Patterson Air Force Base

C- 6 AVCO Corporation

C- 7 Boeing Company

C- 8 General Dynamics

C- 9 General Electric Corporation, Space Technology Center

C-10 Giannini Scientific Corporation

C-11 Martin Company

C-12 North American Aviation Incorporated

FACILITY	MODEL NO.	ENTHALPY POTENTIALS (Btu lb^{-1})					HEAT TRANSFER RATE (Btu sec^{-1} ft^{-2})		
		Δh_{meas} CW (4)	Δh_{calc} SRI HW (5)	Δh_{sonic} CW (6)	Δh_{calc} SRI CW (7)	Δh_{calc} FAC CW (8)	$\dot{q}_{FAC}$ CW	$\dot{q}_{SRI}$ CW	$\dot{q}_{SRI}$ HW (9)
Ames Research Center—NASA	T96	5,350	6,865	5,649	7,278			212.0	201
	T97	6,250	5,215	6,599	5,453			162.0	151
	T98	1,250	1,815	1,323	2,053			58.0	48
Table C-1	T99	3,250	4,225	3,222	4,484			132.0	121
	T100	4,750	7,950	5,553	8,226			347.0	330
	T103	2,950	3,590	2,896	3,822			110.0	100
	P7A2	5,250		5,673	7,304			212	
	P7A3	6,150		6,828	5,629			163	
	P7A4 (1)	5,050		5,247	6,304			256	
	P7A5 (2)	4,850			5,903			236	
	P7A6 (3)	4,750			5,915			235	
	P7A7	5,700		7,790	6,278			251	
	P7B1 (1)	5,050		6,664	6,467			261	
	P7B2	4,500		5,305	6,777			281	
Entry Structure Branch—Langley Research Center—NASA	T26	1,760	2,085	1,950	2,385	1,944	209	245	204
	T27	2,805	3,425	2,850	3,764	3,176	360	410	368
	T28	1,215	1,225	1,300	1,508	1,407	136	145	108
	T29	1,230	1,225	1,300	1,508	1,407	136	145	108
Table C-2	P6A2	1,250		1,300	1,508	1,547	136	145	
	P6A7	3,045		2,850	3,764	3,615	360	410	
	P6B1	1,950		1,950	2,385	2,225	209	245	
Applied Materials and Physics Division—Langley Research Center—NASA	T1	3,536	2,851	3,500	3,086			68	63
	T4	1,906	1,294	2,400	1,534			51	43
	T5	2,066	1,551	2,400	1,771			37	32
	T6	5,665	--	5,000	--			93	--
	T7	3,000	2,194	3,450	2,434			88	79
	T8	3,037	2,831	3,150	3,056			65	62
Table C-3	T11	8,350	6,419	5,150	6,629			94	91
	T61	4,630	3,486	6,450	3,721			98	92
	P2A4	2,068		2,331	1,777			37	
	P2A5 (2)	4,860		4,906	4,795			97	
	P4B3	4,232		5,963	4,290			113	
	P5B1	7,520		7,179	5,166			77	
	P5B3 (1)	5,880		5,150				93	
	P5B4 (3)	4,750		4,750				102	
	P5B5	3,328		3,510	3,003			67	
	P5B6	3,436		3,367	2,838			63	
	P5B7	2,835		3,250	2,555			91	
	3C1	5,280		4,750				106	
	3C2	3,580		3,150	3,136			67	
	3C3	2,150		2,550	1,708			36	
	3C4	1,885		2,500	1,534			51	
	3C5	2,570		2,350	2,323			84	
	3C6	4,875		5,150	4,142			91	
	3C7	6,990		6,450	5,680			86	
Manned Spacecraft Center, Houston—NASA	T47	4,850					300		
	T48	8,650					525		
	T51	12,300					807		
Table C-4	T53	5,350					436		
	T54	7,350					528		
	P4B2	7,551					540		
	P4B4	5,887					478		
	P4B5	7,377					534		
	P4B6	4,914					316		
	P4B7	5,274					413		
	P8B2	5,650					295		
	P8B4	4,360					115		
	P8B5	5,650					295		
	P8B6	5,726					300		
	P9A3	11,918					746		
	P9A4	5,131					350		

APPENDIX C

SUMMARY OF CORRELATION DATA

(Based on Tunnel Calibration and Test Data
Reported By All Participating Facilities)

MODEL STAGNATION PRESSURE P_{t_2} (atm)	NOZZLE EXPANSION RATIO A/A*	SHOCK PRESSURE RATIO P_{t_2}/P_{t_1}		$\frac{\dot{q}_{SRI\ HW}}{\dot{m}_t}$ (Btu lb^{-1})	CHAR DENSITY ρ_{CR} (lb ft^{-3})	MASS LOSS RATES (lb sec^{-1} ft^{-2})					FRONT SURFACE TEMP T_{FS} $\epsilon = 0.85$ ($^{\circ}$R)
		Predicted	Measured			$\dot{m}_t$	$\dot{m}_{CR}$	$\dot{m}_V$	$\dot{m}_{CP}$	$\dot{m}_P$	
0.0844	13.0	0.127	0.2019	2,865		0.0705					
0.0878	13.0	0.127	0.2018	2,605		0.0580					
0.0794	13.0	0.127	0.2020	1,395		0.0344					
0.0862	13.0	0.127	0.2019	1,785		0.0678					
0.177	13.0	0.127	0.1292	3,620		0.0912					
0.0824	13.0	0.127	0.2020	1,680		0.0595					
0.0838	13.0	0.127	0.2019		27.9	0.0208	0.00316	0.0180	0.00536	0.0234	4,100
0.0834	13.0	0.127	0.2019		20.9	0.0192	0.00145	0.0171	0.00605	0.0232	3,850
0.164	13.0	0.127	0.2025		31.3	0.0281	0.0045	0.0250	0.00705	0.0321	4,300
0.159	13.0	0.127	0.2015		26.1	0.0328	0.00306	0.0302	0.0105	0.0407	4,230
0.157	13.0	0.127	0.2023		24.3	0.0346	0.00313	0.0322	0.0104	0.0426	4,050
0.159	13.0	0.127	0.2015		25.0	0.0257	0.00258	0.0232	0.00795	0.0312	4,000
0.162	13.0	0.127	0.2017		29.0	0.0275	0.00362	0.0246	0.00780	0.0324	4,290
0.171	13.0	0.127	0.1276		29.0	0.0308	0.0047	0.0279	0.00770	0.0356	4,200
1.05	3.7	0.40	0.3201	1,370		0.149					
1.18	3.7	0.40	0.3198	1,685		0.218					
0.92	3.7	0.40	0.3206	1,175		0.092					
0.92	3.7	0.40	0.3206	1,115		0.097					
0.92	3.7	0.40	0.3206		20.0	0.0332	0.0074	0.0258	0.0023	0.0281	
1.18	3.7	0.40	0.3198		24.0	0.0535	0.0097	0.0438	0.0072	0.0510	
1.05	3.7	0.40	0.3201		23.0	0.0429	0.0098	0.0331	0.0026	0.0357	
0.0483	150.0	0.013	0.0126	1,940		0.0325					
0.110	150.0	0.013	0.0118	1,590		0.0270					
0.0434	150.0	0.013	0.0117	1,840		0.0174					
--	150.0	0.013	--	--		0.0396					
0.130	150.0	0.013	--	1,560		0.0505					
0.0454	150.0	0.013	0.0125	1,980		0.0314					
0.020	150.0	0.013	0.0132	3,180		0.0286					
0.069	150.0	0.013	0.0118	2,370		0.0388					
0.0431	150.0	0.013	0.0117		21.4	0.00736	0.0006	0.00679	0.0015	0.0083	
--	150.0	0.013	--		22.4	0.0151	0.0007	0.0144	0.0041	0.0185	
0.069	150.0	0.013	0.0118		22.4	0.0128	0.0009	0.0119	0.0034	0.0153	
0.0221	150.0	0.013	0.0126		22.4	0.0200	0.0014	0.0186	0.0048	0.0234	
--	150.0	0.013	--		23.4	0.0136	0.0008	0.0128	0.0034	0.0162	
--	150.0	0.013	--		24.0	0.0182	0.0010	0.0172	0.0048	0.0220	
0.0495	150.0	0.013	0.0126		22.7	0.0105	0.0010	0.0095	0.0023	0.0118	
0.0490	150.0	0.013	0.0126		21.9	0.0102	0.0008	0.0094	0.0022	0.0116	
0.126	150.0	0.013	--		23.5	0.0145	0.0013	0.0132	0.0033	0.0165	
--	150.0	0.013	--								
0.0454	150.0	0.013	0.0126								
0.0442	150.0	0.013	0.0118								
0.110	150.0	0.013	0.0118								
0.130	150.0	0.013	--								
0.0480	150.0	0.013	0.0117								
0.0228	150.0	0.013	0.0131								
1.0						0.066					
1.0						0.116					
1.0						0.145					
1.0						0.105					
1.0						0.117					
1.0					32.8	0.0505	0.0057	0.0448	0.021	0.0658	4,890
1.0					35.3	0.0406	0.0073	0.0333	0.0138	0.0471	5,470
1.0					31.2	0.0435	0.0079	0.0356	0.0165	0.0521	4,802
1.0					31.6	0.0338	0.00355	0.0302	0.0150	0.0452	4,482
1.0					27.0	0.0480	0.00226	0.0457	0.021	0.0667	--
1.0					36.2	0.0380	0.00455	0.0334	0.0124	0.0458	4,678
1.0					29.6	0.0185	0.00032	0.0188	0.0088	0.0276	4,012
1.0					33.5	0.0348	0.0033	0.0315	0.0156	0.0471	4,280
1.0					20.6	0.127	0.0180	0.111	0.0423	0.153	--
1.0					40.0	0.0547	0.0095	0.0452	0.0188	0.0640	5,485
1.0					25.8	0.042	0.00153	0.0405	0.0190	0.0595	--

FACILITY	MODEL NO.	ENTHALPY POTENTIALS (Btu lb^{-1})					HEAT TRANSFER RATE (Btu sec^{-1} ft^{-2})			MODEL STAGNATION PRESSURE P_{t_2} (atm)
		Δh_{meas} CW (4)	Δh_{calc} SRI HW (5)	Δh_{sonic} CW (6)	Δh_{calc} SRI CW (7)	Δh_{calc} FAC CW (8)	$\dot{q}_{FAC}$ CW	$\dot{q}_{SRI}$ CW	$\dot{q}_{SRI}$ HW (9)	
Manned Spacecraft Center, Houston—NASA (Continued)	1	13,123					783			1.0
	2	4,116					300			1.0
	3	4,851					280			1.0
	4	8,128					529			1.0
	5	12,996					657			1.0
	6	5,714					320			1.0
	7	7,269					506			1.0
	8	12,893					793			1.0
	4C1	4,680					315			1.0
	4C2	6,418					470			1.0
	4C3	11,488					652			1.0
	4C4	5,073					330	331		1.0
	4C5	7,355					497	381		1.0
	4C6	13,150					778	698		1.0
	4C7	5,336					337	275		1.0
	4C8	5,610					(280)	283		1.0
	4C9	5,230					(323)	296		1.0
	4C10	5,290					(307)	181		1.0
	4C11	4,875					137	134		1.0
	4C12	6,375					345	325		1.0
	4C13	11,531					550	504		1.0
Flight Mechanics Division, Wright-Patterson Air Force Base	T33	1,597	1,792	2,050	2,051			64.7	57.3	0.0996
	T34	2,350	2,108	3,350	2,274			88	82.5	0.149
	T35	1,821	1,650	2,150	1,906			59.2	51.9	0.0962
	T36	3,131	4,742	3,750	5,016			190.2	181.0	0.143
	T37		3,416	3,650	3,684			144	134.0	0.152
Table C-5	P1A2	4,844		--	--			651.4		0.234
	P1A4 (2)	2,758		3,450	3,717			143.4		0.148
	P1A6 (1)	2,828			3,891			152.6		0.153
	P1A7	2,795			3,210			126.3		0.155
	P1A8	2,654			3,238			126.3		0.151
	P6B4	1,677		2,350	2,418			76.3		0.0999
	P1A5	--			4,346			269.3		0.406
	5C1	1,610		2,550			98.5	86.5		0.145
	5C2	2,800		3,550			164.0	150.0		0.152
	5C3	2,730		4,150	3,811	4,828	189.0	149.0		0.152
	5C4	2,670		4,150			202.5	136.5		0.150
	5C5	1,610					--	--		0.137
	5C6	4,412					--	660.8		0.183
	5C7	4,750					598.4	488.0		0.183
	5C8	--					249.3	242.2		0.391
AVCO Corporation	T18	4,450	--	--	4,668	6,550	104	74	68	0.0250
	T14	4,850	4,945	9,039	5,121	7,608	122	82	76	0.0255
	T17	14,350	16,390	9,039	16,858	27,101	322	200	195	0.0140
Table C-6	T16	9,650	10,160	9,033	10,342	16,425	202	127	122	0.0150
	T15	10,250	9,520	10,259	9,789	11,729	102	85	82	0.0075
	T13	5,050	5,510	5,048	5,758	5,060	44	50	47	0.0075
	P2B1 (1)	4,550		9,050	5,564	8,068	116	80		0.025
	P2B3 (2)	4,950		8,690	5,843	7,790	112	84		0.025
	P2B4 (3)	4,950		8,690	5,843	7,790	117	84		0.0255
	P2B2	14,350		9,050	18,122	26,680	317	215		0.014
	P2B5	9,950		9,759	9,673	11,499	100	84		0.0075
	P2B6	14,850		9,350	15,345	19,000	155	125		0.0066
	P2B7	4,750		5,150	5,873	5,405	47	51		0.0075
Boeing Company	T40	6,210	17,885		18,087	19,571	291	269	256	0.022
	T41	4,700	17,490		17,692		--	238	220	0.018
	T45	14,330	31,880		32,174	31,204	551	568	555	0.031
Table C-7	T46	10,080	28,680		28,945	28,922	511	511	495	0.031
	P1B5	3,850			23,001		--	407		0.041
	P1B3 (1)	4,680			20,032		--	246		0.015
	P1B6 (2)	4,660			17,975		--	235		0.017
	P1B1	14,380					592	570		--
	P1B2	4,440			29,007	33,803	719	617		0.045
	P1B4	10,200			31,911	35,507	656	590		0.034
	P1B7	4,900			29,799	32,256	605	559		0.035
	P3B4	6,240			17,755	19,689	299	270		0.023
	P3B5	14,030			35,239	34,000	591	612		0.030

APPENDIX C Continued

NOZZLE EXPANSION RATIO A/A^*	SHOCK PRESSURE RATIO P_{t_2}/P_{t_1}		$\frac{\dot{q}_{SRI_{HW}}}{\dot{m}_t}$ (Btu lb^{-1})	CHAR DENSITY ρ_{CR} (lb ft^{-3})	MASS LOSS RATES (lb sec^{-1} ft^{-2})					FRONT SURFACE TEMP T_{FS}, $\epsilon = 0.85$ (°R)
	Predicted	Measured			$\dot{m}_t$	$\dot{m}_{CR}$	$\dot{m}_V$	$\dot{m}_{CP}$	$\dot{m}_P$	
					0.129					
					0.0992					
					0.0821					
					0.117					
					0.127					
					0.0845					
					0.113					
					0.146					
640	0.003	0.0008	1,940		0.0296					
640	0.003	0.0042	1,740		0.0474					
640	0.003	0.0042	1,600		0.0325					
640	0.003	0.0040	2,300		0.0786					
3,310	0.0006	0.0043	2,040		0.0655					
640	0.003	0.0139								
640	0.003	0.0044		22.7	0.0212	0.0016	0.0196	0.0056	0.0252	
640	0.003	0.0042		25.8	0.0191	0.0019	0.0173	0.0048	0.0221	--
640	0.003	0.0043		24.4	0.0214	0.0016	0.0198	0.0056	0.0254	--
640	0.003	0.0043		23.8	0.0232	0.0016	0.0216	0.0059	0.0275	--
3,310	0.0006	0.0008		21.4	0.0133	0.0013	0.0120	0.0029	0.0149	--
640	0.003	0.0043		21.8	0.0320	0.0027	0.0347	0.0085	0.0432	--
		0.0043								
9.0	0.17	0.207			0.0782					
9.0	0.17	0.186	1,925		0.0397					
9.0	0.17	0.201	4,370		0.0446					
9.0	0.17	0.178	3,360		0.0364					
9.0	0.17	0.198	3,475		0.0236					
9.0	0.17	0.176	3,200		0.0147					
9.0	0.17	0.183								
9.0	0.17	0.185		20.6	0.0156	0.00174	1.39	0.0031	0.0170	3,870
9.0	0.17	0.183		21.0	0.0152	0.00127	1.39	0.0033	0.0172	3,780
9.0	0.17	0.201		20.0	0.0167	0.0044	1.23	0.0044	0.0167	3,430
9.0	0.17	0.202		21.7	0.0222	0.00088	2.13	0.0059	0.0273	3,520
9.0	0.17	0.194		19.7	0.00966	0.00030	0.936	0.0025	0.0118	3,140
9.0	0.17	0.175		20.3	0.0139	0.00079	1.31	0.0031	0.0162	3,200
				20.8	0.00749	0.00045	0.705	0.0015	0.00858	2,980
18.4	0.09		5,225		0.0503					
18.4	0.09		4,240		0.0550					
18.4	0.09		7,410		0.0760					
18.4	0.09		7,020		0.0720					
18.4	0.09									
18.4	0.09			28.2	0.0354	0.0020	0.0334	0.0105	0.0439	
18.4	0.09			24.6	0.0243	0.0010	0.0233	0.0080	0.0313	
18.4	0.09			24.8	0.0270	0.00093	0.0261	0.0086	0.0347	
18.4	0.09			20.8	0.0380	0.0020	0.0360	0.0120	0.0480	
18.4	0.09			28.9	0.0445	0.0018	0.0427	0.0140	0.0567	
18.4	0.09			25.3	0.0362	0.0012	0.0350	0.0132	0.0482	
18.4	0.09			25.2	0.0356	0.0017	0.0339	0.0123	0.0462	
18.4	0.09			22.0	0.0248	0.00105	0.0237	0.0078	0.0315	
18.4	0.09			19.5	0.0314	0.00077	0.0306	0.0108	0.0414	

FACILITY	MODEL NO.	ENTHALPY POTENTIALS (Btu lb^{-1})					HEAT TRANSFER RATE (Btu sec^{-1} ft^{-2})			MODEL STAGNATION PRESSURE P_{t_2} (atm)
		Δh_{meas} CW (4)	Δh_{calc} SRI HW (5)	Δh_{sonic} CW (6)	Δh_{calc} SRI CW (7)	Δh_{calc} FAC CW (8)	$\dot{q}_{FAC}$ CW	$\dot{q}_{SRI}$ CW	$\dot{q}_{SRI}$ HW (9)	
General Dynamics	T49	4,750		8,850		6,047	398			0.421
	T50						--	--	--	0.490
	T52	5,350	1,560	>20,000	1,770	1,864	36	34	30	0.037
Table C-8	T56	2,650	3,350	4,850	3,620		--	434	401	1.43
	T86	3,550	5,770	5,850	6,000	7,120	535	451	434	0.56
	T44	15,000					245			0.72
	P6A5 (3)	4,750		8,350		6,150	387			0.394
	P6A6	2,650		20,000	2,972			381		1.63
	P6B2 (1)	4,750				5,947	372			0.388
	P8B1	3,550		5,080	5,671	6,151	461	425		0.557
	P8B3	4,750				5,920	376			0.400
	P9B3 (2)	5,350		>20,000	2,071	1,708	33	40		0.037
	P7B4	16,850				3,420	318			0.84
	8C1	4,750		8,250	6,100		394	397		0.422
	8C2	4,750		9,050	6,100		384	370		0.367
	8C3	3,550		5,350	5,860		550	519		0.77
	8C4	3,150		4,850	2,480			317		1.63
General Electric Space Technology Center	T62	13,400	12,470	10,703	12,715			320	312	0.0630
	T63	3,060	11,075	2,963	11,147			215	208	0.0370
	T64	3,030		2,963	11,147			215		0.0370
Table C-9	T65	12,970	7,350	10,526	7,576			69	67	0.00825
	T66	7,850	10,275	5,188	10,527			214	204	0.0411
	T70	5,510	6,940	4,393	7,181			131	122	0.0331
	T75	5,250	5,035	4,505	5,254			44.7	41.7	0.0072
	P5A2 (2)	5,540		10,351	7,181			131		0.0331
	P5A3	13,290		4,393	12,715			320		0.0630
	P5A5 (1)	5,510		10,351	7,181			131		0.0331
	P5A6	7,970		5,303	10,527			214		0.0411
	P5A7 (3)	5,550		10,351	7,181			131		0.0331
	P8A2 (3)	5,620		10,351	7,181			131		0.0331
	P8A3	5,450		4,970	5,254			44.7		0.0072
	P8A4	12,970		10,526	7,576			69.0		0.00825
	9C1	12,930								
	9C2	13,020								
	9C3	12,750								
	9C4	13,020								
	9C5	8,140								
	9C6	8,200								
	9C7	8,450								
	9C8	5,510								
	9C9	5,430								
	9C10	5,330								
	9C11	5,570								
	9C12	3,100								
	9C13	3,100								
	9C14	12,850						330		
	9C15	12,850						324		
	9C16	8,350						212		
	9C17	8,350						215		
	9C18	4,850						133		
	9C19	4,850						129		
	9C20	2,850						217		
	9C21	2,850						214		
	9C22	12,850						75.3		
	9C23	12,850						64.0		
	9C24	12,850						67.2		
	9C25	4,850						44.5		
	9C26	4,850						44.9		
	9C27	5,500								0.0331
	9C28	12,980								0.0630
	9C29	8,550								0.0411
	9C30	2,960								0.0370
	9C31	12,930								0.00825
	9C32	5,440								0.00720

APPENDIX C Continued

NOZZLE EXPANSION RATIO A/A*	SHOCK PRESSURE RATIO P_{t_2}/P_{t_1}		$\dot{q}_{SRI}$ HW / $\dot{m}_t$ (Btu lb^{-1})	CHAR DENSITY ρ_{CR} (lb ft^{-3})	MASS LOSS RATES (lb sec^{-1} ft^{-2})					FRONT SURFACE TEMP T_{FS}, ϵ = 0.85 (°R)
	Predicted	Measured			$\dot{m}_t$	$\dot{m}_{CR}$	$\dot{m}_V$	$\dot{m}_{CP}$	$\dot{m}_P$	
7.2	0.20	0.130			0.157					
7.2	0.20				0.208 (10)					
7.2	0.20	0.0685	1,160		0.0259					
7.2	0.20		1,110		0.362 (10)					
7.2	0.20		2,220		0.196 (10)					
7.2	0.20				0.0604					
7.2	0.20	0.123		21.0	0.0559	0.008	0.0551	0.020	0.0751	
7.2	0.20	0.109		29.6	0.200	0.0480	0.152	0.0046	0.157	
7.2	0.20	0.119		32.2	0.0364	0.0039	0.0325	0.0120	0.0445	
7.2	0.20	0.0828		28.0	0.0440	0.0014	0.0426	0.0151	0.0577	
7.2	0.20	0.123		30.0	0.0374	0.0024	0.0350	0.0127	0.0477	
7.2	0.20	0.0685		22.0	0.00965	0.0007	0.0090	0.0024	0.0114	
7.2	0.20	0.118		25.0	0.0259	0.0013	0.0246	0.0106	0.0352	
7.2	0.20	0.133								
7.2	0.20	0.112								
7.2	0.20	0.114								
7.2	0.20	0.109								
58.0	0.03	0.0391	3,160		0.0953					
58.0	0.03	0.0316	3,400		0.0611					
58.0	0.03	0.0325	--		0.0546					
020	0.002	0.0052	2,900		0.0228					
58.0	0.03	0.0334	3,280		0.0629					
58.0	0.03	0.0306	2,230		0.0556					
1,020	0.002	0.0066	2,790		0.0150					
58.0	0.03	0.0396		23.4	0.0218	0.0021	0.0197	0.00495	0.0247	2,790
58.0	0.03	0.0306		31.0	0.0348	0.00405	0.0308	0.00925	0.0401	3,210
58.0	0.03	0.0331		22.6	0.0179	0.0019	0.0160	0.00372	0.0197	2,830
58.0	0.03			23.2	0.0239	0.00236	0.0215	0.00603	0.0273	2,970
58.0	0.03			23.2	0.0242	0.0017	0.0225	0.00580	0.0283	--
1,020	0.002	0.0064		17.0	0.0236	0.0018	0.0218	0.00730	0.0291	2,770
1,020	0:002	0.0052		21.0	0.0071	0.00062	0.0065	0.00145	0.00795	2,490
58.0	0.03			21.0	0.0113	0.00129	0.0100	0.00223	0.0122	2,400
58.0	0.03									
58.0	0.03									
58.0	0.03									
58.0	0.03									
58.0	0.03									
58.0	0.03									
58.0	0.03									
58.0	0.03									
58.0	0.03									
58.0	0.03									
58.0	0.03									
58.0	0.03									
58.0	0.03									
58.0	0.03									
58.0	0.03									
58.0	0.03									
58.0	0.03									
58.0	0.03									
58.0	0.03									
58.0	0.03									
58.0	0.03									
1,020	0.002									
1,020	0.002									
1,020	0.002									
1,020	0.002									
58.0	0.03									
58.0	0.03									
58.0	0.03									
58.0	0.03									
1,020	0.002									
1,020	0.002									

FACILITY	MODEL NO.	ENTHALPY POTENTIALS (Btu lb^{-1})					HEAT TRANSFER RATE (Btu sec^{-1} ft^{-2})			MODEL STAGNATION PRESSURE P_{t_2}
		Δh_{meas} CW (4)	Δh_{calc} SRI HW (5)	Δh_{sonic} CW (6)	Δh_{calc} SRI CW (7)	Δh_{calc} FAC CW (8)	$\dot{q}_{FAC}$ CW	$\dot{q}_{SRI}$ CW (11)	$\dot{q}_{SRI}$ HW	
Giannini Scientific Corporation	T20	4,955	5,620	4,550		4,924	107	(128)		0.047
	T23	14,960	13,220	>9,850		15,166	334	(296)		0.048
	T24	9,875	6,760	9,250		9,569	219	(160)		0.052
	T21	2,875	3,200	2,650		3,025	72.5	(82)		0.057
Table C-10	T22	4,815	3,555	4,650		4,073	59.4	(55)		0.021
	P3A2	4,850		4,520		4,993	107.1			0.046
	P3A3	4,705		4,466		4,964	106.9			0.046
	P3B3	14,900		>9,850		15,111	332			0.048
	P3B1	9,885		8,675		8,106	118			0.021
	P3A5(1)	4,828		4,726		4,887	137			0.078
	P3A6(2)	4,860		4,789		4,130	138			0.077
	P3A7(3)	4,825		4,726		4,887	137			0.078
	P3B2	4,860		4,650		4,073	58.6			0.020
	10C1	4,770		4,590	5,905	4,977	106.9	127.7		0.046
	10C2	4,805								0.043
	10C3	4,855			5,783	4,911	107.1	125.7		0.047
	10C4	14,805		14,350	13,354	14,956	332.7	296.4		0.049
	10C5	15,725				15,123	332.7			0.048
	10C6	9,835		9,200	7,097	9,662	218.4	160.7		0.051
	10C7	2,835		2,750	3,387	2,974	71.9	81.8		0.058
	10C8	4,855		4,860	5,193	4,919	136.6	144.5		0.077
	10C9	4,875			3,886	4,130	58.9	55.1		0.020
	10C10	4,850				4,176	58.9			0.020
	10C11	9,824		8,610	9,215	8,106	117.8	133.9		0.021
	10C12	9,904				8,066	117.8			0.021
								(11)		
Martin Company	T72	4,936		5,020	7,179	5,747	95	(119)		0.0271
	T74	5,070				5,686	94			0.0271
	T76	4,776				5,729	94			0.0267
Table C-11	T67	12,360		8,200	16,496	20,004	268	(221)		0.0178
	T68	12,100				19,299	260			0.0180
	T71	12,160				19,948	268			0.0179
	T79	2,863		2,000	3,403	3,592	38	(36)		0.0111
	T82	2,900				3,576	38			0.0112
	T84	2,923				3,686	39			0.0111
	T81	10,285		1,800	11,201	9,586	95	(111)		0.00974
	T83	10,083				9,356	93			0.00980
	T87	9,987				9,687	96			0.00974
	T77	4,760		5,150	4,981	2,669	45	(84)		0.0282
	T78	4,920				2,702	45			0.0275
	T88	5,115		800	5,496	5,898	44	(41)		0.00552
	T80	5,070				6,104	45			0.00539
								(11)		
	P9B4	4,844		4,868		6,038	100	(126)		0.0272
	P9B5	4,630				6,000	99			0.0270
	P9B6	4,901				6,005	100			0.0275
	P2A6	11,460		5,728		19,394	262	(214)		0.0182
	P2A7	12,410				19,733	266			0.0180
	P3B6	11,530				19,882	268			0.0180
	P10A4	10,069		1,900		9,505	93	(111)		0.0097
	P10A3	9,725				9,656	95			0.0096
	P10A5	9,350				9,757	96			0.0096
	P7B6(1)	4,870		4,750		8,357	129	(118)		0.0240
	P8A5(1)	5,103				8,415	132			0.0244
	P8A6(1)	4,883				8,450	132			0.0242
	P8A7(2)	4,838		4,800			132	(121)		0.0242
	P9A5(2)	5,030					132			0.0244
	P9A6(2)	4,588					132			0.0244
	P9A7(3)	4,711					137	(121)		0.0246
	P9B1(3)	4,830					129			0.0245
	P9B2(3)	4,944					132			0.0245

NOZZLE EXPANSION RATIO A/A^*	SHOCK PRESSURE RATIO P_{t_2}/P_{t_1}		$\frac{\dot{q}_{SRI}}{\dot{m}_t}$ HW (Btu lb^{-1})	CHAR DENSITY (lb ft^{-3}) ρ_{CR}	MASS LOSS RATES (lb sec^{-1} ft^{-2})					FRONT SURFACE TEMP T_{FS} $\epsilon = 0.85$ (°R)
	Predicted	Measured			$\dot{m}_t$	$\dot{m}_{CR}$	$\dot{m}_V$	$\dot{m}_{CP}$	$\dot{m}_P$	
9.0	0.17	0.204			0.0440					
9.0	0.17	0.154			0.0586					
9.0	0.17	0.186			0.0483					
9.0	0.17	0.211			0.0430					
9.0	0.17	0.256			0.0215					
9.0	0.17	0.200		22.4	0.0187	0.00104	--	--	--	3,510
9.0	0.17	0.201		21.4	0.0158	0.00079	0.015	0.0038	0.0188	3,870
9.0	0.17	0.154		24.0	0.0275	0.00105	0.0265	0.0077	0.0352	4,180
9.0	0.17	0.263		21.7	0.0152	0.00099	0.0151	0.0036	0.0187	3,870
9.0	0.17	0.216		26.0	0.0185	0.00127	0.01730	0.0044	0.0229	4,040
9.0	0.17			22.5	0.0197	--	--	--	--	3,820
9.0	0.17			22.0	0.0233	--	--	--	--	3,390
9.0	0.17	0.241		19.4	0.0103	0.00064	0.00966	0.0020	0.0123	3,205
9.0	0.17	0.201								
9.0	0.17									
9.0	0.17	0.204								
9.0	0.17	0.158								
9.0	0.17	0.154								
9.0	0.17	0.184								
9.0	0.17	0.216								
9.0	0.17	0.213								
9.0	0.17	0.241								
9.0	0.17	0.235								
9.0	0.17	0.266								
9.0	0.17	0.266								
9.0	0.17	0.201			0.0333					
9.0	0.17	0.201			0.0325					
9.0	0.17	0.197			0.0354					
9.0	0.17	0.195			0.0504					
9.0	0.17	0.217			0.0501					
9.0	0.17	0.223			0.0504					
9.0	0.17	0.136			0.0148					
9.0	0.17	0.137			0.0141					
9.0	0.17	0.134			0.0144					
9.0	0.17	0.494			0.0288					
9.0	0.17	0.498			0.0277					
9.0	0.17	0.494			0.0282					
9.0	0.17	0.132			0.0308					
9.0	0.17	0.130			0.0726					
9.0	0.17	0.526			0.0129					
9.0	0.17	0.457			0.0134					
9.0	0.17	0.203		22.5	0.0157	0.0014	0.0143	0.0034	0.0177	3,790
9.0	0.17	0.202		23.9	0.0150	0.0015	0.0135	0.0031	0.0166	3,630
9.0	0.17	0.205		22.8	0.0156	0.0018	0.0138	0.0031	0.0169	3,370
9.0	0.17	0.223		21.1	0.0217	0.0014	0.0203	0.0060	0.0263	3,880
9.0	0.17	0.224		22.6	0.0216	0.0014	0.0202	0.0056	0.0258	--
9.0	0.17	0.224		21.8	0.0212	0.0009	0.0203	0.0059	0.0262	3,780
9.0	0.17	0.483		21.7	0.0132	0.0009	0.0123	0.0032	0.0155	3,700
9.0	0.17	0.485		23.1	0.0127	0.0010	0.0117	0.0029	0.0146	3,460
9.0	0.17	0.471		22.0	0.0128	0.0010	0.0118	0.0029	0.0147	3,435
9.0	0.17	0.211		22.6	0.0165	0.0018	0.0147	0.0035	0.0182	3,660
9.0	0.17	0.216		23.0	0.0167	0.0018	0.0149	0.0037	0.0186	3,610
9.0	0.17	0.213		24.0	0.0167	0.0023	0.0144	0.0033	0.0177	3,480
9.0	0.17	0.213		23.8	0.0190	0.0021	0.0169	0.0039	0.0208	3,430
9.0	0.17	0.212		23.6	0.0184	0.0017	0.0167	0.0043	0.0210	3,170
9.0	0.17	0.212		21.7	0.0188	0.0018	0.0171	0.0042	0.0213	3,480
9.0	0.17	0.215		21.9	0.0220	--	--	--	--	--
9.0	0.17	0.213		20.8	0.0220	--	--	--	--	--
9.0	0.17	0.215		22.8	0.0210	--	--	--	--	--

FACILITY	MODEL NO.	ENTHALPY POTENTIALS (Btu lb^{-1})					HEAT TRANSFER RATE (Btu sec^{-1} ft^{-2})		
		Δh_{meas} CW (4)	Δh_{calc} SRI HW (5)	Δh_{sonic} CW (6)	Δh_{calc} SRI CW (7)	Δh_{calc} FAC CW (8)	$\dot{q}_{FAC}$ CW	$\dot{q}_{SRI}$ CW	$\dot{q}_{SRI}$ HW
Martin Company (Continued)	P9B7	5,020		4,959		2,757	47	(84)	
	B10A2	4,960				2,697	45		
	P10A6	5,050		1,000		6,104	45	(42)	
	P9A2	4,630				6,203	45		
	11C1	4,890		4,700			99		
	11C2	4,633		4,780	7,452	5,868	97	123	
	11C3	5,021			7,578	6,005	100	126	
	11C4	5,000				5,934	99		
	11C5	12,280		8,000			268		
	11C6	11,958		8,050	16,520	20,004	268	221	
	11C7	11,480			15,567	19,246	260	210	
	11C8	12,430				19,948	268		
	11C9	2,838		1,900			38		
	11C10	2,900		1,850	3,408	3,592	38	36	
	11C11	10,276					96		
	11C12	9,837		1,900	11,252	9,818	97	111	
	11C13	9,363			11,924	9,788	97	118	
	11C14	4,972		4,900	7,532	8,228	128	117	
	11C15	4,707					44		
	11C16	5,119		4,850	5,043	2,763	45	82	
	11C17	5,094					48	93	
	11C18	5,094		900	5,583	2,877	45		
	11C19	5,070		900	5,705	6,104	45	42	
	11C20	4,870		900	5,570	5,968	44	41	
North American Aviation, Incorporated	T55	2,430	2,080	2,530	2,333	2,386	105	102.5	87.6
	T57	5,520	5,410	5,690	5,674	5,163	226	248	232
	T58	2,620	2,088	2,690	2,332	2,961	103	81	70
	T59	1,300	920	1,400	1,155	1,221	54	51	37.3
Table C-12	T60	10,300	9,250	9,850	9,528	9,616	434	--	--
	P3A4 (3)	5,400		5,790	4,952	5,150	226	217	
	P4A2	2,450		2,630	2,395	2,403	106	105.5	
	P4A3 (1)	5,465		5,830	5,560	5,186	227	243	
	P4A4 (2)	5,550		5,750	5,102	5,186	228	223	
	P4A5 (3)	5,639		5,750	5,377	5,186	231	235	
	P4A6 (1)	5,620		5,750	5,171	5,186	230	226	
	P4A7	2,620		2,670	2,407	3,019	105	83.6	
	P6B7	10,015		9,850	9,736	9,480	431	442	
	P6B6	3,040		3,170	2,542	3,732	244	166	
	12C1	2,946		2,710		2,890	127.8		
	12C2	5,513		5,750		5,172	224		
	12C3	2,580		2,630		2,911	100		
	12C4	1,300		1,350		1,269	55.1		
	12C5	9,980		9,850		9,337	382		
	12C6	3,180		3,350		3,414	219		
	12C7	2,607		2,780	2,253			100	
	12C8	5,567		5,790	5,368			234	
	12C9	5,707		5,810	5,986			263	
	12C10	5,373		5,810	5,020			220	
	12C11	2,640		2,850	2,525			87.7	
	12C12	1,826		1,420	1,743			77	
	12C13	9,103		9,850	8,020			365	
	12C14	3,015		3,150	2,833			185	

(1) Phenolic-nylon model, long run time in the steady-state series, nominal total heat load 6000 Btu ft^{-2} for all facilities.

(2) Phenolic-nylon model, medium run time in the steady-state series, same tunnel conditions as (1).

(3) Phenolic-nylon model, short run time in the steady-state series, same tunnel conditions as (1).

(4) $\Delta h_{\substack{meas \\ CW}} = h_{t_{FAC}} - h_{CW}$ Enthalpy measured by the facility minus a fixed wall enthalpy $h_{CW} = 150$.

(5) $\Delta h_{\substack{calc \\ SRI \\ HW}} = 24\, \dot{q}_{\substack{SRI \\ CW}} (R_{eff})^{0.5} (P_{t_2})^{-0.5} + h_{CW} - h_{HW}$

Enthalpy calculated from SRI calorimeter plus a fixed wall enthalpy $h_{CW} = 150$ minus hot-wall enthalpy equal to enthalpy of air at surface temperature of the Teflon. Teflon temperature estimated by assuming that its vapor pressure equals model stagnation pressure P_{t_2}.

MODEL STAGNATION PRESSURE P_{t_2} (atm)	NOZZLE EXPANSION RATIO A/A*	SHOCK PRESSURE RATIO P_{t_2}/P_{t_1}		$\frac{\dot{q}_{SRI\ HW}}{\dot{m}_t}$ (Btu lb^{-1})	CHAR DENSITY ρ_{CR} (lb ft^{-3})	MASS LOSS RATES (lb sec^{-1} ft^{-2})					FRONT SURFACE TEMP T_{FS} $\epsilon = 0.85$ ($^{\circ}$R)
		Predicted	Measured			$\dot{m}_t$	$\dot{m}_{CR}$	$\dot{m}_V$	$\dot{m}_{CP}$	$\dot{m}_P$	
0.0276	9.0	0.17	0.130		25.8	0.0151	0.0023	0.0128	0.0025	0.0153	3,595
0.0276	9.0	0.17	0.130		26.2	0.0152	0.0024	0.0128	0.0024	0.0152	3,900
0.00539	9.0	0.17	0.457		23.2	0.00699	0.0005	0.00648	0.0015	0.00800	2,800
0.00522	9.0	0.17	0.396		22.5	0.00721	0.0006	0.00664	0.0014	0.00808	2,810
0.0271	9.0	0.17	0.200								
0.0271	9.0	0.17	0.199								
0.0275	9.0	0.17	0.201								
0.0276	9.0	0.17	0.202								
0.0178	9.0	0.17									
0.0179	9.0	0.17	0.205								
0.0181	9.0	0.17	0.225								
0.0179	9.0	0.17	0.209								
0.0111	9.0	0.17									
0.0111	9.0	0.17	0.136								
0.00974	9.0	0.17	0.510								
0.00968	9.0	0.17	0.482								
0.00974	9.0	0.17	0.510								
0.0240	9.0	0.17	0.212								
0.0276	9.0	0.17	0.130								
0.0263	9.0	0.17	0.125								
0.0276	9.0	0.17	0.130								
0.00552	9.0	0.17									
0.00539	9.0	0.17	0.457								
0.00539	9.0	0.17	0.457								
0.192	12.8	0.128	0.149	1,420		0.0645					
0.190	12.8	0.128	0.148	2,225		0.106					
0.120	12.8	0.128	0.148	1,335		0.0546					
0.194	12.8	0.128	0.149	1,280		0.0313					
0.202	12.8	0.128	0.169			0.129					
0.191	12.8	0.128	0.148		23.0	0.0342	0.00224	0.0320	0.00985	0.0418	3,840
0.193	12.8	0.128	0.148		22.8	0.0187	0.00232	0.0164	0.00376	0.0201	3,410
0.190	12.8	0.128	0.148		26.2	0.0296	0.0031	0.0265	0.00745	0.0339	3,934
0.190	12.8	0.128	0.148		23.3	0.0304	0.00175	0.0286	0.00945	0.0380	4,027
0.190	12.8	0.128	0.148		23.3	0.0358	0.0023	0.0335	0.0102	0.0437	3,870
0.190	12.8	0.128	0.148		28.4	0.0303	0.0039	0.0264	0.0070	0.0334	4,027
0.120	12.8	0.128	0.148		21.8	0.0160	0.0025	0.0135	0.00262	0.0161	3,430
0.205	12.8	0.128	0.169		31.0	0.0416	0.0043	0.0373	0.0118	0.0491	4,240
0.424	12.8	0.128	0.143		23.0	0.0318	0.0059	0.0259	0.0045	0.0304	3,840
0.194	12.8	0.128	0.147								
0.186	12.8	0.128	0.145								
0.117	12.8	0.128	0.145								
0.187	12.8	0.128	0.145								
0.166	12.8	0.128	0.136								
0.408	12.8	0.128	0.146								
0.196	12.8	0.128	0.148								
0.189	12.8	0.128	0.146								
0.192	12.8	0.128	0.149								
0.191	12.8	0.128	0.149								
0.120	12.8	0.128	0.148								
0.194	12.8	0.128	0.149								
0.206	12.8	0.128	0.170								
0.424	12.8	0.128	0.143								

(6) $\Delta h_{\underset{CW}{sonic}} = (280\ A^*P_{t_1}W^{-1})^{2.5} - h_{CW}$

Enthalpy measured by sonic flow method minus a fixed wall enthalpy $h_{CW} = 150$, Ref. TND1333 and TND2132.

(7) $\Delta h_{\underset{CW}{\underset{SRI}{calc}}} = 24\ \dot{q}_{\underset{CW}{SRI}}(R_{eff})^{0.5}(P_{t_2})^{-0.5}$ Enthalpy calculated from SRI calorimeter reading.

(8) $\Delta h_{\underset{CW}{\underset{FAC}{calc}}} = 24\ \dot{q}_{\underset{CW}{FAC}}(R_{eff})^{0.5}(P_{t_2})^{-0.5}$ Enthalpy calculated from facility calorimeter reading.

(9) $\dot{q}_{\underset{HW}{SRI}} = \dot{q}_{\underset{CW}{SRI}} \Delta h_{\underset{HW}{\underset{SRI}{calc}}} \Big/ \Delta h_{\underset{CW}{\underset{SRI}{calc}}}$

(10) Data not used in correlations because model eroded asymmetrically.

(11) SRI calorimeter cold wall heating rate estimated from calibration runs.